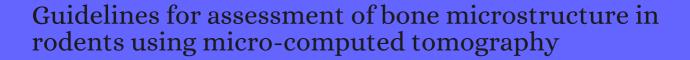
# CITATION REPORT List of articles citing



DOI: 10.1002/jbmr.141 Journal of Bone and Mineral Research, 2010, 25, 1468-86.

Source: https://exaly.com/paper-pdf/48109584/citation-report.pdf

**Version:** 2024-04-10

This report has been generated based on the citations recorded by exaly.com for the above article. For the latest version of this publication list, visit the link given above.

The third column is the impact factor (IF) of the journal, and the fourth column is the number of citations of the article.

#	Paper	IF	Citations
2308	Two-Dimensional Magnesium Phosphate Nanosheets Form Highly Thixotropic Gels That Up-Regulate Bone Formation.		
2307	Muscle changes can account for bone loss after botulinum toxin injection. <b>2010</b> , 87, 541-9		23
2306	Application of in vivo micro-computed tomography in the temporal characterisation of subchondral bone architecture in a rat model of low-dose monosodium iodoacetate-induced osteoarthritis. <b>2011</b> , 13, R210		67
2305	CXC receptor knockout mice: characterization of skeletal features and membranous bone healing in the adult mouse. <b>2011</b> , 48, 267-74		12
2304	Increasing duration of type 1 diabetes perturbs the strength-structure relationship and increases brittleness of bone. <b>2011</b> , 48, 733-40		77
2303	Suberoylanilide hydroxamic acid (SAHA; vorinostat) causes bone loss by inhibiting immature osteoblasts. <b>2011</b> , 48, 1117-26		60
2302	Dose response of bone-targeted enzyme replacement for murine hypophosphatasia. <b>2011</b> , 49, 250-6		41
2301	Serial FIB/SEM imaging for quantitative 3D assessment of the osteocyte lacuno-canalicular network. <b>2011</b> , 49, 304-11		107
2300	The bone architecture is enhanced with combined PTH and alendronate treatment compared to monotherapy while maintaining the state of surface mineralization in the OVX rat. <b>2011</b> , 49, 225-32		23
2299	Attenuated anabolic response to exercise in lamin A/C haploinsufficient mice. 2011, 49, 412-8		12
2298	MicroCT morphometry analysis of mouse cancellous bone: intra- and inter-system reproducibility. <b>2011</b> , 49, 580-7		40
2297	Low bone accrual is associated with osteocyte apoptosis in alcohol-induced osteopenia. <b>2011</b> , 49, 543-	52	41
2296	Development of micro-CT protocols for in vivo follow-up of mouse bone architecture without major radiation side effects. <b>2011</b> , 49, 613-22		69
2295	Different effects on bone strength and cell differentiation in pre pubertal caloric restriction versus hypothalamic suppression. <b>2011</b> , 49, 810-8		5
2294	Deriving tissue density and elastic modulus from microCT bone scans. <b>2011</b> , 49, 931-8		35
2293	Comparison of 2D and 3D bone microarchitecture evaluation at the femoral neck, among postmenopausal women with hip fracture or hip osteoarthritis. <b>2011</b> , 49, 1055-61		28
2292	Erythropoietin stimulates bone formation, cell proliferation, and angiogenesis in a femoral segmental defect model in mice. <b>2011</b> , 49, 1037-45		68

2291	The importance of murine cortical bone microstructure for microcrack initiation and propagation. <b>2011</b> , 49, 1186-93		34
2290	In vivo validation of a computational bone adaptation model using open-loop control and time-lapsed micro-computed tomography. <b>2011</b> , 49, 1166-72		24
2289	Mouse tail vertebrae adapt to cyclic mechanical loading by increasing bone formation rate and decreasing bone resorption rate as shown by time-lapsed in vivo imaging of dynamic bone morphometry. <b>2011</b> , 49, 1340-50		84
2288	In vivo loading increases mechanical properties of scaffold by affecting bone formation and bone resorption rates. <b>2011</b> , 49, 1357-64		30
2287	Gene Therapy Applications for Fracture Repair. 2011,		
2286	Erythropoietin couples erythropoiesis, B-lymphopoiesis, and bone homeostasis within the bone marrow microenvironment. <b>2011</b> , 117, 5631-42		100
2285	Subchondral trabecular structural changes in the proximal tibia in an ovine model of increased bone turnover. <b>2011</b> , 218, 619-24		8
2284	Microcomputed tomography-based structural analysis of various bone tissue regeneration models. <b>2011</b> , 6, 105-10		59
2283	Lamin A/C deficiency is associated with fat infiltration of muscle and bone. <b>2011</b> , 132, 552-9		44
2282	Imaging technologies for preclinical models of bone and joint disorders. <b>2011</b> , 1, 11		41
2281	Direct visualization and quantification of bone growth into porous titanium implants using micro computed tomography. <b>2011</b> , 22, 1321-32		42
2280	In vivo bone regeneration with injectable chitosan/hydroxyapatite/collagen composites and mesenchymal stem cells. <b>2011</b> , 5, 301-310		13
2279	Interferon-[plays a role in bone formation in vivo and rescues osteoporosis in ovariectomized mice. Journal of Bone and Mineral Research, <b>2011</b> , 26, 1472-83	6.3	101
2278	Osteal macrophages promote in vivo intramembranous bone healing in a mouse tibial injury model. <i>Journal of Bone and Mineral Research</i> , <b>2011</b> , 26, 1517-32	6.3	303
2277	Chlorthalidone improves vertebral bone quality in genetic hypercalciuric stone-forming rats. Journal of Bone and Mineral Research, <b>2011</b> , 26, 1904-12	6.3	22
2276	Connexin43 deficiency reduces the sensitivity of cortical bone to the effects of muscle paralysis. Journal of Bone and Mineral Research, <b>2011</b> , 26, 2151-60	6.3	66
2275	Thyroid hormone receptor Imediates thyroid hormone effects on bone remodeling and bone mass. <i>Journal of Bone and Mineral Research</i> , <b>2011</b> , 26, 2036-44	6.3	34
2274	FGF-23/Klotho signaling is not essential for the phosphaturic and anabolic functions of PTH. <i>Journal of Bone and Mineral Research</i> , <b>2011</b> , 26, 2026-35	6.3	44

2273	Regulation of postnatal trabecular bone formation by the osteoblast endothelin A receptor. Journal of Bone and Mineral Research, <b>2011</b> , 26, 2523-36	6.3	29
2272	Cell line IDG-SW3 replicates osteoblast-to-late-osteocyte differentiation in vitro and accelerates bone formation in vivo. <i>Journal of Bone and Mineral Research</i> , <b>2011</b> , 26, 2634-46	6.3	160
2271	Physiological function of the angiotensin AT1a receptor in bone remodeling. <i>Journal of Bone and Mineral Research</i> , <b>2011</b> , 26, 2959-66	6.3	42
2270	Automated quantitative microstructural analysis of metastatically involved vertebrae: effects of stereologic model and spatial resolution. <b>2011</b> , 33, 188-94		7
2269	Vertical ground reaction forces diminish in mice after botulinum toxin injection. <b>2011</b> , 44, 637-43		19
2268	Bone Gla protein increases HIF-1alpha-dependent glucose metabolism and induces cartilage and vascular calcification. <b>2011</b> , 31, e55-71		89
2267	Hypoxia-inducible factor-1⊕rotein negatively regulates load-induced bone formation. <b>2011</b> , 286, 44449-	-56	26
2266	Standardized three-dimensional volumes of interest with adapted surfaces for more precise subchondral bone analyses by micro-computed tomography. <b>2011</b> , 17, 475-84		15
2265	HES1 (hairy and enhancer of split 1) is a determinant of bone mass. <b>2011</b> , 286, 2648-57		39
2264	Targeted ablation of the PTH/PTHrP receptor in osteocytes impairs bone structure and homeostatic calcemic responses. <b>2011</b> , 209, 21-32		153
2264			153
2263	homeostatic calcemic responses. <b>2011</b> , 209, 21-32	-80	
2263	homeostatic calcemic responses. <b>2011</b> , 209, 21-32  High-Resolution Imaging Techniques for Bone Quality Assessment. <b>2011</b> , 891-925	-80	1
2263 2262 2261	homeostatic calcemic responses. <b>2011</b> , 209, 21-32  High-Resolution Imaging Techniques for Bone Quality Assessment. <b>2011</b> , 891-925  Sclerostin antibody increases bone volume and enhances implant fixation in a rat model. <b>2012</b> , 94, 1670-  Multiple exposures to unloading decrease bone's responsivity but compound skeletal losses in	-80	1 42
2263 2262 2261	High-Resolution Imaging Techniques for Bone Quality Assessment. <b>2011</b> , 891-925  Sclerostin antibody increases bone volume and enhances implant fixation in a rat model. <b>2012</b> , 94, 1670-1670.  Multiple exposures to unloading decrease bone's responsivity but compound skeletal losses in C57BL/6 mice. <b>2012</b> , 303, R159-67	-80	1 42 16
2263 2262 2261 2260	High-Resolution Imaging Techniques for Bone Quality Assessment. 2011, 891-925  Sclerostin antibody increases bone volume and enhances implant fixation in a rat model. 2012, 94, 1670- Multiple exposures to unloading decrease bone's responsivity but compound skeletal losses in C57BL/6 mice. 2012, 303, R159-67  3-dimensional imaging modalities for phenotyping genetically engineered mice. 2012, 49, 106-15  Indentation experiments and simulation of ovine bone using a viscoelastic-plastic damage model.	-80	1 42 16
2263 2262 2261 2260 2259	homeostatic calcemic responses. 2011, 209, 21-32  High-Resolution Imaging Techniques for Bone Quality Assessment. 2011, 891-925  Sclerostin antibody increases bone volume and enhances implant fixation in a rat model. 2012, 94, 1670-  Multiple exposures to unloading decrease bone's responsivity but compound skeletal losses in C57BL/6 mice. 2012, 303, R159-67  3-dimensional imaging modalities for phenotyping genetically engineered mice. 2012, 49, 106-15  Indentation experiments and simulation of ovine bone using a viscoelastic-plastic damage model. 2012, 27, 368-377  Induction of osteoclastogenesis and bone loss by human autoantibodies against citrullinated	-80	1 42 16 14 2

2255	NELL1 promotes bone regeneration in polyethylene particle-induced osteolysis. <b>2012</b> , 18, 1344-51		4
2254	Imaging of cellular spread on a three-dimensional scaffold by means of a novel cell-labeling technique for high-resolution computed tomography. <b>2012</b> , 18, 167-75		4
2253	Micro-tomographic Characterization of Dissolution-induced Local Porosity Changes including Fines Migration in Carbonate Rock. <b>2012</b> ,		5
2252	A soluble bone morphogenetic protein type IA receptor increases bone mass and bone strength. <b>2012</b> , 109, 12207-12		38
2251	Reconstruction of bone microstructure from few projections with convex-concave and non local regularization. <b>2012</b> ,		1
2250	Selenium deficiency decreases antioxidative capacity and is detrimental to bone microarchitecture in mice. <b>2012</b> , 142, 1526-31		50
2249	Low-dose, ionizing radiation and age-related changes in skeletal microarchitecture. <b>2012</b> , 2012, 481983		22
2248	Rac signaling in osteoblastic cells is required for normal bone development but is dispensable for hematopoietic development. <b>2012</b> , 119, 736-44		20
2247	The effect of a Beare-Stevenson syndrome Fgfr2 Y394C mutation on early craniofacial bone volume and relative bone mineral density in mice. <b>2012</b> , 221, 434-42		11
2246	A comparative study of the trabecular bony architecture of the talus in humans, non-human primates, and Australopithecus. <b>2012</b> , 63, 536-51		54
2245	Mechanisms of bone fragility in a mouse model of glucocorticoid-treated rheumatoid arthritis: implications for insufficiency fracture risk. <b>2012</b> , 64, 3649-59		35
2244	Sclerostin antibody prevents particle-induced implant loosening by stimulating bone formation and inhibiting bone resorption in a rat model. <b>2012</b> , 64, 4012-20		42
2243	Connexin 43 deficiency attenuates loss of trabecular bone and prevents suppression of cortical bone formation during unloading. <i>Journal of Bone and Mineral Research</i> , <b>2012</b> , 27, 2359-72	6.3	71
2242	Class IA phosphatidylinositol 3-kinase regulates osteoclastic bone resorption through protein kinase B-mediated vesicle transport. <i>Journal of Bone and Mineral Research</i> , <b>2012</b> , 27, 2464-75	6.3	28
2241	Microarchitecture and bone quality in the human calcaneus: local variations of fabric anisotropy. Journal of Bone and Mineral Research, <b>2012</b> , 27, 2562-72	6.3	20
2240	Osteopetrosis rescue upon RANKL administration to Rankl(-/-) mice: a new therapy for human RANKL-dependent ARO. <i>Journal of Bone and Mineral Research</i> , <b>2012</b> , 27, 2501-10	6.3	36
2239	Effects of different therapeutic ultrasound intensities on fracture healing in rats. <b>2012</b> , 38, 745-52		24
2238	Computed radiographic and ultrasonic evaluation of bone regeneration during tibial distraction osteogenesis in rabbits. <b>2012</b> , 38, 1744-58		4

2237	Stimulated angiogenesis for fracture healing augmented by low-magnitude, high-frequency vibration in a rat model-evaluation of pulsed-wave doppler, 3-D power Doppler ultrasonography and micro-CT microangiography. <b>2012</b> , 38, 2120-9		43	
2236	Transient muscle paralysis degrades bone via rapid osteoclastogenesis. <b>2012</b> , 26, 1110-8		35	
2235	Vitamin D supplementation protects against bone loss associated with chronic alcohol administration in female mice. <b>2012</b> , 343, 401-12		36	
2234	A paradigm for the development and evaluation of novel implant topologies for bone fixation: in vivo evaluation. <b>2012</b> , 45, 2651-7		11	
2233	Three-dimensional structure of the shell plate assembly of the chiton Tonicella marmorea and its biomechanical consequences. <b>2012</b> , 177, 314-28		53	
2232	Imaging the vasculature by microCT; ain't no bones about it. <b>2012</b> , 50, 400			
2231	Proteinase-activated receptor-2 is required for normal osteoblast and osteoclast differentiation during skeletal growth and repair. <b>2012</b> , 50, 704-12		22	
2230	Anatomical distribution of the degree of mineralization of bone tissue in human femoral neck: impact on biomechanical properties. <b>2012</b> , 50, 876-84		35	
2229	Micro and macroarchitectural changes at the tibia after botulinum toxin injection in the growing rat. <b>2012</b> , 50, 858-64		20	
2228	Villin promoter-mediated transgenic expression of transient receptor potential cation channel, subfamily V, member 6 (TRPV6) increases intestinal calcium absorption in wild-type and vitamin D receptor knockout mice. <i>Journal of Bone and Mineral Research</i> , <b>2012</b> , 27, 2097-107	6.3	49	
2227	Regulation of bone mass and osteoclast function depend on the F-actin modulator SWAP-70. Journal of Bone and Mineral Research, <b>2012</b> , 27, 2085-96	6.3	27	
2226	Minimally invasive mandibular bone augmentation using injectable hydrogels. <b>2012</b> , 6 Suppl 3, s15-23		35	
2225	Early effects of zoledronic acid and teriparatide on bone microarchitecture, remodeling and collagen crosslinks: comparison between iliac crest and lumbar vertebra in ewes. <b>2012</b> , 51, 714-9		10	
2224	High resolution micro arthrography of hard and soft tissues in a murine model. <b>2012</b> , 20, 1011-9		19	
2223	Bone characteristics of late-term embryonic and hatchling broilers: bone development under extreme growth rate. <b>2012</b> , 91, 2614-20		27	
2222	Adult stem cell mobilization enhances intramembranous bone regeneration: a pilot study. <b>2012</b> , 470, 2503-12		12	
2221	Repair of rabbit ulna segmental bone defect using freshly isolated adipose-derived stromal vascular fraction. <b>2012</b> , 14, 296-305		21	
2220	Estimation of an early meaningful time point of bone parameter changes in application to an osteoporotic rat model with in vivo microcomputed tomography measurements. <b>2012</b> , 46, 237-44		11	

2219	Spectral optimization for micro-CT. <b>2012</b> , 39, 3229-39	8
2218	Anaesthesia and physiological monitoring during in vivo imaging of laboratory rodents: considerations on experimental outcomes and animal welfare. <b>2012</b> , 2, 44	99
2217	Temporal changes in bone composition, architecture, and strength following estrogen deficiency in osteoporosis. <b>2012</b> , 91, 440-9	30
2216	Deletion of Cx43 from osteocytes results in defective bone material properties but does not decrease extrinsic strength in cortical bone. <b>2012</b> , 91, 215-24	51
2215	Impact of an obesogenic diet program on bone densitometry, micro architecture and metabolism in male rat. <b>2012</b> , 11, 91	22
2214	High-frequency, low-magnitude vibration does not prevent bone loss resulting from muscle disuse in mice following botulinum toxin injection. <b>2012</b> , 7, e36486	19
2213	Calcitonin inhibits SDCP-induced osteoclast apoptosis and increases its efficacy in a rat model of osteoporosis. <b>2012</b> , 7, e40272	20
2212	Quantitative ex-vivo micro-computed tomographic imaging of blood vessels and necrotic regions within tumors. <b>2012</b> , 7, e41685	22
2211	Low bone turnover and low BMD in Down syndrome: effect of intermittent PTH treatment. <b>2012</b> , 7, e42967	27
2210	Fracture healing in protease-activated receptor-2 deficient mice. <b>2012</b> , 30, 1271-6	5
2209	Site-specific changes in bone microarchitecture, mineralization, and stiffness during lactation and after weaning in mice. <i>Journal of Bone and Mineral Research</i> , <b>2012</b> , 27, 865-75	61
2208	Bones' adaptive response to mechanical loading is essentially linear between the low strains associated with disuse and the high strains associated with the lamellar/woven bone transition. 6.3  Journal of Bone and Mineral Research, 2012, 27, 1784-93	142
2207	Serum response factor regulates bone formation via IGF-1 and Runx2 signals. <i>Journal of Bone and Mineral Research</i> , <b>2012</b> , 27, 1659-68	30
2206	Relationship between microstructure and degree of mineralization in subchondral bone of osteoarthritis: a synchrotron radiation $\mu$ CT study. <i>Journal of Bone and Mineral Research</i> , <b>2012</b> , 27, 1511- $7^{6.3}$	30
2205	Three-dimensional dynamic bone histomorphometry. <i>Journal of Bone and Mineral Research</i> , <b>2012</b> , 27, 486-95	38
2204	Influence of mineralization and microporosity on tissue elasticity: experimental and numerical investigation on mineralized turkey leg tendons. <b>2012</b> , 90, 319-29	25
2203	The effect of level and downhill running on cortical and trabecular bone in growing rats. 2012, 90, 429-37	15
2202	Local delivery of FTY720 accelerates cranial allograft incorporation and bone formation. <b>2012</b> , 347, 553-66	35

2201	3D characterization of bone strains in the rat tibia loading model. <b>2012</b> , 11, 403-10		29
2200	Phospholipase CI is required for basal but not oestrogen deficiency-induced bone resorption. <b>2012</b> , 42, 49-60		25
2199	Low-dose rhBMP2/7 heterodimer to reconstruct peri-implant bone defects: a micro-CT evaluation. <b>2012</b> , 39, 98-105		27
2198	Spine degeneration in a murine model of chronic human tobacco smokers. <b>2012</b> , 20, 896-905		80
2197	Musculoskeletal changes following non-invasive knee injury using a novel mouse model of post-traumatic osteoarthritis. <b>2012</b> , 20, 773-82		124
2196	Overexpression of DMP1 accelerates mineralization and alters cortical bone biomechanical properties in vivo. <b>2012</b> , 5, 1-8		23
2195	Bone turnover markers correlate with implant fixation in a rat model using LPS-doped particles to induced implant loosening. <b>2012</b> , 100, 918-28		21
2194	Proteoglycan 4: a dynamic regulator of skeletogenesis and parathyroid hormone skeletal anabolism. <i>Journal of Bone and Mineral Research</i> , <b>2012</b> , 27, 11-25	6.3	34
2193	Anti IL-17A therapy inhibits bone loss in TNF-Emediated murine arthritis by modulation of the T-cell balance. <b>2012</b> , 42, 413-23		39
2192	Gremlin1 is required for skeletal development and postnatal skeletal homeostasis. 2012, 227, 269-77		27
2191	The transient receptor potential channel TRPV6 is dynamically expressed in bone cells but is not crucial for bone mineralization in mice. <b>2012</b> , 227, 1951-9		33
2190	Low intensity pulsed ultrasound enhances fracture healing in both ovariectomy-induced osteoporotic and age-matched normal bones. <b>2012</b> , 30, 129-36		36
2189	Comparable outcomes in fracture reduction and bone properties with RANKL inhibition and alendronate treatment in a mouse model of osteogenesis imperfecta. <b>2012</b> , 23, 1141-50		44
2188	Skeletal remodeling following clinically relevant radiation-induced bone damage treated with zoledronic acid. <b>2012</b> , 90, 40-9		10
2187	Longitudinal assessment of in vivo bone dynamics in a mouse tail model of postmenopausal osteoporosis. <b>2012</b> , 90, 108-19		34
2186	Experimental and finite element analysis of the mouse caudal vertebrae loading model: prediction of cortical and trabecular bone adaptation. <b>2012</b> , 11, 221-30		24
2185	Is micro-computed tomography reliable to determine the microstructure of the maxillary alveolar bone?. <b>2013</b> , 24, 730-7		25
2184	The predictive value of trabecular bone score (TBS) on whole lumbar vertebrae mechanics: an ex vivo study. <b>2013</b> , 24, 2455-60		122

2183	Skeletal effects of zoledronic acid in an animal model of chronic kidney disease. <b>2013</b> , 24, 1471-81	35
2182	Adaptation of tibial structure and strength to axial compression depends on loading history in both C57BL/6 and BALB/c mice. <b>2013</b> , 93, 211-21	41
2181	Further analysis of the Crouzon mouse: effects of the FGFR2(C342Y) mutation are cranial bone-dependent. <b>2013</b> , 92, 451-66	36
2180	The influence of therapeutic radiation on the patterns of bone remodeling in ovary-intact and ovariectomized mice. <b>2013</b> , 92, 372-84	10
2179	Micro-computed tomography and compressive characterization of trabecular bone. 2013, 438, 199-205	12
2178	Kinsenoside prevents ovariectomy-induced bone loss and suppresses osteoclastogenesis by regulating classical NF- <b>B</b> pathways. <b>2013</b> , 24, 1663-76	23
2177	Determination of mesenchymal stem cell fate by pigment epithelium-derived factor (PEDF) results in increased adiposity and reduced bone mineral content. <b>2013</b> , 27, 4384-94	57
2176	The effects of minimally invasive laser needle system on suppression of trabecular bone loss induced by skeletal unloading. <b>2013</b> , 28, 1495-502	7
2175	Siglec-15 regulates osteoclast differentiation by modulating RANKL-induced phosphatidylinositol 3-kinase/Akt and Erk pathways in association with signaling Adaptor DAP12. <i>Journal of Bone and Mineral Research</i> , <b>2013</b> , 28, 2463-75	77
2174	Sclerostin deficient mice rapidly heal bone defects by activating []-catenin and increasing intramembranous ossification. <b>2013</b> , 441, 886-90	44
2173	Acceleration of bone development and regeneration through the Wnt/Ecatenin signaling pathway in mice heterozygously deficient for GSK-3 2013, 440, 677-82	29
2172	Maternal hypervitaminosis D reduces fetal bone mass and mineral acquisition and leads to neonatal lethality. <b>2013</b> , 57, 123-31	30
2171	Osteoblastic Wnts differentially regulate bone remodeling and the maintenance of bone marrow mesenchymal stem cells. <b>2013</b> , 55, 258-67	36
2170	Prenatal nutritional manipulation by in ovo enrichment influences bone structure, composition, and mechanical properties. <b>2013</b> , 91, 2784-93	22
2169	Hairy and Enhancer of Split-related with YRPW motif (HEY)2 regulates bone remodeling in mice. <b>2013</b> , 288, 21547-57	14
2168	Insulin-like growth factor-1 receptor in mature osteoblasts is required for periosteal bone formation induced by reloading. <b>2013</b> , 92, 73-78	15
2167	Pharmacological inhibition of PPARIIncreases osteoblastogenesis and bone mass in male C57BL/6 mice. <i>Journal of Bone and Mineral Research</i> , <b>2013</b> , 28, 639-48	58
2166	Glucose-dependent insulinotropic polypeptide (GIP) receptor deletion leads to reduced bone strength and quality. <b>2013</b> , 56, 337-42	78

2165	Age-related changes of vertical and horizontal lumbar vertebral trabecular 3D bone microstructure is different in women and men. <b>2013</b> , 57, 47-55		25
2164	Animal Models of Bone Disease-B. <b>2013</b> , 391-417		3
2163	A commentary on modelling osteoarthritis pain in small animals. <b>2013</b> , 21, 1316-26		96
2162	Metaphyseal and diaphyseal bone loss in the tibia following transient muscle paralysis are spatiotemporally distinct resorption events. <b>2013</b> , 57, 413-22		28
2161	Nutritional Influences on Bone Health and Overview of Methods. 2013, 357-370		1
2160	The interaction of force and repetition on musculoskeletal and neural tissue responses and sensorimotor behavior in a rat model of work-related musculoskeletal disorders. <b>2013</b> , 14, 303		85
2159	Preservation of bone structure and function by Lithothamnion sp. derived minerals. <b>2013</b> , 156, 210-20		11
2158	Trabecular bone structural parameters evaluated using dental cone-beam computed tomography: cellular synthetic bones. <b>2013</b> , 12, 115		23
2157	In vitro ceramic scaffold mineralization: comparison between histological and micro-computed tomographical analysis. <b>2013</b> , 41, 2666-75		13
2156	The effect of the Achilles tendon on trabecular structure in the primate calcaneus. <b>2013</b> , 296, 1509-17		18
2155	Serum IGF-1 is insufficient to restore skeletal size in the total absence of the growth hormone receptor. <i>Journal of Bone and Mineral Research</i> , <b>2013</b> , 28, 1575-86	6.3	28
2154	Assessment of Bone Mass and Microarchitecture in Rodents. <b>2013</b> , 59-68		
2153	Tooth periodontal ligament: Direct 3D microCT visualization of the collagen network and how the network changes when the tooth is loaded. <b>2013</b> , 181, 108-15		31
2152	The assessment of trabecular bone parameters and cortical bone strength: a comparison of micro-CT and dental cone-beam CT. <b>2013</b> , 46, 2611-8		36
2151	Inactivation of estrogen receptor \(\frac{1}{2}\)n bone-forming cells induces bone loss in female mice. <b>2013</b> , 27, 478-88		65
2150	Changes in bone sclerostin levels in mice after ovariectomy vary independently of changes in serum sclerostin levels. <i>Journal of Bone and Mineral Research</i> , <b>2013</b> , 28, 618-26	6.3	39
2149	Comparative effects of teriparatide and risedronate in glucocorticoid-induced osteoporosis in men: 18-month results of the EuroGIOPs trial. <i>Journal of Bone and Mineral Research</i> , <b>2013</b> , 28, 1355-68	6.3	119
2148	Comparison of estrogenic responses in bone and uterus depending on the parity status in Lewis rats. <b>2013</b> , 133, 101-9		8

2147	Textural characteristics of model and natural bone tissues and interfacial behavior of bound water. <b>2013</b> , 392, 446-462		5
2146	A novel left heart simulator for the multi-modality characterization of native mitral valve geometry and fluid mechanics. <b>2013</b> , 41, 305-15		38
2145	Lumbar vertebral body bone microstructural scaling in small to medium-sized strepsirhines. <b>2013</b> , 296, 210-26		22
2144	Quantitative imaging of murine osteoarthritic cartilage by phase-contrast micro-computed tomography. <b>2013</b> , 65, 388-96		42
2143	Fourier transform infrared imaging of femoral neck bone: reduced heterogeneity of mineral-to-matrix and carbonate-to-phosphate and more variable crystallinity in treatment-naive fracture cases compared with fracture-free controls. <i>Journal of Bone and Mineral Research</i> , <b>2013</b> ,	6.3	69
2142	28, 150-61  Negative regulation of osteoclast precursor differentiation by CD11b and I2 integrin-B-cell lymphoma 6 signaling. <i>Journal of Bone and Mineral Research</i> , <b>2013</b> , 28, 135-49	6.3	38
2141	Human apolipoprotein E isoforms differentially affect bone mass and turnover in vivo. <i>Journal of Bone and Mineral Research</i> , <b>2013</b> , 28, 236-45	6.3	17
2140	Mobilization of endogenous stem cell populations enhances fracture healing in a murine femoral fracture model. <b>2013</b> , 15, 1136-47		32
2139	Diminished response to in vivo mechanical loading in trabecular and not cortical bone in adulthood of female C57Bl/6 mice coincides with a reduction in deformation to load. <b>2013</b> , 55, 335-46		105
2138	Osteo-promoting effects of insulin-like growth factor I (IGF-I) in a mouse model of type 1 diabetes. <b>2013</b> , 57, 36-40		19
2137	Trabecular bone adapts to long-term cyclic loading by increasing stiffness and normalization of dynamic morphometric rates. <b>2013</b> , 55, 325-34		38
2136	A review of mouse critical size defect models in weight bearing bones. <b>2013</b> , 55, 241-7		32
2135	Previous exposure to simulated microgravity does not exacerbate bone loss during subsequent exposure in the proximal tibia of adult rats. <b>2013</b> , 56, 461-73		13
2134	Spatiotemporal disorder in the axial skeleton development of the Mesp2-null mouse: a model of spondylocostal dysostosis and spondylothoracic dysostosis. <b>2013</b> , 53, 248-58		12
2133	Fifteen days of microgravity causes growth in calvaria of mice. <b>2013</b> , 56, 290-5		33
2132	A comparative evaluation of cone beam CT and micro-CT on trabecular bone structures in the human mandible. <b>2013</b> , 42, 20130145		50
2131	The kidney sodium-phosphate co-transporter alters bone quality in an age and gender specific manner. <b>2013</b> , 53, 546-53		3
2130	Male mice housed in groups engage in frequent fighting and show a lower response to additional bone loading than females or individually housed males that do not fight. <b>2013</b> , 54, 113-7		51

2129	Effect of X-ray irradiation on the elastic strain evolution in the mineral phase of bovine bone under creep and load-free conditions. <b>2013</b> , 9, 5305-12	6
2128	3D image registration is critical to ensure accurate detection of longitudinal changes in trabecular bone density, microstructure, and stiffness measurements in rat tibiae by in vivo microcomputed tomography (CT). <b>2013</b> , 56, 83-90	37
2127	Glucose-dependent insulinotropic polypeptide receptor deficiency leads to modifications of trabecular bone volume and quality in mice. <b>2013</b> , 53, 221-30	64
2126	Soft diet causes greater alveolar osteopenia in the mandible than in the maxilla. 2013, 58, 907-11	25
2125	A quantitative framework for the 3D characterization of the osteocyte lacunar system. 2013, 57, 142-54	73
2124	Deferoxamine expedites consolidation during mandibular distraction osteogenesis. <b>2013</b> , 55, 384-90	42
2123	The importance of the intracortical canal network for murine bone mechanics. <b>2013</b> , 53, 120-8	24
2122	New insights to the role of aryl hydrocarbon receptor in bone phenotype and in dioxin-induced modulation of bone microarchitecture and material properties. <b>2013</b> , 273, 219-26	28
2121	Bone cysts after osteochondral allograft repair of cartilage defects in goats suggest abnormal interaction between subchondral bone and overlying synovial joint tissues. <b>2013</b> , 57, 259-68	26
2120	Optimization and characterization of a rat model of prostate cancer-induced bone pain using behavioral, pharmacological, radiological, histological and immunohistochemical methods. <b>2013</b> , 106, 33-46	22
2119	Modeling distinct osteosarcoma subtypes in vivo using Cre:lox and lineage-restricted transgenic shRNA. <b>2013</b> , 55, 166-78	57
2118	TRPV4 deficiency causes sexual dimorphism in bone metabolism and osteoporotic fracture risk. <b>2013</b> , 57, 443-54	28
2117	PTH prevents the adverse effects of focal radiation on bone architecture in young rats. <b>2013</b> , 55, 449-57	42
2116	Mineralization kinetics in murine trabecular bone quantified by time-lapsed in vivo micro-computed tomography. <b>2013</b> , 56, 55-60	34
2115	Vitamin D receptor in osteoblasts is a negative regulator of bone mass control. <b>2013</b> , 154, 1008-20	117
2114	Sclerostin antibody treatment improves bone mass, bone strength, and bone defect regeneration in rats with type 2 diabetes mellitus. <i>Journal of Bone and Mineral Research</i> , <b>2013</b> , 28, 627-38	84
2113	Non-nuclear-initiated actions of the estrogen receptor protect cortical bone mass. <b>2013</b> , 27, 649-56	49
2112	Targeted disruption of leucine-rich repeat kinase 1 but not leucine-rich repeat kinase 2 in mice causes severe osteopetrosis. <i>Journal of Bone and Mineral Research</i> , <b>2013</b> , 28, 1962-74	35

2111 Characterisation of Trabecular Bone Structure. <b>2013</b> , 31-51		17
2110 Effects of radiation and surgery on healing of femoral fractures in a rat model. <b>2013</b> , 31, 1323-31		16
Inhibition of Call+/calmodulin-dependent protein kinase kinase 2 stimulates osteoblast formation and inhibits osteoclast differentiation. <i>Journal of Bone and Mineral Research</i> , <b>2013</b> , 28, 1599-610	6.3	35
Cartilage oligomeric matrix protein enhances osteogenesis by directly binding and activating bon morphogenetic protein-2. <b>2013</b> , 55, 23-35	e	34
2107 High-Resolution Imaging. <b>2013</b> , 149-159		
2106 Inducible brown adipose tissue, or beige fat, is anabolic for the skeleton. <b>2013</b> , 154, 2687-701		94
WNT-LRP5 signaling induces Warburg effect through mTORC2 activation during osteoblast differentiation. <b>2013</b> , 17, 745-55		226
Pyk2 regulates megakaryocyte-induced increases in osteoblast number and bone formation.  Journal of Bone and Mineral Research, <b>2013</b> , 28, 1434-45	6.3	22
Osteoblast-targeted suppression of PPARlincreases osteogenesis through activation of mTOR signaling. <b>2013</b> , 31, 2183-92		59
Effects of lithium on extraction socket healing in rats assessed with micro-computed tomography	<i>'</i> .	
<b>21</b> 02 <b>2013</b> , 71, 1335-40		7
2101 Skeletal Aging and Osteoporosis. <b>2013</b> ,		3
<b>2013</b> , 71, 1335-40		
2101 Skeletal Aging and Osteoporosis. 2013,	6.3	3
2101 Skeletal Aging and Osteoporosis. 2013, 2100 Bone and Joints. 2013, 2761-2858  Partial reductions in mechanical loading yield proportional changes in bone density, bone		3
2101 Skeletal Aging and Osteoporosis. 2013,  2100 Bone and Joints. 2013, 2761-2858  Partial reductions in mechanical loading yield proportional changes in bone density, bone architecture, and muscle mass. <i>Journal of Bone and Mineral Research</i> , 2013, 28, 875-85		3 12 62
2101 Skeletal Aging and Osteoporosis. 2013, 2100 Bone and Joints. 2013, 2761-2858  2009 Partial reductions in mechanical loading yield proportional changes in bone density, bone architecture, and muscle mass. <i>Journal of Bone and Mineral Research</i> , 2013, 28, 875-85  2008 CHAPTER 2:Bone Structural Adaptation and Wolff's Law. 2013, 17-45  Quantification of external root resorption by low- vs high-resolution cone-beam computed		3 12 62 3
2101 Skeletal Aging and Osteoporosis. 2013,  2100 Bone and Joints. 2013, 2761-2858  2099 Partial reductions in mechanical loading yield proportional changes in bone density, bone architecture, and muscle mass. <i>Journal of Bone and Mineral Research</i> , 2013, 28, 875-85  2098 CHAPTER 2:Bone Structural Adaptation and Wolff's Law. 2013, 17-45  Quantification of external root resorption by low- vs high-resolution cone-beam computed tomography and periapical radiography: A volumetric and linear analysis. 2013, 143, 77-91		3 12 62 3 43

2093	Impact of Charcot neuroarthropathy on metatarsal bone mineral density and geometric strength indices. <b>2013</b> , 52, 407-13		8
2092	Bone remodeling is regulated by inner ear vestibular signals. <i>Journal of Bone and Mineral Research</i> , <b>2013</b> , 28, 2136-44	.3	34
2091	Notch signaling in osteocytes differentially regulates cancellous and cortical bone remodeling. <b>2013</b> , 288, 25614-25625		73
2090	Osteoblast lineage-specific effects of notch activation in the skeleton. <b>2013</b> , 154, 623-34		98
2089	Roux-en-Y gastric bypass surgery but not vertical sleeve gastrectomy decreases bone mass in male rats. <b>2013</b> , 154, 2015-24		55
2088	Craniosynostosis-associated Fgfr2(C342Y) mutant bone marrow stromal cells exhibit cell autonomous abnormalities in osteoblast differentiation and bone formation. <b>2013</b> , 2013, 292506		14
2087	Greater Skeletal Gains in Ovary Intact Rats at Maturity Are Achieved by Supplementing a Standardized Extract of Butea monosperma Stem Bark that Confers Better Bone Conserving Effect following Ovariectomy and Concurrent Treatment Withdrawal. <b>2013</b> , 2013, 519387		11
2086	Efficacy and safety of echinacoside in a rat osteopenia model. <b>2013</b> , 2013, 926928		15
2085	ADAM17 controls endochondral ossification by regulating terminal differentiation of chondrocytes. <b>2013</b> , 33, 3077-90		40
2084	Partial weight bearing does not prevent musculoskeletal losses associated with disuse. <b>2013</b> , 45, 2052-60		15
2083	A longitudinal study of the effect of experimental osteoporosis on bone trabecular structure in the rat mandibular condyle. <b>2013</b> , 31, 140-50		12
2082	Characterization of rotating gantry micro-CT configuration for the in vivo evaluation of murine trabecular bone. <b>2013</b> , 19, 907-13		3
2081	Multiscale Heterogeneity of Bone Microporosities and Tissue Scaffolds. <b>2013</b> , 592-593, 350-353		
2080	Biomimetic Design of Lightweight Vehicle Structures Based on Animal Bone Properties. <b>2013</b> , 633, 3-14		2
2079	Maternal perinatal diet induces developmental programming of bone architecture. <b>2013</b> , 217, 69-81		20
2078	Deletion of CD74, a putative MIF receptor, in mice enhances osteoclastogenesis and decreases bone mass. <i>Journal of Bone and Mineral Research</i> , <b>2013</b> , 28, 948-59	.3	34
2077	The effect of rosiglitazone on bone mass and fragility is reversible and can be attenuated with alendronate. <i>Journal of Bone and Mineral Research</i> , <b>2013</b> , 28, 1653-65	.3	16
2076	A mouse model for human osteogenesis imperfecta type VI. <i>Journal of Bone and Mineral Research</i> , <b>2013</b> , 28, 1531-6	.3	41

	chemoattractant protein-1 is a mediator of the anabolic action of parathyroid hormone ournal of Bone and Mineral Research, <b>2013</b> , 28, 1975-86	6.3	35
	cive study of automatic thresholding approaches for 3D x-ray microtomography of bone. <b>2013</b> , 40, 091903		8
Micro-comp 2073 99, 71-82	outed tomography imaging and analysis in developmental biology and toxicology. 2013,		19
2072	ermogenesis and impaired bone remodeling in Misty mice. <i>Journal of Bone and Mineral</i> <b>013</b> , 28, 1885-97	6.3	46
	i that control the loss and regain of trabecular bone during unloading and reambulation. <i>Bone and Mineral Research</i> , <b>2013</b> , 28, 1537-49	6.3	19
	antibody inhibits skeletal deterioration due to reduced mechanical loading. <i>Journal of lineral Research</i> , <b>2013</b> , 28, 865-74	6.3	115
3060	receptor regulates extracellular ATP metabolism and the osteogenic response to loading. <i>Journal of Bone and Mineral Research</i> , <b>2013</b> , 28, 1446-56	6.3	27
	tivated protein kinase 2 regulates physiological and pathological bone turnover. <i>Journal Mineral Research</i> , <b>2013</b> , 28, 936-47	6.3	10
2067 Bone micro	structure reconstructions from few projections with level-set regularization. 2013,		1
	hormone (PTH)/PTH-related peptide type 1 receptor (PPR) signaling in osteocytes nabolic and catabolic skeletal responses to PTH. <b>2013</b> , 288, 20122-34		122
	alters serum vitamin D metabolite and fibroblast growth factor 23 concentrations and excretion of calcium. <b>2013</b> , 110, 6199-204		89
	ritas-in serum sanitas? Cell non-autonomous aging compromises differentiation and mesenchymal stromal cells via the oxidative stress pathway. <b>2013</b> , 4, e970		34
	n D3 diet administered during active colitis negatively affects bone metabolism in an cell transfer model. <b>2013</b> , 305, G35-46		12
	ne mechanical and material properties require a functional glucagon-like peptide-1 <b>013</b> , 219, 59-68		68
	re percussion diagnostics and bone density analysis of the implant-bone interface in a stmortem human subject. <b>2013</b> , 28, 1581-8		6
2060 Assessmen <b>2013</b> ,	t of Cancellous Bone Microarchitecture from Poroelastic Ultrasound (PEUS) Theory.		
	romotes bone formation and suppresses bone resorption in postnatal growing mice. Sone and Mineral Research, <b>2013</b> , 28, 1160-9	6.3	84
	ion of Smad-dependent BMP signaling in neural crest cells causes craniosynostosis in all of Bone and Mineral Research, <b>2013</b> , 28, 1422-33	6.3	69

2057	Bone microarchitecture in ankylosing spondylitis and the association with bone mineral density, fractures, and syndesmophytes. <b>2013</b> , 15, R179	74
2056	BMP2 is superior to BMP4 for promoting human muscle-derived stem cell-mediated bone regeneration in a critical-sized calvarial defect model. <b>2013</b> , 22, 2393-408	34
2055	Age-related changes in the 3D hierarchical structure of rat tibia cortical bone characterized by high-resolution micro-CT. <b>2013</b> , 114, 923-33	15
2054	Deferoxamine administration delivers translational optimization of distraction osteogenesis in the irradiated mandible. <b>2013</b> , 132, 542e-548e	21
2053	Darbepoietin-alfa has comparable erythropoietic stimulatory effects to recombinant erythropoietin whilst preserving the bone marrow microenvironment. <b>2013</b> , 98, 686-90	6
2052	Compositional and material properties of rat bone after bisphosphonate and/or Strontium ranelate drug treatment. <b>2013</b> , 16, 52-64	14
2051	Establishment of a murine model for radiation-induced bone loss using micro-computed tomography in adult C3H/HeN mice. <b>2013</b> , 29, 55-62	10
2050	Rib fractures and death from deletion of osteoblast catenin in adult mice is rescued by corticosteroids. <b>2013</b> , 8, e55757	3
2049	Effects of constitutive I-catenin activation on vertebral bone growth and remodeling at different postnatal stages in mice. <b>2013</b> , 8, e74093	15
2048	The effects of antihypertensive drugs on bone mineral density in ovariectomized mice. <b>2013</b> , 28, 1139-44	26
2047	Osseointegration of the titanium implant coated with rhTGF-I2/PLGA particles by electrospray: a preliminary microCT analyzing rabbit study. <b>2014</b> , 52, 298	
2046	Magnetic resonance imaging of the ear for patient-specific reconstructive surgery. <b>2014</b> , 9, e104975	8
2045	Improved anchorage of Ti6Al4V orthopaedic bone implants through oligonucleotide mediated immobilization of BMP-2 in osteoporotic rats. <b>2014</b> , 9, e86151	18
2044	Aberrant bone density in aging mice lacking the adenosine transporter ENT1. <b>2014</b> , 9, e88818	18
2043	Systemic but no local effects of combined zoledronate and parathyroid hormone treatment in experimental autoimmune arthritis. <b>2014</b> , 9, e92359	8
2042	Distinct actions of akt1 on skeletal architecture and function. <b>2014</b> , 9, e93040	8
2041	Caspase-2 maintains bone homeostasis by inducing apoptosis of oxidatively-damaged osteoclasts. <b>2014</b> , 9, e93696	17
2040	Long bone structure and strength depend on BMP2 from osteoblasts and osteocytes, but not vascular endothelial cells. <b>2014</b> , 9, e96862	24

2039	Micro-computed tomography derived anisotropy detects tumor provoked deviations in bone in an orthotopic osteosarcoma murine model. <b>2014</b> , 9, e97381	10
2038	The p38HMAPK function in osteoprecursors is required for bone formation and bone homeostasis in adult mice. <b>2014</b> , 9, e102032	21
2037	SH3BP2 gain-of-function mutation exacerbates inflammation and bone loss in a murine collagen-induced arthritis model. <b>2014</b> , 9, e105518	13
2036	A comparison of micro-CT and dental CT in assessing cortical bone morphology and trabecular bone microarchitecture. <b>2014</b> , 9, e107545	30
2035	Dimethyloxalylglycine prevents bone loss in ovariectomized C57BL/6J mice through enhanced angiogenesis and osteogenesis. <b>2014</b> , 9, e112744	43
2034	Treatment with Rhizoma Dioscoreae extract has protective effect on osteopenia in ovariectomized rats. <b>2014</b> , 2014, 645975	10
2033	High-Fat-Diet-Induced Weight Gain Ameliorates Bone Loss without Exacerbating AIPP Processing and Cognition in Female APP/PS1 Mice. <b>2014</b> , 8, 225	22
2032	The protective effect of Rhizoma Dioscoreae extract against alveolar bone loss in ovariectomized rats via regulating Wnt and p38 MAPK signaling. <b>2014</b> , 6, 5853-70	5
2031	Mineralized Tissue. <b>2014</b> , 31-43	3
2030	High-Resolution CT for Small-Animal Imaging Research. <b>2014</b> , 221-242	3
2029	Fibrodysplasia ossificans progressiva-related activated activin-like kinase signaling enhances osteoclast formation during heterotopic ossification in muscle tissues. <b>2014</b> , 289, 16966-77	23
2028	Implications of high-dosage bisphosphonate treatment on bone tissue in the jaw and knee joint. <b>2014</b> , 95, 436-45	8
2027	Protein kinase C∏PKC∄regulates bone architecture and osteoblast activity. <b>2014</b> , 289, 25509-22	20
2026	Bone quality assessment for total hip arthroplasty with intraoperative trabecular torque measurements. <b>2014</b> , 9, 109	8
2025	Mouse models of telomere dysfunction phenocopy skeletal changes found in human age-related osteoporosis. <b>2014</b> , 7, 583-92	22
2024	Notch pathway inhibition controls myeloma bone disease in the murine MOPC315.BM model. <b>2014</b> , 4, e217	35
2023	Effects of immediate and delayed loading on peri-implant trabecular structures: a cone beam CT evaluation. <b>2014</b> , 16, 873-83	19
	Inhibition of apoptosis signal-regulating kinase 1 enhances endochondral bone formation by	

2021	Central adiponectin administration reveals new regulatory mechanisms of bone metabolism in mice. <b>2014</b> , 306, E1418-30		48
2020	Total body irradiation is permissive for mesenchymal stem cell-mediated new bone formation following local transplantation. <b>2014</b> , 20, 3212-27		14
2019	Tissue-type plasminogen activator deficiency delays bone repair: roles of osteoblastic proliferation and vascular endothelial growth factor. <b>2014</b> , 307, E278-88		25
2018	Intermittently administered parathyroid hormone [1-34] promotes tendon-bone healing in a rat model. <b>2014</b> , 15, 17366-79		19
2017	Genistein supplementation increases bone turnover but does not prevent alcohol-induced bone loss in male mice. <b>2014</b> , 239, 1380-9		4
2016	Tissue-nonspecific alkaline phosphatase deficiency causes abnormal craniofacial bone development in the Alpl(-/-) mouse model of infantile hypophosphatasia. <b>2014</b> , 67, 81-94		65
2015	WNT7B promotes bone formation in part through mTORC1. <b>2014</b> , 10, e1004145		96
2014	An in vivo ovine model of bone tissue alterations in simulated microgravity conditions. <b>2014</b> , 136, 02102	20	6
2013	Deletion of P58(IPK), the Cellular Inhibitor of the Protein Kinases PKR and PERK, Causes Bone Changes and Joint Degeneration in Mice. <b>2014</b> , 5, 174		10
2012	Direct stimulation of bone mass by increased GH signalling in the osteoblasts of Socs2-/- mice. <b>2014</b> , 223, 93-106		10
2011	Biomechanics of metastatic disease in the vertebral column. <b>2014</b> , 36, 493-501		11
2010	Rapid, automated imaging of mouse articular cartilage by microCT for early detection of osteoarthritis and finite element modelling of joint mechanics. <b>2014</b> , 22, 1419-28		57
2009	Effects of the peroxisome proliferator-activated receptor (PPAR)-lagonist GW501516 on bone and muscle in ovariectomized rats. <b>2014</b> , 155, 2178-89		12
2008	Skeletal response of male mice to anabolic hormone therapy in the absence of the Igfals gene. <b>2014</b> , 155, 987-99		4
2007	Early-onset type 2 diabetes impairs skeletal acquisition in the male TALLYHO/JngJ mouse. <b>2014</b> , 155, 3806-16		61
2006	Impaired musculoskeletal response to age and exercise in PPARI(-/-) diabetic mice. <b>2014</b> , 155, 4686-96		11
2005	Diet-derived phenolic acids regulate osteoblast and adipocyte lineage commitment and differentiation in young mice. <i>Journal of Bone and Mineral Research</i> , <b>2014</b> , 29, 1043-53	6.3	29
2004	Image interpolation allows accurate quantitative bone morphometry in registered micro-computed tomography scans. <b>2014</b> , 17, 539-48		22

2003	Age-related impairment of bones' adaptive response to loading in mice is associated with sex-related deficiencies in osteoblasts but no change in osteocytes. <i>Journal of Bone and Mineral Research</i> , <b>2014</b> , 29, 1859-71	6.3	69
2002	Bone matrix quality after sclerostin antibody treatment. <i>Journal of Bone and Mineral Research</i> , <b>2014</b> , 29, 1597-607	6.3	36
2001	Intervention timing of strontium treatment on estrogen depletion-induced osteoporosis in rats: bone microstructure and mechanics. <b>2014</b> , 32, 477-84		3
2000	CTLA-4Ig-induced T cell anergy promotes Wnt-10b production and bone formation in a mouse model. <b>2014</b> , 66, 990-9		35
1999	Physiological functions of osteoblast lineage and T cell-derived RANKL in bone homeostasis. Journal of Bone and Mineral Research, <b>2014</b> , 29, 830-42	6.3	51
1998	Oxytocin reverses ovariectomy-induced osteopenia and body fat gain. <b>2014</b> , 155, 1340-52		46
1997	Quantitative phenotyping of bone fracture repair: a review. <b>2014</b> , 3, 550		17
1996	Testosterone dose dependently prevents bone and muscle loss in rodents after spinal cord injury. <b>2014</b> , 31, 834-45		41
1995	Dysapoptosis of osteoblasts and osteocytes increases cancellous bone formation but exaggerates cortical porosity with age. <i>Journal of Bone and Mineral Research</i> , <b>2014</b> , 29, 103-17	6.3	52
1994	Disruption of Lrp4 function by genetic deletion or pharmacological blockade increases bone mass and serum sclerostin levels. <b>2014</b> , 111, E5187-95		83
1993	Posterolateral lumbar fusion using Escherichia coli-derived rhBMP-2/hydroxyapatite in the mini pig. <b>2014</b> , 14, 2959-67		13
1992	Identical subchondral bone microarchitecture pattern with increased bone resorption in rheumatoid arthritis as compared to osteoarthritis. <b>2014</b> , 22, 2083-92		18
1991	3D assessment of cortical bone porosity and tissue mineral density using high-resolution μCT: effects of resolution and threshold method. <i>Journal of Bone and Mineral Research</i> , <b>2014</b> , 29, 142-50	6.3	73
1990	Reproducibility of results in preclinical studies: a perspective from the bone field. <i>Journal of Bone and Mineral Research</i> , <b>2014</b> , 29, 2131-40	6.3	33
1989	Role of TGF-II in a mouse model of high turnover renal osteodystrophy. <i>Journal of Bone and Mineral Research</i> , <b>2014</b> , 29, 1141-57	6.3	23
1988	Cortical and trabecular bone benefits of mechanical loading are maintained long term in mice independent of ovariectomy. <i>Journal of Bone and Mineral Research</i> , <b>2014</b> , 29, 1131-40	6.3	23
1987	Gene-by-diet interactions influence calcium absorption and bone density in mice. <i>Journal of Bone and Mineral Research</i> , <b>2014</b> , 29, 657-65	6.3	23
1986	Epiphyseal chondrocyte secondary ossification centers require thyroid hormone activation of Indian hedgehog and osterix signaling. <i>Journal of Bone and Mineral Research</i> , <b>2014</b> , 29, 2262-75	6.3	49

1985	Quality of bone healing: perspectives and assessment techniques. <b>2014</b> , 22 Suppl 1, 39-49		5
1984	Nemo-like kinase regulates postnatal skeletal homeostasis. <b>2014</b> , 229, 1736-43		5
1983	Resveratrol as anti-aging therapy for age-related bone loss. <b>2014</b> , 17, 439-45		31
1982	Three-dimensional reconstruction of neovasculature in solid tumors and basement membrane matrix using ex vivo X-ray microcomputed tomography. <b>2014</b> , 21, 159-70		8
1981	Emodin regulates bone remodeling by inhibiting osteoclastogenesis and stimulating osteoblast formation. <i>Journal of Bone and Mineral Research</i> , <b>2014</b> , 29, 1541-53	6.3	52
1980	Osteoclast-derived complement component 3a stimulates osteoblast differentiation. <i>Journal of Bone and Mineral Research</i> , <b>2014</b> , 29, 1522-30	6.3	106
1979	Vitamin K catabolite inhibition of ovariectomy-induced bone loss: structure-activity relationship considerations. <b>2014</b> , 58, 1658-66		3
1978	Micro-computed tomography assessment of vertebral column defects in retinoic acid-induced rat model of myelomeningocele. <b>2014</b> , 100, 453-62		9
1977	Inhibition of miR-92a enhances fracture healing via promoting angiogenesis in a model of stabilized fracture in young mice. <i>Journal of Bone and Mineral Research</i> , <b>2014</b> , 29, 316-26	6.3	85
1976	Deficiency of Sef is associated with increased postnatal cortical bone mass by regulating Runx2 activity. <i>Journal of Bone and Mineral Research</i> , <b>2014</b> , 29, 1217-31	6.3	12
1975	Influence of segmentation on micro-CT images of trabecular bone. <b>2014</b> , 256, 75-81		24
1974	Effects of parathyroid hormone on bone mass, bone strength, and bone regeneration in male rats with type 2 diabetes mellitus. <b>2014</b> , 155, 1197-206		53
1973	Poly(vinylidene-trifluoroethylene)/barium titanate composite for in vivo support of bone formation. <b>2014</b> , 29, 104-12		32
1972	Microcomputed tomography: approaches and applications in bioengineering. <b>2014</b> , 5, 144		68
1971	The effect of erythropoietin on bone. <b>2014</b> , 85, 1-27		6
1970	Osteoporotic rat models for evaluation of osseointegration of bone implants. <b>2014</b> , 20, 493-505		28
1969	Truncated-correlation photothermal coherence tomography of artificially demineralized animal bones: two- and three-dimensional markers for mineral loss monitoring. <b>2014</b> , 19, 026015		12
1968	Bone vascularization: a way to study bone microarchitecture?. <b>2014</b> ,		

1967	Imaging methods for detection of joint degeneration. <b>2014</b> , 235-265	1
1966	T cell costimulation molecules CD80/86 inhibit osteoclast differentiation by inducing the IDO/tryptophan pathway. <b>2014</b> , 6, 235ra60	110
1965	Impaired bone resorption and woven bone formation are associated with development of osteonecrosis of the jaw-like lesions by bisphosphonate and anti-receptor activator of NF-B ligand antibody in mice. <b>2014</b> , 184, 3084-93	62
1964	A Longitudinal Low Dose IT Analysis of Bone Healing in Mice: A Pilot Study. <b>2014</b> , 2014, 791539	1
1963	The role of the renal ammonia transporter Rhcg in metabolic responses to dietary protein. <b>2014</b> , 25, 2040-52	16
1962	Inhibitory effects of obovatol on osteoclast differentiation and bone resorption. <b>2014</b> , 723, 473-80	6
1961	Topographical variations in articular cartilage and subchondral bone of the normal rat knee are age-related. <b>2014</b> , 196, 278-85	6
1960	Vitamin K-dependent carboxylation of osteocalcin affects the efficacy of teriparatide (PTH(1-34)) for skeletal repair. <b>2014</b> , 64, 95-101	17
1959	Adiponectin receptor 1 regulates bone formation and osteoblast differentiation by GSK-3I/II-catenin signaling in mice. <b>2014</b> , 64, 147-54	49
1958	The effect of enoxacin on osteoclastogenesis and reduction of titanium particle-induced osteolysis via suppression of JNK signaling pathway. <b>2014</b> , 35, 5721-30	79
1957	Nano-structural, compositional and micro-architectural signs of cortical bone fragility at the superolateral femoral neck in elderly hip fracture patients vs. healthy aged controls. <b>2014</b> , 55, 19-28	46
1956	Comparison of Faxitronâlversus MicroCT imaging of the skeleton of the suckling rat. <b>2014</b> , 48, 44-50	5
1955	Trabecular microfractures in the femoral head with osteoporosis: analysis of microcallus formations by synchrotron radiation micro CT. <b>2014</b> , 64, 82-7	19
1954	Recherche sur le cadavre : perspectives en anthropologie l§ionnelle par utilisation dâŪn modle animal tudie en microtomographie. <b>2014</b> , 5, 83-90	
1953	Notch1 and Notch2 expression in osteoblast precursors regulates femoral microarchitecture. <b>2014</b> , 62, 22-8	29
1952	Mineralocorticoid receptor function in bone metabolism and its role in glucocorticoid-induced osteopenia. <b>2014</b> , 447, 407-12	24
1951	Investigating the role of DNA damage in tobacco smoking-induced spine degeneration. <b>2014</b> , 14, 416-23	34
1950	The correlation between mineralization degree and bone tissue stiffness in the porcine mandibular condyle. <b>2014</b> , 32, 29-37	8

1949	Risedronate improves bone architecture and strength faster than alendronate in ovariectomized rats on a low-calcium diet. <b>2014</b> , 32, 653-9		7	
1948	Combined effects of botulinum toxin injection and hind limb unloading on bone and muscle. <b>2014</b> , 94, 327-37		32	
1947	Three-dimensional image registration improves the long-term precision of in vivo micro-computed tomographic measurements in anabolic and catabolic mouse models. <b>2014</b> , 94, 282-92		20	
1946	1,25(OH)âDâlınduces a mineralization defect and loss of bone mineral density in genetic hypercalciuric stone-forming rats. <b>2014</b> , 94, 531-43		14	
1945	Impact of a functionalized olive oil extract on the uterus and the bone in a model of postmenopausal osteoporosis. <b>2014</b> , 53, 1073-81		27	
1944	Skeletal Imaging. <b>2014</b> , 93-113		2	
1943	Influence of fat/carbohydrate ratio on progression of fatty liver disease and on development of osteopenia in male rats fed alcohol via total enteral nutrition (TEN). <b>2014</b> , 48, 133-44		5	
1942	The C-terminal domain of chondroadherin: a new regulator of osteoclast motility counteracting bone loss. <i>Journal of Bone and Mineral Research</i> , <b>2014</b> , 29, 1833-46	6.3	14	
1941	Retention assessment of magnetic nanoparticles in rat arteries with micro-computed tomography. <b>2014</b> , 59, 1271-81		5	
1940	Melatonin dietary supplement as an anti-aging therapy for age-related bone loss. <b>2014</b> , 17, 341-6		36	
1939	The Clinical Biomechanics Award 2012 - presented by the European Society of Biomechanics: large scale simulations of trabecular bone adaptation to loading and treatment. <b>2014</b> , 29, 355-62		40	
1938	Reductions in serum IGF-1 during aging impair health span. <b>2014</b> , 13, 408-18		45	
1937	Circulating interleukin-8 levels explain breast cancer osteolysis in mice and humans. <b>2014</b> , 61, 176-85		41	
1936	Deletion of a single II catenin allele in osteocytes abolishes the bone anabolic response to loading. Journal of Bone and Mineral Research, <b>2014</b> , 29, 705-15	6.3	93	
1935	Dietary protein level and source differentially affect bone metabolism, strength, and intestinal calcium transporter expression during ad libitum and food-restricted conditions in male rats. <b>2014</b> , 144, 821-9		21	
1934	Influence of object location in different FOVs on trabecular bone microstructure measurements of human mandible: a cone beam CT study. <b>2014</b> , 43, 20130329		13	
1933	Anti-apoptotic Bcl-2 family member Mcl-1 regulates cell viability and bone-resorbing activity of osteoclasts. <b>2014</b> , 58, 1-10		9	
1932	Balancing the rates of new bone formation and polymer degradation enhances healing of weight-bearing allograft/polyurethane composites in rabbit femoral defects. <b>2014</b> , 20, 115-29		39	

1931	Acceleration of bone regeneration by local application of lithium: Wnt signal-mediated osteoblastogenesis and Wnt signal-independent suppression of osteoclastogenesis. <b>2014</b> , 90, 397-405	53
1930	Loss of functional NADPH oxidase 2 protects against alcohol-induced bone resorption in female p47phox-/- mice. <b>2014</b> , 38, 672-82	21
1929	IPTCP granules mixed with reticulated hyaluronic acid induce an increase in bone apposition. <b>2014</b> , 9, 015001	12
1928	Quantitative analysis of bone and soft tissue by micro-computed tomography: applications to ex vivo and in vivo studies. <b>2014</b> , 3, 564	86
1927	Inhibition of osteoclastogenesis and inflammatory bone resorption by targeting BET proteins and epigenetic regulation. <b>2014</b> , 5, 5418	78
1926	Low-dose bone morphogenetic protein-2/stromal cell-derived factor-1 cotherapy induces bone regeneration in critical-size rat calvarial defects. <b>2014</b> , 20, 1444-53	51
1925	Micro-CT of rodents: state-of-the-art and future perspectives. <b>2014</b> , 30, 619-34	121
1924	Bone quality is affected by food restriction and by nutrition-induced catch-up growth. <b>2014</b> , 223, 227-39	19
1923	DPP IV inhibitor treatment attenuates bone loss and improves mechanical bone strength in male diabetic rats. <b>2014</b> , 307, E447-55	51
1922	Morbid obesity attenuates the skeletal abnormalities associated with leptin deficiency in mice. <b>2014</b> , 223, M1-15	25
1921	Stk11 (Lkb1) deletion in the osteoblast lineage leads to high bone turnover, increased trabecular bone density and cortical porosity. <b>2014</b> , 69, 98-108	12
1920	NF- <b>B</b> RelB negatively regulates osteoblast differentiation and bone formation. <i>Journal of Bone and Mineral Research</i> , <b>2014</b> , 29, 866-77	47
1919	The effects of misalignment during in vivo loading of bone: techniques to detect the proximity of objects in three-dimensional models. <b>2014</b> , 47, 3156-61	10
1918	Pulsed electromagnetic fields partially preserve bone mass, microarchitecture, and strength by promoting bone formation in hindlimb-suspended rats. <i>Journal of Bone and Mineral Research</i> , <b>2014</b> , 6.3 29, 2250-61	78
1917	Disruption of glucocorticoid signaling in chondrocytes delays metaphyseal fracture healing but does not affect normal cartilage and bone development. <b>2014</b> , 69, 12-22	22
1916	The influence of age on adaptive bone formation and bone resorption. <b>2014</b> , 35, 9290-301	79
1915	Reference point indentation is not indicative of whole mouse bone measures of stress intensity fracture toughness. <b>2014</b> , 69, 174-9	29
1914	Diet and gene interactions influence the skeletal response to polyunsaturated fatty acids. <b>2014</b> , 68, 100-7	21

1913	Comparison of loading rate-dependent injury modes in a murine model of post-traumatic osteoarthritis. <b>2014</b> , 32, 79-88		52
1912	Increased osteopontin contributes to inhibition of bone mineralization in FGF23-deficient mice. Journal of Bone and Mineral Research, <b>2014</b> , 29, 693-704	6.3	67
1911	Role of donor and host cells in muscle-derived stem cell-mediated bone repair: differentiation vs. paracrine effects. <b>2014</b> , 28, 3792-809		33
1910	In vivo fluorescence reflectance imaging of protease activity in a mouse model of post-traumatic osteoarthritis. <b>2014</b> , 22, 1461-9		25
1909	Influence of aromatase inhibition on the bone-protective effects of testosterone. <i>Journal of Bone and Mineral Research</i> , <b>2014</b> , 29, 2405-13	6.3	23
1908	The mechanism of anti-osteoporosis effects of 3-hydroxybutyrate and derivatives under simulated microgravity. <b>2014</b> , 35, 8273-83		43
1907	Hypericin suppresses osteoclast formation and wear particle-induced osteolysis via modulating ERK signalling pathway. <b>2014</b> , 90, 276-87		47
1906	Ell'ocotrienol protects against ovariectomy-induced bone loss via mevalonate pathway as HMG-CoA reductase inhibitor. <b>2014</b> , 67, 200-7		36
1905	Inkjet-based biopatterning of SDF-1 augments BMP-2-induced repair of critical size calvarial bone defects in mice. <b>2014</b> , 67, 95-103		36
1904	Could the median-palate accommodate wide-bodied implants in order to support maxillary over-dentures? A radiomorphometric study of human cadavers. <b>2014</b> , 25, 101-9		3
1903	N-acetylcysteine supplementation decreases osteoclast differentiation and increases bone mass in mice fed a high-fat diet. <b>2014</b> , 144, 289-96		22
1902	Tsc2 is a molecular checkpoint controlling osteoblast development and glucose homeostasis. <b>2014</b> , 34, 1850-62		45
1901	Moderate intensity resistive exercise improves metaphyseal cancellous bone recovery following an initial disuse period, but does not mitigate decrements during a subsequent disuse period in adult rats. <b>2014</b> , 66, 296-305		9
1900	Effects of sequential osteoporosis treatments on trabecular bone in adult rats with low bone mass. <b>2014</b> , 25, 1735-50		19
1899	Lanthanum carbonate stimulates bone formation in a rat model of renal insufficiency with low bone turnover. <b>2014</b> , 32, 484-93		6
1898	The PTH-GB-protein kinase A cascade controls NAC localization to regulate bone mass. <b>2014</b> , 34, 1622-3	33	15
1897	Interdependence of muscle atrophy and bone loss induced by mechanical unloading. <i>Journal of Bone and Mineral Research</i> , <b>2014</b> , 29, 1118-30	6.3	71
1896	Additive effect of PTH (1-34) and zoledronate in the prevention of disuse osteopenia in rats. <b>2014</b> , 66, 287-95		31

1895	Methods to analyze bone regenerative response to different rhBMP-2 doses in rabbit craniofacial defects. <b>2014</b> , 20, 749-60	11
1894	Estrogen receptor #n osteocytes regulates trabecular bone formation in female mice. <b>2014</b> , 60, 68-77	74
1893	Generation of the first autosomal dominant osteopetrosis type II (ADO2) disease models. <b>2014</b> , 59, 66-75	25
1892	Beneficial effects of a N-terminally modified GIP agonist on tissue-level bone material properties. <b>2014</b> , 63, 61-8	30
1891	Whole body vibration during fracture healing intensifies the effects of estradiol and raloxifene in estrogen-deficient rats. <b>2014</b> , 64, 187-94	23
1890	Quantitative trait loci that modulate trabecular bone's risk of failure during unloading and reloading. <b>2014</b> , 64, 25-32	8
1889	Hepatic lipase is expressed by osteoblasts and modulates bone remodeling in obesity. <b>2014</b> , 62, 90-8	6
1888	Advanced oxidation protein products accelerate bone deterioration in aged rats. <b>2014</b> , 50, 64-71	23
1887	Effect of bisphosphonates on the rapidly growing male murine skeleton. <b>2014</b> , 155, 1188-96	16
1886	Mineralizing surface is the main target of mechanical stimulation independent of age: 3D dynamic in vivo morphometry. <b>2014</b> , 66, 15-25	77
1885	Aryl hydrocarbon receptor catabolic activity in bone metabolism is osteoclast dependent in vivo. <b>2014</b> , 450, 416-22	23
1884	A comparison of bone regeneration with human mesenchymal stem cells and muscle-derived stem cells and the critical role of BMP. <b>2014</b> , 35, 6859-70	61
1883	Effect of interval-training exercise on subchondral bone in a chemically-induced osteoarthritis model. <b>2014</b> , 22, 1176-85	23
1882	Mechanical unloading of bone in microgravity reduces mesenchymal and hematopoietic stem cell-mediated tissue regeneration. <b>2014</b> , 13, 181-201	53
1881	Increased fracture callus mineralization and strength in cathepsin K knockout mice. <b>2014</b> , 66, 72-81	21
1880	Species-specific homing mechanisms of human prostate cancer metastasis in tissue engineered bone. <b>2014</b> , 35, 4108-15	82
1879	Longitudinal quantitative evaluation of the mid-palatal suture after rapid expansion using in vivo micro-CT. <b>2014</b> , 59, 414-23	5
1878	Hypoxia-inducible factor-1#estricts the anabolic actions of parathyroid hormone. <b>2014</b> , 2, 14005	16

1877	Nrf2 is required for normal postnatal bone acquisition in mice. <b>2014</b> , 2, 14033		29
1876	Validating cone-beam computed tomography for peri-implant bone morphometric analysis. <b>2014</b> , 2, 14010		15
1875	SH3BP2 cherubism mutation potentiates TNF-Induced osteoclastogenesis via NFATc1 and TNF-Imediated inflammatory bone loss. <i>Journal of Bone and Mineral Research</i> , <b>2014</b> , 29, 2618-35	6.3	45
1874	An Assessment of the Influence of Micro-porosity for Effective Permeability Using Local Flux Analysis on Tomographic Images. <b>2014</b> ,		7
1873	Adipose-Derived Mesenchymal Stem Cells Prevent Systemic Bone Loss in Collagen-Induced Arthritis. <b>2015</b> , 195, 5136-48		45
1872	Effects of methionine restriction and endurance exercise on bones of ovariectomized rats: a study of histomorphometry, densitometry, and biomechanical properties. <b>2015</b> , 119, 517-26		9
1871	WNT5A has anti-prostate cancer effects in vitro and reduces tumor growth in the skeleton in vivo. Journal of Bone and Mineral Research, <b>2015</b> , 30, 471-80	6.3	32
1870	Myelosuppressive therapies significantly increase pro-inflammatory cytokines and directly cause bone loss. <i>Journal of Bone and Mineral Research</i> , <b>2015</b> , 30, 886-97	6.3	34
1869	Inner Ear Vestibular Signals Regulate Bone Remodeling via the Sympathetic Nervous System. Journal of Bone and Mineral Research, <b>2015</b> , 30, 1103-11	6.3	34
1868	Establishing biomechanical mechanisms in mouse models: practical guidelines for systematically evaluating phenotypic changes in the diaphyses of long bones. <i>Journal of Bone and Mineral Research</i> , <b>2015</b> , 30, 951-66	6.3	154
1867	A transgenic mouse model of OI type V supports a neomorphic mechanism of the IFITM5 mutation. Journal of Bone and Mineral Research, <b>2015</b> , 30, 489-98	6.3	21
1866	Gender-Specific Differences in the Skeletal Response to Continuous PTH in Mice Lacking the IGF1 Receptor in Mature Osteoblasts. <i>Journal of Bone and Mineral Research</i> , <b>2015</b> , 30, 1064-76	6.3	10
1865	Bone volume fraction and fabric anisotropy are better determinants of trabecular bone stiffness than other morphological variables. <i>Journal of Bone and Mineral Research</i> , <b>2015</b> , 30, 1000-8	6.3	93
1864	The Effects of Androgens on Murine Cortical Bone Do Not Require AR or ERsignaling in Osteoblasts and Osteoclasts. <i>Journal of Bone and Mineral Research</i> , <b>2015</b> , 30, 1138-49	6.3	59
1863	A comprehensive study of long-term skeletal changes after spinal cord injury in adult rats. <b>2015</b> , 3, 150	28	20
1862	Application of a Collagenated Biphasic Calcium Phosphate Loaded with Fibroblast Growth Factor-2 in the Rabbit Sinus: A Pilot Study. <b>2015</b> , 30, 1197-204		3
1861	A nonterminal equine mandibular model of bone healing. <b>2015</b> , 44, 314-21		4
1860	Effective Small Interfering RNA Therapy to Treat CLCN7-dependent Autosomal Dominant Osteopetrosis Type 2. <b>2015</b> , 4, e248		14

1859	Amlexanox Suppresses Osteoclastogenesis and Prevents Ovariectomy-Induced Bone Loss. <b>2015</b> , 5, 13	575	36
1858	A Novel, Stable, Estradiol-Stimulating, Osteogenic Yam Protein with Potential for the Treatment of Menopausal Syndrome. <b>2015</b> , 5, 10179		13
1857	Ciliary neurotrophic factor has intrinsic and extrinsic roles in regulating B cell differentiation and bone structure. <b>2015</b> , 5, 15529		12
1856	Administration of soluble activin receptor 2B increases bone and muscle mass in a mouse model of osteogenesis imperfecta. <b>2015</b> , 3, 14042		36
1855	Mechanical competence of ovariectomy-induced compromised bone after single or combined treatment with high-frequency loading and bisphosphonates. <b>2015</b> , 5, 10795		14
1854	Heidelberg-mCT-Analyzer: a novel method for standardized microcomputed-tomography-guided evaluation of scaffold properties in bone and tissue research. <b>2015</b> , 2, 150496		10
1853	Imaging technologies and basic considerations for welfare of laboratory rodents. 2015, 44, 97-105		2
1852	Computed Tomography and Optical Imaging of Osteogenesis-angiogenesis Coupling to Assess Integration of Cranial Bone Autografts and Allografts. <b>2015</b> , e53459		4
1851	Characterization of trabecular bone plate-rod microarchitecture using multirow detector CT and the tensor scale: Algorithms, validation, and applications to pilot human studies. <b>2015</b> , 42, 5410-25		18
1850	Characterization of the MPS I-H knock-in mouse reveals increased femoral biomechanical integrity with compromised material strength and altered bone geometry. <b>2015</b> , 5, 3-11		5
1849	Skin wound trauma, following high-dose radiation exposure, amplifies and prolongs skeletal tissue loss. <b>2015</b> , 81, 487-494		5
1848	Amphiregulin lacks an essential role for the bone anabolic action of parathyroid hormone. <b>2015</b> , 417, 158-65		5
1847	Immobilization induced osteopenia is strain specific in mice. <b>2015</b> , 2, 59-67		29
1846	Refine, reduce, replace: Imaging of fibrosis and arthritis in animal models. <b>2015</b> , 29, 715-40		5
1845	Prolonged performance of a high repetition low force task induces bone adaptation in young adult rats, but loss in mature rats. <b>2015</b> , 72, 204-17		17
1844	Aberrant Activation of TGF-In Subchondral Bone at the Onset of Rheumatoid Arthritis Joint Destruction. <i>Journal of Bone and Mineral Research</i> , <b>2015</b> , 30, 2033-43	6.3	27
1843	NF- <b>B</b> decoy oligodeoxynucleotide inhibits wear particle-induced inflammation in a murine calvarial model. <b>2015</b> , 103, 3872-8		20
1842	Improved resolution of 3D printed scaffolds by shrinking. <b>2015</b> , 103, 1415-23		4

1841	OPG-Fc but Not Zoledronic Acid Discontinuation Reverses Osteonecrosis of the Jaws (ONJ) in Mice. Journal of Bone and Mineral Research, <b>2015</b> , 30, 1627-40	6.3	52
1840	IGF-I Signaling in Osterix-Expressing Cells Regulates Secondary Ossification Center Formation, Growth Plate Maturation, and Metaphyseal Formation During Postnatal Bone Development.  Journal of Bone and Mineral Research, 2015, 30, 2239-48	6.3	24
1839	Dysregulated TGF-I signaling alters bone microstructure in a mouse model of Loeys-Dietz syndrome. <b>2015</b> , 33, 1447-54		7
1838	Extending Rest between Unloading Cycles Does Not Enhance Bone's Long-Term Recovery. <b>2015</b> , 47, 2191-200		3
1837	Effects of particle size and porosity on in vivo remodeling of settable allograft bone/polymer composites. <b>2015</b> , 103, 1641-51		19
1836	Blockage of Src by Specific siRNA as a Novel Therapeutic Strategy to Prevent Destructive Repair in Steroid-Associated Osteonecrosis in Rabbits. <i>Journal of Bone and Mineral Research</i> , <b>2015</b> , 30, 2044-57	6.3	25
1835	Calcilytic Ameliorates Abnormalities of Mutant Calcium-Sensing Receptor (CaSR) Knock-In Mice Mimicking Autosomal Dominant Hypocalcemia (ADH). <i>Journal of Bone and Mineral Research</i> , <b>2015</b> , 30, 1980-93	6.3	40
1834	Stable Incretin Mimetics Counter Rapid Deterioration of Bone Quality in Type 1 Diabetes Mellitus. <b>2015</b> , 230, 3009-18		50
1833	The development and validation of micro-CT of large deep frozen specimens. <b>2015</b> , 37, 63-72		3
1832	Structural and Qualitative Bone Remodeling Around Repetitive Loaded Implants in Rabbits. <b>2015</b> , 17 Suppl 2, e699-710		15
1831	Osteoblast-Specific Loss of IGF1R Signaling Results in Impaired Endochondral Bone Formation During Fracture Healing. <i>Journal of Bone and Mineral Research</i> , <b>2015</b> , 30, 1572-84	6.3	40
1830	Mice Deficient in AKAP13 (BRX) Are Osteoporotic and Have Impaired Osteogenesis. <i>Journal of Bone and Mineral Research</i> , <b>2015</b> , 30, 1887-95	6.3	11
1829	Paradoxical effects of partial leptin deficiency on bone in growing female mice. 2015, 298, 2018-29		11
1828	Effects of Glucosinolates from Turnip (Brassica rapa L.) Root on Bone Formation by Human Osteoblast-Like MG-63 Cells and in Normal Young Rats. <b>2015</b> , 29, 902-9		12
1827	Contradictory Role of CD97 in Basal and Tumor Necrosis Factor-Induced Osteoclastogenesis In Vivo. <b>2016</b> , 68, 1301-13		11
1826	Ergonomic task reduction prevents bone osteopenia in a rat model of upper extremity overuse. <b>2015</b> , 53, 206-21		11
1825	Whole-body vibration improves fracture healing and bone quality in rats with ovariectomy-induced osteoporosis. <b>2015</b> , 30, 727-35		17
1824	Swimming Activity Prevents the Unloading Induced Loss of Bone Mass, Architecture, and Strength in Rats. <b>2015</b> , 2015, 507848		13

1823	Bone formation around rhBMP-2-coated implants in rabbit sinuses with or without absorbable collagen sponge grafting. <b>2015</b> , 45, 238-46	7
1822	The Osteogenesis Effect and Underlying Mechanisms of Local Delivery of gAPN in Extraction Sockets of Beagle Dogs. <b>2015</b> , 16, 24946-64	10
1821	Using Micro-CT Derived Bone Microarchitecture to Analyze Bone Stiffness - A Case Study on Osteoporosis Rat Bone. <b>2015</b> , 6, 80	17
1820	Distributional variations in trabecular architecture of the mandibular bone: an in vivo micro-CT analysis in rats. <b>2015</b> , 10, e0116194	8
1819	Aryl hydrocarbon receptors in osteoclast lineage cells are a negative regulator of bone mass. <b>2015</b> , 10, e0117112	24
1818	The effect of locomotion on the mobilization of minerals from the maternal skeleton. <b>2015</b> , 10, e0122702	1
1817	The Tissue Fibrinolytic System Contributes to the Induction of Macrophage Function and CCL3 during Bone Repair in Mice. <b>2015</b> , 10, e0123982	17
1816	Time Related Changes of Mineral and Collagen and Their Roles in Cortical Bone Mechanics of Ovariectomized Rabbits. <b>2015</b> , 10, e0127973	15
1815	Intramembranous bone healing process subsequent to tooth extraction in mice: micro-computed tomography, histomorphometric and molecular characterization. <b>2015</b> , 10, e0128021	73
1814	Structural and Mechanical Improvements to Bone Are Strain Dependent with Axial Compression of the Tibia in Female C57BL/6 Mice. <b>2015</b> , 10, e0130504	41
1813	Characterization of Heterotopic Ossification Using Radiographic Imaging: Evidence for a Paradigm Shift. <b>2015</b> , 10, e0141432	11
1812	In vivo small animal micro-CT using nanoparticle contrast agents. <b>2015</b> , 6, 256	83
1811	Quantification of osseointegration of plasma-polymer coated titanium alloyed implants by means of microcomputed tomography versus histomorphometry. <b>2015</b> , 2015, 103137	6
1810	Temporal changes of microarchitectural and mechanical parameters of cancellous bone in the osteoporotic rabbit. <b>2015</b> , 2015, 263434	12
1809	In Vivo MicroCT Monitoring of Osteomyelitis in a Rat Model. <b>2015</b> , 2015, 587857	24
1808	Insight into bone-derived biological apatite: ultrastructure and effect of thermal treatment. <b>2015</b> , 2015, 601025	3
1807	Epoxyeicosanoids suppress osteoclastogenesis and prevent ovariectomy-induced bone loss. <b>2015</b> , 29, 1092-101	46
1806	Microarchitectural and mechanical characterization of the sickle bone. <b>2015</b> , 48, 220-228	8

1805	Activation of Nfatc2 in osteoblasts causes osteopenia. <b>2015</b> , 230, 1689-95	11
1804	Attenuation of hind-limb suspension-induced bone loss by curcumin is associated with reduced oxidative stress and increased vitamin D receptor expression. <b>2015</b> , 26, 2665-76	30
1803	Modic (endplate) changes in the lumbar spine: bone micro-architecture and remodelling. <b>2015</b> , 24, 1926-34	43
1802	Decitabine represses osteoclastogenesis through inhibition of RANK and NF-B. 2015, 27, 969-77	10
1801	Characterization of bone turnover and energy metabolism in a rat model of primary and secondary osteoporosis. <b>2015</b> , 67, 287-96	9
1800	Wnt-Lrp5 signaling regulates fatty acid metabolism in the osteoblast. <b>2015</b> , 35, 1979-91	90
1799	Novel role for cyclophilin A in regulation of chondrogenic commitment and endochondral ossification. <b>2015</b> , 35, 2119-30	8
1798	Ovariectomy-Induced Osteopenia Influences the Middle and Late Periods of Bone Healing in a Mouse Femoral Osteotomy Model. <b>2015</b> , 18, 356-65	14
1797	Vertical Trabeculae are Thinned More Than Horizontal Trabeculae in Skeletal-Unloaded Rats. <b>2015</b> , 97, 516-26	9
1796	Micro-Computed tomography (CT) based assessment of dental regenerative therapy in the canine mandible model. <b>2015</b> , 9417,	1
1795	Gambogic acid inhibits osteoclast formation and ovariectomy-induced osteoporosis by suppressing the JNK, p38 and Akt signalling pathways. <b>2015</b> , 469, 399-408	26
1794	The frequency of osteolytic bone metastasis is determined by conditions of the soil, not the number of seeds; evidence from in vivo models of breast and prostate cancer. <b>2015</b> , 34, 124	36
1793	The inhibitory effects of a RANKL-binding peptide on articular and periarticular bone loss in a murine model of collagen-induced arthritis: a bone histomorphometric study. <b>2015</b> , 17, 251	23
1792	Co-administration of aspirin and allogeneic adipose-derived stromal cells attenuates bone loss in ovariectomized rats through the anti-inflammatory and chemotactic abilities of aspirin. <b>2015</b> , 6, 200	28
1791	Loss of bone strength in HLA-B27 transgenic rats is characterized by a high bone turnover and is mainly osteoclast-driven. <b>2015</b> , 75, 183-91	7
1790	Quantitative morphometric patterns in cartilage and bone from the humeral heads of end-stage osteoarthritis patients. <b>2015</b> , 23, 1377-87	10
1789	Improved bone defect healing by a superagonistic GDF5 variant derived from a patient with multiple synostoses syndrome. <b>2015</b> , 73, 111-9	10
1788	Bone quality and biomechanical function: a lesson from human ossicles. <b>2015</b> , 73, 105-10	20

1787	71, 14-21		4
1786	The chemokine receptor CCR5 plays a role in post-traumatic cartilage loss in mice, but does not affect synovium and bone. <b>2015</b> , 23, 454-61		35
1785	Repositioning Potential of PAK4 to Osteoclastic Bone Resorption. <i>Journal of Bone and Mineral Research</i> , <b>2015</b> , 30, 1494-507	6.3	6
1784	Strain energy density gradients in bone marrow predict osteoblast and osteoclast activity: a finite element study. <b>2015</b> , 48, 866-74		28
1783	Links between mechanical behavior of cancellous bone and its microstructural properties under dynamic loading. <b>2015</b> , 48, 498-503		25
1782	Osteoblast menin regulates bone mass in vivo. <b>2015</b> , 290, 3910-24		21
1781	The $201$ binding domain of chondroadherin inhibits breast cancer-induced bone metastases and impairs primary tumour growth: a preclinical study. <b>2015</b> , 358, 67-75		12
1780	Single-Limb Irradiation Induces Local and Systemic Bone Loss in a Murine Model. <i>Journal of Bone and Mineral Research</i> , <b>2015</b> , 30, 1268-79	6.3	50
1779	3,3'-Diindolylmethane increases bone mass by suppressing osteoclastic bone resorption in mice. <b>2015</b> , 127, 75-82		14
1778	Micro-CT analysis of the rodent jaw bone micro-architecture: A systematic review. <b>2015</b> , 2, 14-24		32
1777	Siglec-15 is a potential therapeutic target for postmenopausal osteoporosis. <b>2015</b> , 71, 217-26		34
1776	Mesenchymal stem cell expression of stromal cell-derived factor-1□augments bone formation in a model of local regenerative therapy. <b>2015</b> , 33, 174-84		10
1775	Influence of differences in the hardness and calcium content of diets on the growth of craniofacial bone in rats. <b>2015</b> , 85, 969-79		13
1774	Age-related changes in vertebral and iliac crest 3D bone microstructuredifferences and similarities. <b>2015</b> , 26, 219-28		22
1773	Novel bilayer bacterial nanocellulose scaffold supports neocartilage formation in vitro and in vivo. <b>2015</b> , 44, 122-33		113
1772	Adverse Effects of Osteocytic Constitutive Activation of ECatenin on Bone Strength and Bone Growth. <i>Journal of Bone and Mineral Research</i> , <b>2015</b> , 30, 1184-94	6.3	31
1771	High bone mass in adult mice with diet-induced obesity results from a combination of initial increase in bone mass followed by attenuation in bone formation; implications for high bone mass and decreased bone quality in obesity. <b>2015</b> , 410, 35-41		86
1770	Skeletal maturity leads to a reduction in the strain magnitudes induced within the bone: a murine tibia study. <b>2015</b> , 13, 301-10		61

1769	Improvement of the skeletal and dental hypophosphatasia phenotype in Alpl-/- mice by administration of soluble (non-targeted) chimeric alkaline phosphatase. <b>2015</b> , 72, 137-47		39	
1768	Loss of SH3 domain-binding protein 2 function suppresses bone destruction in tumor necrosis factor-driven and collagen-induced arthritis in mice. <b>2015</b> , 67, 656-67		23	
1767	Myelomeningocele: How we can improve the assessment of the most severe form of spina bifida. <b>2015</b> , 1619, 84-90		10	
1766	Autologous implantation of BMP2-expressing dermal fibroblasts to improve bone mineral density and architecture in rabbit long bones. <b>2015</b> , 33, 1455-65		7	
1765	Relationship between serum uric Acid and bone mineral density in the general population and in rats with experimental hyperuricemia. <i>Journal of Bone and Mineral Research</i> , <b>2015</b> , 30, 992-9	6.3	43	
1764	Identifying Novel Clinical Surrogates to Assess Human Bone Fracture Toughness. <i>Journal of Bone and Mineral Research</i> , <b>2015</b> , 30, 1290-300	6.3	70	
1763	Fracture discrimination by combined bone mineral density (BMD) and microarchitectural texture analysis. <b>2015</b> , 96, 274-83		26	
1762	Pathophysiological Mechanism of Bone Loss in Type 2 Diabetes Involves Inverse Regulation of Osteoblast Function by PGC-1\(\text{h}\)nd Skeletal Muscle Atrogenes: AdipoR1 as a Potential Target for Reversing Diabetes-Induced Osteopenia. <b>2015</b> , 64, 2609-23		42	
1761	Choline kinase I mutant mice exhibit reduced phosphocholine, elevated osteoclast activity, and low bone mass. <b>2015</b> , 290, 1729-42		21	
1760	Bioactive silica nanoparticles reverse age-associated bone loss in mice. <b>2015</b> , 11, 959-967		28	
1759	Estrogen Deficiency-Associated Bone Loss in the Maxilla: A Methodology to Quantify the Changes in the Maxillary Intra-radicular Alveolar Bone in an Ovariectomized Rat Osteoporosis Model. <b>2015</b> , 21, 458-66		21	
1758	The use of nano-computed tomography to enhance musculoskeletal research. <b>2015</b> , 56, 106-19		29	
1757	Genetic regulation of bone strength: a review of animal model studies. 2015, 4, 714		9	
1756	Mechanical loading causes site-specific anabolic effects on bone following exposure to ionizing radiation. <b>2015</b> , 81, 260-269		13	
1755	Ionizing Radiation Stimulates Expression of Pro-Osteoclastogenic Genes in Marrow and Skeletal Tissue. <b>2015</b> , 35, 480-7		35	
1754	A comparison of tissue engineering based repair of calvarial defects using adipose stem cells from normal and osteoporotic rats. <b>2015</b> , 78, 1-10		17	
1753	Sialic acid-binding immunoglobulin-like lectin 15 (Siglec-15) mediates periarticular bone loss, but not joint destruction, in murine antigen-induced arthritis. <b>2015</b> , 79, 65-70		19	
1752	Age dependent regulation of bone-mass and renal function by the MEPE ASARM-motif. <b>2015</b> , 79, 131-42	2	20	

1751	Osteoblast-specific overexpression of amphiregulin leads to transient increase in femoral cancellous bone mass in mice. <b>2015</b> , 81, 36-46	6
1750	Exercise does not enhance aged bone's impaired response to artificial loading in C57Bl/6 mice. <b>2015</b> , 81, 47-52	13
1749	Kindlin-2 controls TGF-□signalling and Sox9 expression to regulate chondrogenesis. <b>2015</b> , 6, 7531	71
1748	Bone microarchitecture at muscle attachment sites: The relationship between macroscopic scores of entheses and their cortical and trabecular microstructural design. <b>2015</b> , 157, 81-93	18
1747	Glutamic acid ameliorates estrogen deficiency-induced menopausal-like symptoms in ovariectomized mice. <b>2015</b> , 35, 774-83	10
1746	Changes of elastic constants and anisotropy patterns in trabecular bone during disuse-induced bone loss assessed by poroelastic ultrasound. <b>2015</b> , 137,	4
1745	mTORC1 Signaling Promotes Osteoblast Differentiation from Preosteoblasts. <b>2015</b> , 10, e0130627	49
1744	Chronic kidney disease induced by adenine: a suitable model of growth retardation in uremia. <b>2015</b> , 309, F57-62	37
1743	Quantification of trabecular spatial orientation from low-resolution images. <b>2015</b> , 18, 1392-9	3
1742	Treatment of Radix Dipsaci extract prevents long bone loss induced by modeled microgravity in hindlimb unloading rats. <b>2015</b> , 53, 110-6	19
1741	Local delivery of the cationic steroid antibiotic CSA-90 enables osseous union in a rat open fracture model of Staphylococcus aureus infection. <b>2015</b> , 97, 302-9	22
1740	Compromised vertebral structural and mechanical properties associated with progressive kidney disease and the effects of traditional pharmacological interventions. <b>2015</b> , 77, 50-6	22
1739	Non-severe burn injury leads to depletion of bone volume that can be ameliorated by inhibiting TNF- <b>B2015</b> , 41, 558-64	18
1738	A DNA segment spanning the mouse Tnfsf11 transcription unit and its upstream regulatory domain rescues the pleiotropic biologic phenotype of the RANKL null mouse. <i>Journal of Bone and Mineral</i> 6.3 <i>Research</i> , <b>2015</b> , 30, 855-68	13
1737	Multi-level femoral morphology and mechanical properties of rats of different ages. 2015, 76, 76-87	26
1736	Rhizoma Dioscoreae extract protects against alveolar bone loss in ovariectomized rats via microRNAs regulation. <b>2015</b> , 7, 1333-51	2
1735	Osteoblast function and bone histomorphometry in a murine model of Rett syndrome. <b>2015</b> , 76, 23-30	12
1734	Periodontal Defects in the A116T Knock-in Murine Model of Odontohypophosphatasia. <b>2015</b> , 94, 706-14	29

1733	Single and combined effect of high-frequency loading and bisphosphonate treatment on the bone micro-architecture of ovariectomized rats. <b>2015</b> , 26, 303-13	23
1732	Checkpoint kinase Chk2 controls renal Cyp27b1 expression, calcitriol formation, and calcium-phosphate metabolism. <b>2015</b> , 467, 1871-80	7
1731	Botulinum Toxin-induced Muscle Paralysis Inhibits Heterotopic Bone Formation. <b>2015</b> , 473, 2825-30	5
1730	Effect of alendronate on post-traumatic osteoarthritis induced by anterior cruciate ligament rupture in mice. <b>2015</b> , 17, 30	42
1729	Association of mesenchymal stem cells and osteoblasts for bone repair. <b>2015</b> , 10, 127-33	10
1728	Age- and Sex-Specific Bone Structure Patterns Portend Bone Fragility in Radii and Tibiae in Relation to Osteodensitometry: A High-Resolution Peripheral Quantitative Computed Tomography Study in 385 Individuals. <b>2015</b> , 70, 1269-75	37
1727	Soy protein is beneficial but high-fat diet and voluntary running are detrimental to bone structure in mice. <b>2015</b> , 35, 523-31	9
1726	Androgens inhibit the osteogenic response to mechanical loading in adult male mice. <b>2015</b> , 156, 1343-53	27
1725	Loss of BMPR2 leads to high bone mass due to increased osteoblast activity. <b>2015</b> , 128, 1308-15	36
1724	Diacylglycerol Kinase [DGK] Is a Critical Regulator of Bone Homeostasis Via Modulation of c-Fos Levels in Osteoclasts. <i>Journal of Bone and Mineral Research</i> , <b>2015</b> , 30, 1852-63	18
1723	Involuntary wheel running improves but does not fully reverse the deterioration of bone structure of obese rats despite decreasing adiposity. <b>2015</b> , 97, 145-55	17
1722	Piroxicam treatment augments bone abnormalities in interleukin-10 knockout mice. <b>2015</b> , 21, 257-66	11
1721	Erythropoietin directly stimulates osteoclast precursors and induces bone loss. <b>2015</b> , 29, 1890-900	71
1720	Mesenchymal stromal cell implantation for stimulation of long bone healing aggravates Staphylococcus aureus induced osteomyelitis. <b>2015</b> , 21, 165-77	29
1719	Impaired bone homeostasis in amyotrophic lateral sclerosis mice with muscle atrophy. <b>2015</b> , 290, 8081-94	24
1718	High Bone Mass-Causing Mutant LRP5 Receptors Are Resistant to Endogenous Inhibitors In Vivo. <i>Journal of Bone and Mineral Research</i> , <b>2015</b> , 30, 1822-30	17
1717	Monitoring in vivo (re)modeling: a computational approach using 4D microCT data to quantify bone surface movements. <b>2015</b> , 75, 210-21	49
1716	On the effects of leaflet microstructure and constitutive model on the closing behavior of the mitral valve. <b>2015</b> , 14, 1281-302	46

1715	and the Wnt Inhibitors Sclerostin and Dickkopf-1. <b>2015</b> , 156, 3517-27	37
1714	Role of T-cell reconstitution in HIV-1 antiretroviral therapy-induced bone loss. <b>2015</b> , 6, 8282	56
1713	Comprehensive analysis of translational osteochondral repair: Focus on the histological assessment. <b>2015</b> , 50, 19-36	19
1712	Extra-intestinal calcium handling contributes to normal serum calcium levels when intestinal calcium absorption is suboptimal. <b>2015</b> , 81, 502-512	14
1711	Defective cancellous bone structure and abnormal response to PTH in cortical bone of mice lacking Cx43 cytoplasmic C-terminus domain. <b>2015</b> , 81, 632-643	28
1710	Thyrostimulin Regulates Osteoblastic Bone Formation During Early Skeletal Development. <b>2015</b> , 156, 3098-113	33
1709	Genome-Wide Mapping and Interrogation of the Nmp4 Antianabolic Bone Axis. 2015, 29, 1269-85	8
1708	Reproducibility of compartmental subchondral bone morphometry in the mouse tibiofemoral joint. <b>2015</b> , 81, 649-653	5
1707	The Impact of Strontium Ranelate on Metaphyseal Bone Healing in Ovariectomized Rats. <b>2015</b> , 97, 391-401	30
1706	High resolution peripheral quantitative computed tomography for the assessment of morphological and mechanical bone parameters. <b>2015</b> , 55, 352-362	3
1705	Engraftment and bone mass are enhanced by PTHrP 1-34 in ectopically transplanted vertebrae (vossicle model) and can be non-invasively monitored with bioluminescence and fluorescence imaging. <b>2015</b> , 24, 955-69	
1704	Osteopathology in the Equine Distal Phalanx Associated With the Development and Progression of Laminitis. <b>2015</b> , 52, 928-44	18
1703	Tenting effect of the elevated sinus membrane over an implant with adjunctive use of a hydroxyapatite-powdered collagen membrane in rabbits. <b>2015</b> , 26, 663-70	12
1702	NLRP12 provides a critical checkpoint for osteoclast differentiation. <b>2015</b> , 112, 10455-60	17
1701	Mutation in Osteoactivin Promotes Receptor Activator of NFB Ligand (RANKL)-mediated Osteoclast Differentiation and Survival but Inhibits Osteoclast Function. <b>2015</b> , 290, 20128-46	25
1700	Locally limited inhibition of bone resorption and orthodontic relapse by recombinant osteoprotegerin protein. <b>2015</b> , 18 Suppl 1, 187-95	18
1699	Comparison of the effects of heparin and the direct factor Xa inhibitor, rivaroxaban, on bone microstructure and metabolism in adult rats. <b>2015</b> , 56, 477-82	3
1698	Epigenetic Control of Skeletal Development by the Histone Methyltransferase Ezh2. <b>2015</b> , 290, 27604-17	108

1697	Sclerostin antibody and interval treadmill training effects in a rodent model of glucocorticoid-induced osteopenia. <b>2015</b> , 81, 691-701	24
1696	D-amino acid inhibits biofilm but not new bone formation in an ovine model. <b>2015</b> , 473, 3951-61	16
1695	Osteoporotic bone of miR-150-deficient mice: Possibly due to low serum OPG-mediated osteoclast activation. <b>2015</b> , 3, 5-10	11
1694	Disuse rescues the age-impaired adaptive response to external loading in mice. <b>2015</b> , 26, 2703-8	14
1693	Prunetin signals via G-protein-coupled receptor, GPR30(GPER1): Stimulation of adenylyl cyclase and cAMP-mediated activation of MAPK signaling induces Runx2 expression in osteoblasts to promote bone regeneration. <b>2015</b> , 26, 1491-501	33
1692	Igfbp2 Deletion in Ovariectomized Mice Enhances Energy Expenditure but Accelerates Bone Loss. <b>2015</b> , 156, 4129-40	21
1691	Bone Marrow Stress Decreases Osteogenic Progenitors. <b>2015</b> , 97, 476-86	6
1690	In vivo monitoring of bone architecture and remodeling after implant insertion: The different responses of cortical and trabecular bone. <b>2015</b> , 81, 468-477	35
1689	Three-dimensional evaluation of human jaw bone microarchitecture: correlation between the microarchitectural parameters of cone beam computed tomography and micro-computer tomography. <b>2015</b> , 120, 762-70	12
1688	Fatostatin, an SREBP inhibitor, prevented RANKL-induced bone loss by suppression of osteoclast differentiation. <b>2015</b> , 1852, 2432-41	12
1687	Focal enhancement of the skeleton to exercise correlates with responsivity of bone marrow mesenchymal stem cells rather than peak external forces. <b>2015</b> , 218, 3002-9	31
1686	Spatial distribution of soluble insulin in pig subcutaneous tissue: Effect of needle length, injection speed and injected volume. <b>2015</b> , 79, 96-101	9
1685	[High resolution peripheral quantitative computed tomography for the assessment of morphological and mechanical bone parameters]. <b>2015</b> , 55, 352-62	24
1684	Bone status of acetylcholinesterase-knockout mice. <b>2015</b> , 29, 222-30	10
1683	Three-Dimensional Micro-Computed Tomography Analyses of Induced Periapical Lesions in Transgenic Mice. <b>2015</b> , 39, 402-7	4
1682	Ultrastructural alterations of osteocyte morphology via loaded implants in rabbit tibiae. <b>2015</b> , 48, 4130-4141	19
1681	Sclerostin inhibition prevents spinal cord injury-induced cancellous bone loss. <i>Journal of Bone and Mineral Research</i> , <b>2015</b> , 30, 681-9	45
1680	The kynurenine pathway of tryptophan degradation is activated during osteoblastogenesis. <b>2015</b> , 33, 111-21	50

## (2015-2015)

1679	mTORC2 signaling promotes skeletal growth and bone formation in mice. <i>Journal of Bone and Mineral Research</i> , <b>2015</b> , 30, 369-78	6.3	64
1678	Bone fracture toughness and strength correlate with collagen cross-link maturity in a dose-controlled lathyrism mouse model. <i>Journal of Bone and Mineral Research</i> , <b>2015</b> , 30, 455-64	6.3	88
1677	Lipocalin 2: a new mechanoresponding gene regulating bone homeostasis. <i>Journal of Bone and Mineral Research</i> , <b>2015</b> , 30, 357-68	6.3	52
1676	Lack of prolidase causes a bone phenotype both in human and in mouse. <b>2015</b> , 72, 53-64		15
1675	Deletion of connexin43 in osteoblasts/osteocytes leads to impaired muscle formation in mice. Journal of Bone and Mineral Research, <b>2015</b> , 30, 596-605	6.3	59
1674	Thrombin receptor deficiency leads to a high bone mass phenotype by decreasing the RANKL/OPG ratio. <b>2015</b> , 72, 14-22		17
1673	SPR4-peptide alters bone metabolism of normal and HYP mice. <b>2015</b> , 72, 23-33		6
1672	Effects of load-bearing exercise on skeletal structure and mechanics differ between outbred populations of mice. <b>2015</b> , 72, 1-8		25
1671	Core binding factor $\square$ of osteoblasts maintains cortical bone mass via stabilization of Runx2 in mice. <i>Journal of Bone and Mineral Research</i> , <b>2015</b> , 30, 715-22	6.3	24
1670	Micro-computed tomography assessment of human alveolar bone: bone density and three-dimensional micro-architecture. <b>2015</b> , 17, 307-13		33
1669	Skeletal site-specific response to ovariectomy in a rat model: change in bone density and microarchitecture. <b>2015</b> , 26, 392-398		52
1668	Double incretin receptor knock-out (DIRKO) mice present with alterations of trabecular and cortical micromorphology and bone strength. <b>2015</b> , 26, 209-18		34
1667	Anti-sclerostin antibody treatment in a rat model of progressive renal osteodystrophy. <i>Journal of Bone and Mineral Research</i> , <b>2015</b> , 30, 499-509	6.3	87
1666	Systemic injection of CK2.3, a novel peptide acting downstream of bone morphogenetic protein receptor BMPRIa, leads to increased trabecular bone mass. <b>2015</b> , 33, 208-15		17
1665	Osteoporosis and Osteoarthritis. 2015,		2
1664	Pre-clinical characterization of tissue engineering constructs for bone and cartilage regeneration. <b>2015</b> , 43, 681-96		20
1663	Bone marrow transplantation improves autoinflammation and inflammatory bone loss in SH3BP2 knock-in cherubism mice. <b>2015</b> , 71, 201-9		9
1662	Intrinsic Sex-Linked Variations in Osteogenic and Adipogenic Differentiation Potential of Bone Marrow Multipotent Stromal Cells. <b>2015</b> , 230, 296-307		20

1661	Planar cell polarity aligns osteoblast division in response to substrate strain. <i>Journal of Bone and Mineral Research</i> , <b>2015</b> , 30, 423-35	6.3	16
1660	Mitral Valves: A Computational Framework. <b>2015</b> , 223-255		6
1659	Multiscale Modeling in Biomechanics and Mechanobiology. 2015,		6
1658	MicroCT Imaging of Red fox Talus: A Non-Invasive Approach to Evaluate Age at Death. <b>2015</b> , 57, 194-21		5
1657	Providing Flaxseed Oil but Not Menhaden Oil Protects against OVX Induced Bone Loss in the Mandible of Sprague-Dawley Rats. <b>2016</b> , 8,		7
1656	Orexin Plays a Role in Growth Impediment Induced by Obstructive Sleep Breathing in Rats. <b>2016</b> , 39, 887-97		9
1655	Microstructure of Concrete. <b>2016</b> ,		12
1654	Murine models of breast cancer bone metastasis. <b>2016</b> , 5, 804		67
1653	Marrow Adipose Tissue Expansion Coincides with Insulin Resistance in MAGP1-Deficient Mice. <b>2016</b> , 7, 87		14
1652	Bone loss and aggravated autoimmune arthritis in HLA-DRI1-bearing humanized mice following oral challenge with Porphyromonas gingivalis. <b>2016</b> , 18, 249		41
1651	Inhibition of Midkine Augments Osteoporotic Fracture Healing. <b>2016</b> , 11, e0159278		15
1650	Sc65-Null Mice Provide Evidence for a Novel Endoplasmic Reticulum Complex Regulating Collagen Lysyl Hydroxylation. <b>2016</b> , 12, e1006002		38
1649	A Non-Destructive Method for Distinguishing Reindeer Antler (Rangifer tarandus) from Red Deer Antler (Cervus elaphus) Using X-Ray Micro-Tomography Coupled with SVM Classifiers. <b>2016</b> , 11, e01496	58	3
1648	Governing Equations of Tissue Modelling and Remodelling: A Unified Generalised Description of Surface and Bulk Balance. <b>2016</b> , 11, e0152582		8
1647	Cortical Bone Morphological and Trabecular Bone Microarchitectural Changes in the Mandible and Femoral Neck of Ovariectomized Rats. <b>2016</b> , 11, e0154367		29
1646	A Comparative Study of Five Association Tests Based on CpG Set for Epigenome-Wide Association Studies. <b>2016</b> , 11, e0156895		13
1645	Does Anticoagulant Medication Alter Fracture-Healing? A Morphological and Biomechanical Evaluation of the Possible Effects of Rivaroxaban and Enoxaparin Using a Rat Closed Fracture Model. <b>2016</b> , 11, e0159669		9
1644	Ultrastructure Organization of Human Trabeculae Assessed by 3D sSAXS and Relation to Bone Microarchitecture. <b>2016</b> , 11, e0159838		16

1643	Influence of Implant Neck Design on Bone Formation Under Mechanical Repetitive Loading: Histomorphometric and Microcomputed Tomographic Studies in Rabbit Tibiae. <b>2016</b> , 25, 171-8		1
1642	Effect of Resorbable Collagen Plug on Bone Regeneration in Rat Critical-Size Defect Model. <b>2016</b> , 25, 163-70		6
1641	Six Weeks of Daily Abaloparatide Treatment Increased Vertebral and Femoral Bone Mineral Density, Microarchitecture and Strength in Ovariectomized Osteopenic Rats. <b>2016</b> , 99, 489-499		35
1640	Binding to COMP Reduces the BMP2 Dose for Spinal Fusion in a Rat Model. <b>2016</b> , 41, E829-E836		9
1639	A novel rat model for subchondral microdamage in acute knee injury: a potential mechanism in post-traumatic osteoarthritis. <b>2016</b> , 24, 1776-1785		27
1638	Skeletal effect of casein and whey protein intake during catch-up growth in young male Sprague-Dawley rats. <b>2016</b> , 116, 59-69		20
1637	Thyroid hormone receptor-D1 signaling is critically involved in regulating secondary ossification via promoting transcription of the Ihh gene in the epiphysis. <b>2016</b> , 310, E846-54		10
1636	High-fat diet exacerbates pain-like behaviors and periarticular bone loss in mice with CFA-induced knee arthritis. <b>2016</b> , 24, 1106-15		20
1635	Transcriptional Modulator Ifrd1 Regulates Osteoclast Differentiation through Enhancing the NF- <b>B</b> /NFATc1 Pathway. <b>2016</b> , 36, 2451-63		15
1634	Biological reaction to polyethylene particles in a murine calvarial model is highly influenced by age. <b>2016</b> , 34, 574-80		7
1633	Peri-implant bone adaptations to overloading in rat tibiae: experimental investigations and numerical predictions. <b>2016</b> , 27, 1444-1453		8
1632	Bone morphogenetic protein type I receptor inhibition induces cleft palate associated with micrognathia and cleft lower lip in mice. <b>2016</b> , 106, 612-23		5
1631	Suppression of p38EMAPK Signaling in Osteoblast Lineage Cells Impairs Bone Anabolic Action of Parathyroid Hormone. <i>Journal of Bone and Mineral Research</i> , <b>2016</b> , 31, 985-93	6.3	11
1630	Systemic administration of omeprazole interferes with bone healing and implant osseointegration: an in vivo study on rat tibiae. <b>2016</b> , 43, 193-203		35
1629	The Transcriptional Modulator Interferon-Related Developmental Regulator 1 in Osteoblasts Suppresses Bone Formation and Promotes Bone Resorption. <i>Journal of Bone and Mineral Research</i> , <b>2016</b> , 31, 573-84	6.3	19
1628	Ameloblastin, an Extracellular Matrix Protein, Affects Long Bone Growth and Mineralization. Journal of Bone and Mineral Research, <b>2016</b> , 31, 1235-46	6.3	14
1627	Regulation of Sclerostin Expression in Multiple Myeloma by Dkk-1: A Potential Therapeutic Strategy for Myeloma Bone Disease. <i>Journal of Bone and Mineral Research</i> , <b>2016</b> , 31, 1225-34	6.3	72
1626	Local bone quality affects the outcome of prosthetic total knee arthroplasty. <b>2016</b> , 34, 240-8		17

1625	Odanacatib Restores Trabecular Bone of Skeletally Mature Female Rabbits With Osteopenia but Induces Brittleness of Cortical Bone: A Comparative Study of the Investigational Drug With PTH, Estrogen, and Alendronate. <i>Journal of Bone and Mineral Research</i> , <b>2016</b> , 31, 615-29	6.3	9	
1624	Strontium Ranelate Reduces the Fracture Incidence in a Growing Mouse Model of Osteogenesis Imperfecta. <i>Journal of Bone and Mineral Research</i> , <b>2016</b> , 31, 1003-14	6.3	10	
1623	Sclerostin Antibody Treatment Improves the Bone Phenotype of Crtap(-/-) Mice, a Model of Recessive Osteogenesis Imperfecta. <i>Journal of Bone and Mineral Research</i> , <b>2016</b> , 31, 1030-40	6.3	50	
1622	Conditional Deletion of Murine Fgf23: Interruption of the Normal Skeletal Responses to Phosphate Challenge and Rescue of Genetic Hypophosphatemia. <i>Journal of Bone and Mineral Research</i> , <b>2016</b> , 31, 1247-57	6.3	39	
1621	Mechanical Vibration Mitigates the Decrease of Bone Quantity and Bone Quality of Leptin Receptor-Deficient Db/Db Mice by Promoting Bone Formation and Inhibiting Bone Resorption. <i>Journal of Bone and Mineral Research</i> , <b>2016</b> , 31, 1713-24	6.3	21	
1620	Deletion of FGFR3 in Osteoclast Lineage Cells Results in Increased Bone Mass in Mice by Inhibiting Osteoclastic Bone Resorption. <i>Journal of Bone and Mineral Research</i> , <b>2016</b> , 31, 1676-87	6.3	19	
1619	Histone Acetyltransferase GCN5 Regulates Osteogenic Differentiation of Mesenchymal Stem Cells by Inhibiting NF- <b>B</b> . <i>Journal of Bone and Mineral Research</i> , <b>2016</b> , 31, 391-402	6.3	33	
1618	Pharmacodynamic Actions of a Long-Acting PTH Analog (LA-PTH) in Thyroparathyroidectomized (TPTX) Rats and Normal Monkeys. <i>Journal of Bone and Mineral Research</i> , <b>2016</b> , 31, 1405-12	6.3	42	
1617	The Effect of Vibration Treatments Combined with Teriparatide or Strontium Ranelate on Bone Healing and Muscle in Ovariectomized Rats. <b>2016</b> , 99, 408-22		23	
1616	Histone H3K9 Acetyltransferase PCAF Is Essential for Osteogenic Differentiation Through Bone Morphogenetic Protein Signaling and May Be Involved in Osteoporosis. <b>2016</b> , 34, 2332-41		41	
1615	Autophagy-linked FYVE containing protein WDFY3 interacts with TRAF6 and modulates RANKL-induced osteoclastogenesis. <b>2016</b> , 73, 73-84		14	
1614	Inhibition of substance P signaling aggravates the bone loss in ovariectomy-induced osteoporosis. <b>2016</b> , 122, 112-121		12	
1613	Effects of a Hot-Water Extract of Allium hookeri Roots on Bone Formation in Human Osteoblast-Like MG-63 Cells In Vitro and in Rats In Vivo. <b>2016</b> , 82, 1410-1415		12	
1612	Deficiency of the intermediate filament synemin reduces bone mass in vivo. <b>2016</b> , 311, C839-C845		16	
1611	The vestibular system is critical for the changes in muscle and bone induced by hypergravity in mice. <b>2016</b> , 4, e12979		22	
1610	NADPH oxidase gp91 contributes to RANKL-induced osteoclast differentiation by upregulating NFATc1. <b>2016</b> , 6, 38014		33	
1609	Characterization of genetically engineered mouse models carrying Col2a1-cre-induced deletions of Lrp5 and/or Lrp6. <b>2016</b> , 4, 15042		12	
1608	Validation of downregulated microRNAs during osteoclast formation and osteoporosis progression. <b>2016</b> , 13, 2273-80		14	

1607	Effects of Spaceflight on Bone Microarchitecture in the Axial and Appendicular Skeleton in Growing Ovariectomized Rats. <b>2015</b> , 5, 18671	21
1606	Multi-level tomography reconstructions with level-set and TV regularization methods. 2016,	
1605	Lysine-specific demethylase 1 inhibitor rescues the osteogenic ability of mesenchymal stem cells under osteoporotic conditions by modulating H3K4 methylation. <b>2016</b> , 4, 16037	27
1604	Bone micro-architectural analysis of mandible and tibia in ovariectomised rats: A quantitative structural comparison between undecalcified histological sections and micro-CT. <b>2016</b> , 5, 253-62	16
1603	Three-dimensional micro computed tomography analysis of the lung vasculature and differential adipose proteomics in the Sugen/hypoxia rat model of pulmonary arterial hypertension. <b>2016</b> , 6, 586-596	13
1602	Differential effects of IGF-1 deficiency during the life span on structural and biomechanical properties in the tibia of aged mice. <b>2016</b> , 38, 38	12
1601	Sostdc1 deficiency accelerates fracture healing by promoting the expansion of periosteal mesenchymal stem cells. <b>2016</b> , 88, 20-30	25
1600	Intrauterine stress induces bone loss in adult offspring of C3H/HeJ mice having high bone mass phenotype but not C57BL/6J mice with low bone mass phenotype. <b>2016</b> , 87, 114-9	3
1599	Osteogenic efficacy of strontium hydroxyapatite micro-granules in osteoporotic rat model. <b>2016</b> , 31, 499-509	29
1598	Pigment epithelium-derived factor restoration increases bone mass and improves bone plasticity in a model of osteogenesis imperfecta type VI via Wnt3a blockade. <b>2016</b> , 30, 2837-48	24
1597	Efficient storage of microCT data preserving bone morphometry assessment. <b>2016</b> , 53, 292-300	
1596	IL-3 Decreases Cartilage Degeneration by Downregulating Matrix Metalloproteinases and Reduces Joint Destruction in Osteoarthritic Mice. <b>2016</b> , 196, 5024-35	15
1595	Longitudinal Use of Micro-computed Tomography Does Not Alter Microarchitecture of the Proximal Tibia in Sham or Ovariectomized Sprague-Dawley Rats. <b>2016</b> , 98, 631-41	18
1594	Moderate chronic kidney disease impairs bone quality in C57Bl/6J mice. <b>2016</b> , 86, 1-9	14
1593	Zoledronate prevents lactation induced bone loss and results in additional post-lactation bone mass in mice. <b>2016</b> , 87, 27-36	13
1592	Modeling vitamin D insufficiency and moderate deficiency in adult mice via dietary cholecalciferol restriction. <b>2016</b> , 41, 290-299	14
1591	Anthocyanin-Rich Blackcurrant Extract Attenuates Ovariectomy-Induced Bone Loss in Mice. <b>2016</b> , 19, 390-7	18
1590	A new stable GIP-Oxyntomodulin hybrid peptide improved bone strength both at the organ and tissue levels in genetically-inherited type 2 diabetes mellitus. <b>2016</b> , 87, 102-13	22

1589	Sulfated hyaluronan improves bone regeneration of diabetic rats by binding sclerostin and enhancing osteoblast function. <b>2016</b> , 96, 11-23	43
1588	Sprouty2 regulates endochondral bone formation by modulation of RTK and BMP signaling. <b>2016</b> , 88, 170-179	9
1587	Effects of developmental exposure to perfluorooctanoic acid (PFOA) on long bone morphology and bone cell differentiation. <b>2016</b> , 301, 14-21	42
1586	LGR4 acts as a key receptor for R-spondin 2 to promote osteogenesis through Wnt signaling pathway. <b>2016</b> , 28, 989-1000	42
1585	Nano-Computed Tomography: Technique and Applications. <b>2016</b> , 188, 146-54	39
1584	Bone formation of human mesenchymal stem cells harvested from reaming debris is stimulated by low-dose bone morphogenetic protein-7 application in vivo. <b>2016</b> , 13, 404-8	15
1583	Rapid phenotyping of knockout mice to identify genetic determinants of bone strength. <b>2016</b> , 231, R31-46	24
1582	HBM Mice Have Altered Bone Matrix Composition and Improved Material Toughness. <b>2016</b> , 99, 384-95	4
1581	NGF-TrkA Signaling by Sensory Nerves Coordinates the Vascularization and Ossification of Developing Endochondral Bone. <b>2016</b> , 16, 2723-2735	74
1580	WITHDRAWN: Prolyl hydroxylase domain proteins regulate bone mass through their expression in osteoblasts. <b>2016</b> ,	
1579	Coadministration of puerarin (low dose) and zinc attenuates bone loss and suppresses bone marrow adiposity in ovariectomized rats. <b>2016</b> , 166, 20-26	13
1578	Experimental and Numerical Investigation on Stress Dependence of Sandstone Electrical Properties and Deviations from Archie's Law. <b>2016</b> ,	5
1577	Glucose Transporter-4 Facilitates Insulin-Stimulated Glucose Uptake in Osteoblasts. <b>2016</b> , 157, 4094-4103	51
1576	Effect of dietary calcium deficiency and altered diet hardness on the jawbone growth: A micro-CT and bone histomorphometric study in rats. <b>2016</b> , 72, 200-210	11
1575	Myocardin-related transcription factor A (MRTFA) regulates the fate of bone marrow mesenchymal stem cells and its absence in mice leads to osteopenia. <b>2016</b> , 5, 970-979	16
1574	Effect of micro-computed tomography voxel size and segmentation method on trabecular bone microstructure measures in mice. <b>2016</b> , 5, 136-40	51
1573	Comparison of micro-CT post-processing methods for evaluating the trabecular bone volume fraction in a rat ACL-transection model. <b>2016</b> , 49, 3559-3563	4
1572	Impact of P2RX7 ablation on the morphological, mechanical and tissue properties of bones in a murine model of duchenne muscular dystrophy. <b>2016</b> , 49, 3444-3451	5

## (2016-2016)

1571	Short-range ultraviolet irradiation with LED device effectively increases serum levels of 25(OH)D. <b>2016</b> , 164, 256-263	8
1570	Ethanolic extract of Schizonepeta tenuifolia attenuates osteoclast formation and activation in vitro and protects against lipopolysaccharide-induced bone loss in vivo. <b>2016</b> , 16, 301	5
1569	Glucose-dependent insulinotropic polypeptide (GIP) dose-dependently reduces osteoclast differentiation and resorption. <b>2016</b> , 91, 102-12	25
1568	Combined treatment with a transforming growth factor beta inhibitor (1D11) and bortezomib improves bone architecture in a mouse model of myeloma-induced bone disease. <b>2016</b> , 91, 81-91	34
1567	FGF23 Regulates Bone Mineralization in a 1,25(OH)2 D3 and Klotho-Independent Manner. <i>Journal of Bone and Mineral Research</i> , <b>2016</b> , 31, 129-42	82
1566	Changes in the Fracture Resistance of Bone with the Progression of Type 2 Diabetes in the ZDSD Rat. <b>2016</b> , 99, 289-301	36
1565	Peri-implant osseointegration after low-level laser therapy: micro-computed tomography and resonance frequency analysis in an animal model. <b>2016</b> , 31, 1789-1795	14
1564	The PPAREAgonist Fenofibrate Improves the Musculoskeletal Effects of Exercise in Ovariectomized Rats. <b>2016</b> , 157, 3924-3934	5
1563	Effect of combined treatment with zoledronic acid and parathyroid hormone on mouse bone callus structure and composition. <b>2016</b> , 92, 70-78	16
1562	Mechanical and material properties of cortical and trabecular bone from cannabinoid receptor-1-null (Cnr1(-/-)) mice. <b>2016</b> , 38, 1044-54	7
1561	Simulating the Lunar Environment: Partial Weightbearing and High-LET Radiation-Induce Bone Loss and Increase Sclerostin-Positive Osteocytes. <b>2016</b> , 186, 254-63	18
1560	Only minor differences in renal osteodystrophy features between wild-type and sclerostin knockout mice with chronic kidney disease. <b>2016</b> , 90, 828-34	17
1559	Role of ERMISS in the Effect of Estradiol on Cancellous and Cortical Femoral Bone in Growing Female Mice. <b>2016</b> , 157, 2533-44	17
1558	Zoledronate treatment has different effects in mouse strains with contrasting baseline bone mechanical phenotypes. <b>2016</b> , 27, 3637-3643	9
1557	Characterization of BMP signaling dependent osteogenesis using a BMP depletable avianized bone marrow stromal cell line (TVA-BMSC). <b>2016</b> , 91, 39-52	15
1556	Longitudinal imaging of the ageing mouse. <b>2016</b> , 160, 93-116	31
1555	Polymerization shrinkage assessment of dental resin composites: a literature review. <b>2016</b> , 104, 257-70	56
1554	Loss of Type I Collagen Telopeptide Lysyl Hydroxylation Causes Musculoskeletal Abnormalities in a Zebrafish Model of Bruck Syndrome. <i>Journal of Bone and Mineral Research</i> , <b>2016</b> , 31, 1930-1942	45

1553	Overexpression of HSPA1A enhances the osteogenic differentiation of bone marrow mesenchymal stem cells via activation of the Wnt/I-catenin signaling pathway. <b>2016</b> , 6, 27622	28
1552	Myeloid thrombomodulin lectin-like domain inhibits osteoclastogenesis and inflammatory bone loss. <b>2016</b> , 6, 28340	9
1551	Protein Phosphatase PP5 Controls Bone Mass and the Negative Effects of Rosiglitazone on Bone through Reciprocal Regulation of PPAR[Peroxisome Proliferator-activated Receptor land RUNX2 (Runt-related Transcription Factor 2). <b>2016</b> , 291, 24475-24486	18
1550	The effect of local delivery of adiponectin from biodegradable microsphere-scaffold composites on new bone formation in adiponectin knockout mice. <b>2016</b> , 4, 4771-4779	5
1549	Understanding Bone Strength from Finite Element Models: Concepts for Non-engineers. <b>2016</b> , 14, 161-166	2
1548	X-ray computed tomography for fast and non-destructive multiple pearl inspection. <b>2016</b> , 6, 32-37	4
1547	Prolyl hydroxylase domain proteins regulate bone mass through their expression in osteoblasts. <b>2016</b> , 594, 125-130	4
1546	Preexisting Periapical Inflammatory Condition Exacerbates Tooth Extraction-induced Bisphosphonate-related Osteonecrosis of the Jaw Lesions in Mice. <b>2016</b> , 42, 1641-1646	26
1545	Promotion of osteointegration under diabetic conditions by tantalum coating-based surface modification on 3-dimensional printed porous titanium implants. <b>2016</b> , 148, 440-452	38
1544	Quercetin-loaded solid lipid nanoparticles improve osteoprotective activity in an ovariectomized rat model: a preventive strategy for post-menopausal osteoporosis. <b>2016</b> , 6, 97613-97628	23
1543	Differential Responses to Vitamin D2 and Vitamin D3 Are Associated With Variations in Free 25-Hydroxyvitamin D. <b>2016</b> , 157, 3420-30	28
1542	Antagonizing midkine accelerates fracture healing in mice by enhanced bone formation in the fracture callus. <b>2016</b> , 173, 2237-49	19
1541	Specific bone region localization of osteolytic versus osteoblastic lesions in a patient-derived xenograft model of bone metastatic prostate cancer. <b>2016</b> , 3, 229-239	3
1540	Cranial vault thickness in non-human primates: Allometric and geometric analyses of the vault and its component layers. <b>2016</b> , 101, 90-100	1
1539	Poly(Vinylidene Fluoride-Trifluorethylene)/barium titanate membrane promotes de novo bone formation and may modulate gene expression in osteoporotic rat model. <b>2016</b> , 27, 180	16
1538	Disruption of c-Kit Signaling in Kit(W-sh/W-sh) Growing Mice Increases Bone Turnover. <b>2016</b> , 6, 31515	9
1537	Ras signaling regulates osteoprogenitor cell proliferation and bone formation. <b>2016</b> , 7, e2405	15
1536	SIKs control osteocyte responses to parathyroid hormone. <b>2016</b> , 7, 13176	79

1535	Allogeneic Mesenchymal Stem Cell Therapy Promotes Osteoblastogenesis and Prevents Glucocorticoid-Induced Osteoporosis. <b>2016</b> , 5, 1238-46	52	
1534	GDF11 decreases bone mass by stimulating osteoclastogenesis and inhibiting osteoblast differentiation. <b>2016</b> , 7, 12794	97	
1533	Repetitive Stresses Generate Osteochondral Lesions in Skeletally Immature Rabbits. <b>2016</b> , 44, 2957-2966	2	
1532	sFRP4-dependent Wnt signal modulation is critical for bone remodeling during postnatal development and age-related bone loss. <b>2016</b> , 6, 25198	41	
1531	Binary tomography reconstruction from few projections with Total Variation regularization for bone microstructure studies. <b>2016</b> , 24, 177-89	1	
1530	Inhibition of GSK-3 increases trabecular bone volume but not cortical bone volume in adenine-induced uremic mice with severe hyperparathyroidism. <b>2016</b> , 4, e13010	5	
1529	Pharmacological Regulation of In Situ Tissue Stem Cells Differentiation for Soft Tissue Calcification Treatment. <b>2016</b> , 34, 1083-96	14	
1528	IGF-1 Regulates Vertebral Bone Aging Through Sex-Specific and Time-Dependent Mechanisms. <i>Journal of Bone and Mineral Research</i> , <b>2016</b> , 31, 443-54	27	
1527	Neurotrophin-3 Induces BMP-2 and VEGF Activities and Promotes the Bony Repair of Injured Growth Plate Cartilage and Bone in Rats. <i>Journal of Bone and Mineral Research</i> , <b>2016</b> , 31, 1258-74	32	
1526	Skeletal Mineralization Deficits and Impaired Biogenesis and Function of Chondrocyte-Derived Matrix Vesicles in Phospho1(-/-) and Phospho1/Pi t1 Double-Knockout Mice. <i>Journal of Bone and Mineral Research</i> , <b>2016</b> , 31, 1275-86	32	
1525	Circadian Clock Regulates Bone Resorption in Mice. <i>Journal of Bone and Mineral Research</i> , <b>2016</b> , 31, 13446555	50	
1524	Stress-Induced Activation of Apoptosis Signal-Regulating Kinase 1 Promotes Osteoarthritis. <b>2016</b> , 231, 944-53	10	
1523	Contribution of mechanical unloading to trabecular bone loss following non-invasive knee injury in mice. <b>2016</b> , 34, 1680-1687	20	
1522	Assessment of jawbone trabecular bone structure amongst osteoporotic women by cone-beam computed tomography: the OSTEOSYR project. <b>2016</b> , 7, 332-340	9	
1521	Bone Matrix Composition Following PTH Treatment is Not Dependent on Sclerostin Status. <b>2016</b> , 98, 149-57	8	
1520	Image resolution enhancement for healthy weight-bearing bones based on topology optimization. <b>2016</b> , 49, 3035-3040	13	
1519	Characterization of reactive flow-induced evolution of carbonate rocks using digital core analysis-part 1: Assessment of pore-scale mineral dissolution and deposition. <b>2016</b> , 192, 60-86	22	
1518	Daily leptin blunts marrow fat but does not impact bone mass in calorie-restricted mice. <b>2016</b> , 229, 295-306	22	

1517	Frequency of Teriparatide Administration Affects the Histological Pattern of Bone Formation in Young Adult Male Mice. <b>2016</b> , 157, 2604-20	34
1516	Loss of Oncostatin M Signaling in Adipocytes Induces Insulin Resistance and Adipose Tissue Inflammation in Vivo. <b>2016</b> , 291, 17066-76	17
1515	Techniques to assess bone ultrastructure organization: orientation and arrangement of mineralized collagen fibrils. <b>2016</b> , 13,	72
1514	Skeletal site-specific effects of endurance running on structure and strength of tibia, lumbar vertebrae, and mandible in male Sprague-Dawley rats. <b>2016</b> , 41, 597-604	4
1513	Influence of Fatigue Loading and Bone Turnover on Bone Strength and Pattern of Experimental Fractures of the Tibia in Mice. <b>2016</b> , 99, 99-109	4
1512	Bone mineral properties in growing Col1a2(+/G610C) mice, an animal model of osteogenesis imperfecta. <b>2016</b> , 87, 120-9	22
1511	Development of a protocol to quantify local bone adaptation over space and time: Quantification of reproducibility. <b>2016</b> , 49, 2095-2099	28
1510	Teriparatide Improves Trabecular Osteoporosis but Simultaneously Promotes Ankylosis of the Spine in the Twy Mouse Model for Diffuse Idiopathic Skeletal Hyperostosis. <b>2016</b> , 98, 140-8	6
1509	Correlation of Subchondral Bone Density and Structure from Plain Radiographs with Micro Computed Tomography Ex Vivo. <b>2016</b> , 44, 1698-709	17
1508	Quantitative micro-computed tomography for assessment of age-dependent changes in murine whole-body composition. <b>2016</b> , 5, 70-80	9
1507	Femoral subchondral bone properties of patients with cam-type femoroacetabular impingement. <b>2016</b> , 24, 1000-6	4
1506	Evaluation of Titanium-Coated Pedicle Screws: In Vivo Porcine Lumbar Spine Model. <b>2016</b> , 91, 163-71	5
1505	Bone structure and function in male C57BL/6 mice: Effects of a high-fat Western-style diet with or without trace minerals. <b>2016</b> , 5, 141-149	11
1504	High-resolution mapping of a novel rat blood pressure locus on chromosome 9 to a region containing the Spp2 gene and colocalization of a QTL for bone mass. <b>2016</b> , 48, 409-19	7
1503	Novel methods for microCT-based analyses of vasculature in the renal cortex reveal a loss of perfusable arterioles and glomeruli in eNOS-/- mice. <b>2016</b> , 17, 24	25
1502	Obesity inhibits the osteogenic differentiation of human adipose-derived stem cells. <b>2016</b> , 14, 27	14
1501	Rictor/mTORC2 loss in osteoblasts impairs bone mass and strength. <b>2016</b> , 90, 50-8	18
1500	Reactive Oxygen Species Differentially Regulate Bone Turnover in an Age-Specific Manner in Catalase Transgenic Female Mice. <b>2016</b> , 358, 50-60	6

1499	Three-dimensional polymer coated 45S5-type bioactive glass scaffolds seeded with human mesenchymal stem cells show bone formation in vivo. <b>2016</b> , 27, 119		38
1498	Systemic Treatment with Strontium Ranelate Does Not Influence the Healing of Femoral Mid-shaft Defects in Rats. <b>2016</b> , 98, 206-14		8
1497	Modulation of unloading-induced bone loss in mice with altered ERK signaling. <b>2016</b> , 27, 47-61		10
1496	Minimizing Interpolation Bias and Precision Error in In Vivo μCT-Based Measurements of Bone Structure and Dynamics. <b>2016</b> , 44, 2518-2528		8
1495	Chemical Principles in Tissue Clearing and Staining Protocols for Whole-Body Cell Profiling. <b>2016</b> , 32, 713-741		170
1494	Osteocyte Apoptosis Caused by Hindlimb Unloading is Required to Trigger Osteocyte RANKL Production and Subsequent Resorption of Cortical and Trabecular Bone in Mice Femurs. <i>Journal of Bone and Mineral Research</i> , <b>2016</b> , 31, 1356-65	6.3	95
1493	CCL20/CCR6 Signaling Regulates Bone Mass Accrual in Mice. <i>Journal of Bone and Mineral Research</i> , <b>2016</b> , 31, 1381-90	6.3	13
1492	The Dmp1-SOST Transgene Interacts With and Downregulates the Dmp1-Cre Transgene and the Rosa(Notch) Allele. <b>2016</b> , 117, 1222-32		2
1491	Combined high-fat-resveratrol diet and RIP140 knockout mice reveal a novel relationship between elevated bone mitochondrial content and compromised bone microarchitecture, bone mineral mass, and bone strength in the tibia. <b>2016</b> , 60, 1994-2007		10
1490	Vascular imaging with contrast agent in hard and soft tissues using microcomputed-tomography. <b>2016</b> , 262, 40-9		15
1489	Effects of daidzein on alveolar bone loss and internal microstructures of bone in a rat model of experimental periodontitis: a study using micro-computed tomography. <b>2016</b> , 51, 250-6		8
1488	Cyclooxygenase-2 deficiency impairs muscle-derived stem cell-mediated bone regeneration via cellular autonomous and non-autonomous mechanisms. <b>2016</b> , 25, 3216-3231		20
1487	A novel oxysterol promotes bone regeneration in rabbit cranial bone defects. <b>2016</b> , 10, 591-9		11
1486	Deficiency of circadian clock protein BMAL1 in mice results in a low bone mass phenotype. <b>2016</b> , 84, 194-203		69
1485	Effects of Recombinant Human Bone Morphogenetic Protein-2 Dose and Ceramic Composition on New Bone Formation and Space Maintenance in a Canine Mandibular Ridge Saddle Defect Model. <b>2016</b> , 22, 469-79		12
1484	The effects of strength training and raloxifene on bone health in aging ovariectomized rats. <b>2016</b> , 85, 45-54		23
1483	Canonical Notch activation in osteocytes causes osteopetrosis. <b>2016</b> , 310, E171-82		32
1482	Anabolic and Antiresorptive Modulation of Bone Homeostasis by the Epigenetic Modulator Sulforaphane, a Naturally Occurring Isothiocyanate. <b>2016</b> , 291, 6754-71		45

1481	Novel Wnt Regulator NEL-Like Molecule-1 Antagonizes Adipogenesis and Augments Osteogenesis Induced by Bone Morphogenetic Protein 2. <b>2016</b> , 186, 419-34	48
1480	DMP-1-mediated Ghr gene recombination compromises skeletal development and impairs skeletal response to intermittent PTH. <b>2016</b> , 30, 635-52	19
1479	Sex-Linked Skeletal Phenotype of Lysyl Oxidase Like-1 Mutant Mice. <b>2016</b> , 98, 172-85	16
1478	Neovascularization of osteoporotic metaphyseal bone defects: A morphometric micro-CT study. <b>2016</b> , 105, 7-14	10
1477	Subchondral and epiphyseal bone remodeling following surgical transection and noninvasive rupture of the anterior cruciate ligament as models of post-traumatic osteoarthritis. <b>2016</b> , 24, 698-708	30
1476	Hajdu Cheney Mouse Mutants Exhibit Osteopenia, Increased Osteoclastogenesis, and Bone Resorption. <b>2016</b> , 291, 1538-1551	55
1475	Intermittent hypoxia induces disturbances in craniofacial growth and defects in craniofacial morphology. <b>2016</b> , 61, 115-24	16
1474	Cranial vault thickness in primates: Homo erectus does not have uniquely thick vault bones. <b>2016</b> , 90, 120-34	19
1473	Rictor is required for optimal bone accrual in response to anti-sclerostin therapy in the mouse. <b>2016</b> , 85, 1-8	19
1472	Anabolic actions of Notch on mature bone. <b>2016</b> , 113, E2152-61	39
1471	Sclerostin antibody treatment improves fracture outcomes in a Type I diabetic mouse model. <b>2016</b> , 82, 122-34	48
1470	Cross-correlative 3D micro-structural investigation of human bone processed into bone allografts. <b>2016</b> , 62, 574-84	10
1469	Cortical and trabecular deterioration in mouse models of Roux-en-Y gastric bypass. <b>2016</b> , 85, 23-8	19
1468	Calcitriol Suppression of Parathyroid Hormone Fails to Improve Skeletal Properties in an Animal Model of Chronic Kidney Disease. <b>2016</b> , 43, 20-31	6
1467	Screw insertion in trabecular bone causes peri-implant bone damage. <b>2016</b> , 38, 417-22	26
1466	Osteoprotective Effects of Estrogen in the Maxillary Bone Depend on ER <b>2016</b> , 95, 689-96	18
1465	Performance evaluation of the CT component of the IRIS PET/CT preclinical tomograph. <b>2016</b> , 805, 135-144	4
1464	High fat diet enriched with saturated, but not monounsaturated fatty acids adversely affects femur, and both diets increase calcium absorption in older female mice. <b>2016</b> , 36, 742-50	27

## (2016-2016)

1463	Assessment of a polyelectrolyte multilayer film coating loaded with BMP-2 on titanium and PEEK implants in the rabbit femoral condyle. <b>2016</b> , 36, 310-22	46
1462	Periodontal disease exacerbates systemic ovariectomy-induced bone loss in mice. <b>2016</b> , 83, 241-247	23
1461	Genistein suppresses Prevotella intermedia lipopolysaccharide-induced inflammatory response in macrophages and attenuates alveolar bone loss in ligature-induced periodontitis. <b>2016</b> , 62, 70-9	15
1460	Donepezil regulates energy metabolism and favors bone mass accrual. <b>2016</b> , 84, 131-138	15
1459	3D X-ray ultra-microscopy of bone tissue. <b>2016</b> , 27, 441-55	23
1458	Loss of Gs <del>II</del> n the Postnatal Skeleton Leads to Low Bone Mass and a Blunted Response to Anabolic Parathyroid Hormone Therapy. <b>2016</b> , 291, 1631-1642	29
1457	Test in canine extraction site preservations by using mineralized collagen plug with or without membrane. <b>2016</b> , 30, 1285-99	10
1456	Age-related changes in the fracture resistance of male Fischer F344 rat bone. <b>2016</b> , 83, 220-232	25
1455	Src siRNA prevents corticosteroid-associated osteoporosis in a rabbit model. <b>2016</b> , 83, 190-196	7
1454	Lycopene treatment against loss of bone mass, microarchitecture and strength in relation to regulatory mechanisms in a postmenopausal osteoporosis model. <b>2016</b> , 83, 127-140	35
1453	Effect of Surface Nanotopography on Bone Response to Titanium Implant. <b>2016</b> , 42, 240-7	7
1452	Dual-therapy with ₩B-targeted Sn2 lipase-labile fumagillin-prodrug nanoparticles and zoledronic acid in the Vx2 rabbit tumor model. <b>2016</b> , 12, 201-11	12
1451	Activation of Protein Kinase A in Mature Osteoblasts Promotes a Major Bone Anabolic Response. <b>2016</b> , 157, 112-26	10
1450	Raloxifene improves skeletal properties in an animal model of cystic chronic kidney disease. <b>2016</b> , 89, 95-104	16
1449	Computational Radiology for Orthopaedic Interventions. 2016,	5
1448	Role of osteoclasts in heterotopic ossification enhanced by fibrodysplasia ossificans progressiva-related activin-like kinase 2 mutation in mice. <b>2016</b> , 34, 517-25	5
1447	Interaction between Physical Activity and Smoking on Lung, Muscle, and Bone in Mice. <b>2016</b> , 54, 674-82	14
1446	Combining X-ray computed tomography with relevant techniques for analyzing soilâfoot dynamics âlan overview. <b>2016</b> , 66, 1-19	3

1445	Effect of Doxycycline in Gel Form on Bone Regeneration: Histomorphometric and Tomographic Study in Rat Calvaria. <b>2016</b> , 87, 74-82	11
1444	Bone defect regeneration and cortical bone parameters of type 2 diabetic rats are improved by insulin therapy. <b>2016</b> , 82, 108-15	34
1443	CT Imaging Biomarkers of Bone Damage Induced by Environmental Level of Cadmium Exposure in Male Rats. <b>2016</b> , 170, 146-51	11
1442	Stochastic multiscale modelling of cortical bone elasticity based on high-resolution imaging. <b>2016</b> , 15, 111-31	6
1441	Dual-energy X-ray absorptiometry, peripheral quantitative computed tomography, and micro-computed tomography techniques are discordant for bone density and geometry measurements in the guinea pig. <b>2016</b> , 34, 266-76	2
1440	Evaluation of twelve vibration regimes applied to improve spine properties in ovariectomized rats. <b>2017</b> , 7, 172-180	6
1439	Use of micro-computed tomography for the assessment of periapical lesions in small rodents: a systematic review. <b>2017</b> , 50, 352-366	15
1438	Mesenchymal stem cell expression of SDF-1 synergizes with BMP-2 to augment cell-mediated healing of critical-sized mouse calvarial defects. <b>2017</b> , 11, 1806-1819	20
1437	Osteophyte formation after ACL rupture in mice is associated with joint restabilization and loss of range of motion. <b>2017</b> , 35, 466-473	30
1436	The effect of a flapless alveolar ridge preservation procedure with or without a xenograft on buccal bone crest remodeling compared by histomorphometric and microcomputed tomographic analysis. <b>2017</b> , 28, 938-945	9
1435	MicroCT assessment of bone microarchitecture in implant sites reconstructed with autogenous and xenogenous grafts: a pilot study. <b>2017</b> , 28, 308-313	14
1434	Effects of Sex and Notch Signaling on the Osteocyte Cell Pool. <b>2017</b> , 232, 363-370	10
1433	Different bone remodeling levels of trabecular and cortical bone in response to changes in Wnt/II-catenin signaling in mice. <b>2017</b> , 35, 812-819	34
1432	IT-based trabecular anisotropy can be reproducibly computed from HR-pQCT scans using the triangulated bone surface. <b>2017</b> , 97, 114-120	9
1431	APPLs: More than just adiponectin receptor binding proteins. <b>2017</b> , 32, 76-84	26
1430	Low trabecular bone density in recent sedentary modern humans. <b>2017</b> , 162, 550-560	40
1429	Aerobic Endurance Training Does Not Protect Bone Against Poorly Controlled Type 1 Diabetes in Young Adult Rats. <b>2017</b> , 100, 374-381	2
1428	Soy isoflavone supplementation improves longitudinal bone growth and bone quality in growing female rats. <b>2017</b> , 37, 68-73	7

1427	Unique local bone tissue characteristics in iliac crest bone biopsy from adolescent idiopathic scoliosis with severe spinal deformity. <b>2017</b> , 7, 40265		11
1426	Tgfbr2 is required in osterix expressing cells for postnatal skeletal development. <b>2017</b> , 97, 54-64		11
1425	Comparative 3D micro-CT and 2D histomorphometry analysis of dental implant osseointegration in the maxilla of minipigs. <b>2017</b> , 44, 418-427	,	33
1424	Pulsed electromagnetic field at different stages of knee osteoarthritis in rats induced by low-dose monosodium iodoacetate: Effect on subchondral trabecular bone microarchitecture and cartilage degradation. <b>2017</b> , 38, 227-238		14
1423	Quantifying damage in polycrystalline ice via X-Ray computed micro-tomography. <b>2017</b> , 127, 463-470		7
1422	Sclerostin antibody inhibits skeletal deterioration in mice exposed to partial weight-bearing. <b>2017</b> , 12, 32-38		9
1421	Variations in crestal cortical bone thickness at dental implant sites in different regions of the jawbone. <b>2017</b> , 19, 440-446		29
1420	A Conditional Knockout Mouse Model Reveals a Critical Role of PKD1 in Osteoblast Differentiation and Bone Development. <b>2017</b> , 7, 40505		16
1419	Biodegradable Magnesium Screws Accelerate Fibrous Tissue Mineralization at the Tendon-Bone Insertion in Anterior Cruciate Ligament Reconstruction Model of Rabbit. <b>2017</b> , 7, 40369		23
1418	Cyclin-Dependent Kinase Inhibitor-1-Deficient Mice are Susceptible to Osteoarthritis Associated with Enhanced Inflammation. <i>Journal of Bone and Mineral Research</i> , <b>2017</b> , 32, 991-1001		21
1417	Inhibition of osteoclast differentiation and collagen antibody-induced arthritis by CTHRC1. <b>2017</b> , 97, 153-167		16
1416	Surface Modifications and Surface Characterization of Biomaterials Used in Bone Healing. <b>2017</b> , 405-452		4
1415	Isopsoralen-mediated suppression of bone marrow adiposity and attenuation of the adipogenic commitment of bone marrow-derived mesenchymal stem cells. <b>2017</b> , 39, 527-538		15
1414	Fkbp10 Deletion in Osteoblasts Leads to Qualitative Defects in Bone. <i>Journal of Bone and Mineral Research</i> , <b>2017</b> , 32, 1354-1367		11
1413	Electrical Stimulation of Denervated Rat Skeletal Muscle Ameliorates Bone Fragility and Muscle Loss in Early-Stage Disuse Musculoskeletal Atrophy. <b>2017</b> , 100, 420-430		8
1412	The precision of micro-tomography in bone taphonomic experiments and the importance of registration. <b>2017</b> , 273, 161-167		6
1411	Microscopic dual-energy CT (microDECT): a flexible tool for multichannel ex vivo 3D imaging of biological specimens. <b>2017</b> , 267, 3-26		22
1410	The protective effects of silibinin in the treatment of streptozotocin-induced diabetic osteoporosis in rats. <b>2017</b> , 89, 681-688		<b>2</b> 0

Tissue-Engineered Grafts for Bone and Meniscus Regeneration and Their Assessment Using MRI. **2017**, 149-177

1408	miR-21 deficiency inhibits osteoclast function and prevents bone loss in mice. <b>2017</b> , 7, 43191	71
1407	Image-based modelling of skeletal muscle oxygenation. <b>2017</b> , 14,	13
1406	A novel in silico method to quantify primary stability of screws in trabecular bone. <b>2017</b> , 35, 2415-2424	14
1405	Lipoxin A4 suppresses osteoclastogenesis in RAW264.7 cells and prevents ovariectomy-induced bone loss. <b>2017</b> , 352, 293-303	26
1404	Automated Bone Segmentation and Surface Evaluation of a Small Animal Model of Post-Traumatic Osteoarthritis. <b>2017</b> , 45, 1227-1235	3
1403	Parathyroid hormone's enhancement of bones' osteogenic response to loading is affected by ageing in a dose- and time-dependent manner. <b>2017</b> , 98, 59-67	14
1402	Segmentation of cortical bone using fast level sets. <b>2017</b> ,	
1401	Romosozumab Treatment Converts Trabecular Rods into Trabecular Plates in Male Cynomolgus Monkeys. <b>2017</b> , 101, 82-91	11
1400	Raccoon dog model shows preservation of bone during prolonged catabolism and reduced physical activity. <b>2017</b> , 220, 2196-2202	2
1399	The effect of L-PRF membranes on bone healing in rabbit tibiae bone defects: micro-CT and biomarker results. <b>2017</b> , 7, 46452	17
1398	Hox11 Function Is Required for Region-Specific Fracture Repair. <i>Journal of Bone and Mineral Research</i> , <b>2017</b> , 32, 1750-1760	22
1397	Ablation of Hepatic Production of the Acid-Labile Subunit in Bovine-GH Transgenic Mice: Effects on Organ and Skeletal Growth. <b>2017</b> , 158, 2556-2571	7
1396	Effect of the lipoxygenase-inhibitors baicalein and zileuton on the vertebra in ovariectomized rats. <b>2017</b> , 101, 134-144	14
1395	Utility of quantitative micro-computed tomographic analysis in zebrafish to define gene function during skeletogenesis. <b>2017</b> , 101, 162-171	26
1394	Generalized metabolic bone disease and fracture risk in Rothmund-Thomson syndrome. <b>2017</b> , 26, 3046-3055	6
1393	Exercise improves femoral whole-bone and tissue-level biomechanical properties in hyperphagic OLETF rats. <b>2017</b> , 42, 884-892	2
1392	Human type H vessels are a sensitive biomarker of bone mass. <b>2017</b> , 8, e2760	53

1391	Subantibiotic dose of azithromycin attenuates alveolar bone destruction and improves trabecular microarchitectures in a rat model of experimental periodontitis: A study using micro-computed tomography. <b>2017</b> , 47, 212-217	5
1390	Role of Osteoblast Gi Signaling in Age-Related Bone Loss in Female Mice. <b>2017</b> , 158, 1715-1726	4
1389	A method for measuring the three-dimensional orientation of cortical canals with implications for comparative analysis of bone microstructure in vertebrates. <b>2017</b> , 92, 32-38	13
1388	Trabecular Microstructure and Damage Affect Cement Leakage From the Basivertebral Foramen During Vertebral Augmentation. <b>2017</b> , 42, E939-E948	5
1387	Effects of the bilayer nano-hydroxyapatite/mineralized collagen-guided bone regeneration membrane on site preservation in dogs. <b>2017</b> , 32, 242-256	7
1386	Osteoblast-specific deletion of Hrpt2/Cdc73 results in high bone mass and increased bone turnover. <b>2017</b> , 98, 68-78	6
1385	A robust methodology for the quantitative assessment of the rat jawbone microstructure. <b>2017</b> , 9, 87-94	12
1384	The RhoGAP Myo9b Promotes Bone Growth by Mediating Osteoblastic Responsiveness to IGF-1. <i>Journal of Bone and Mineral Research</i> , <b>2017</b> , 32, 2103-2115	9
1383	Thermal inkjet 3D powder printing of metals and alloys: Current status and challenges. <b>2017</b> , 2, 116-123	17
1382	Early bony changes associated with bisphosphonate-related osteonecrosis of the jaws in rats: A longitudinal in vivo study. <b>2017</b> , 82, 79-85	10
1381	Sustained Notch2 signaling in osteoblasts, but not in osteoclasts, is linked to osteopenia in a mouse model of Hajdu-Cheney syndrome. <b>2017</b> , 292, 12232-12244	20
1380	Raloxifene Improves Bone Mechanical Properties in Mice Previously Treated with Zoledronate. <b>2017</b> , 101, 75-81	7
1379	Sex-Dependent, Osteoblast Stage-Specific Effects of Progesterone Receptor on Bone Acquisition. <i>Journal of Bone and Mineral Research</i> , <b>2017</b> , 32, 1841-1852	9
1378	Automated Quantitative Bone Analysis in In Vivo X-ray Micro-Computed Tomography. <b>2017</b> , 36, 1955-1965	6
1377	Ectopic calcification in pseudoxanthoma elasticum responds to inhibition of tissue-nonspecific alkaline phosphatase. <b>2017</b> , 9,	63
1376	MicroCT analysis of vascular morphometry: a comparison of right lung lobes in the SUGEN/hypoxic rat model of pulmonary arterial hypertension. <b>2017</b> , 7, 522-530	13
1375	Bone Mass Is Compromised by the Chemotherapeutic Trabectedin in Association With Effects on Osteoblasts and Macrophage Efferocytosis. <i>Journal of Bone and Mineral Research</i> , <b>2017</b> , 32, 2116-2127 6.3	16
1374	Differential involvement of Wnt signaling in Bmp regulation of cancellous versus periosteal bone growth. <b>2017</b> , 5, 17016	11

1373	Glucocorticoid suppression of osteocyte perilacunar remodeling is associated with subchondral bone degeneration in osteonecrosis. <b>2017</b> , 7, 44618		48
1372	Teriparatide attenuates scarring around murine cranial bone allograft via modulation of angiogenesis. <b>2017</b> , 97, 192-200		12
1371	Relationships among Bone Quality, Implant Osseointegration, and Wnt Signaling. 2017, 96, 822-831		36
1370	Influence of High-Fat Diet on Bone Tissue: An Experimental Study in Growing Rats. <b>2017</b> , 21, 1337-1343		5
1369	Effects of growth hormone treatment on growth plate, bone, and mineral metabolism of young rats with uremia induced by adenine. <b>2017</b> , 82, 148-154		2
1368	Validation of cortical bone mineral density distribution using micro-computed tomography. <b>2017</b> , 99, 53-61		22
1367	Zoledronic acid improves bone histomorphometry in a murine model of Rett syndrome. <b>2017</b> , 99, 1-7		5
1366	Sex dependent mechanical properties of the human mandibular condyle. <b>2017</b> , 71, 184-191		10
1365	Application of a Parallelizable Perfusion Bioreactor for Physiologic 3D Cell Culture. <b>2017</b> , 203, 316-326		22
1364	On the mechanical characteristics of a self-setting calcium phosphate cement. <b>2017</b> , 68, 296-302		1
1363	Inhibition of cathepsin K promotes osseointegration of titanium implants in ovariectomised rats. <b>2017</b> , 7, 44682		11
1362	Cathepsin K Controls Cortical Bone Formation by Degrading Periostin. <i>Journal of Bone and Mineral Research</i> , <b>2017</b> , 32, 1432-1441	.3	42
1361	Altered Bone Mechanics, Architecture and Composition in the Skeleton of TIMP-3-Deficient Mice. <b>2017</b> , 100, 631-640		7
1360	EZH2 deletion in early mesenchyme compromises postnatal bone microarchitecture and structural integrity and accelerates remodeling. <b>2017</b> , 31, 1011-1027		42
1359	Bone Resorption Is Regulated by Circadian Clock in Osteoblasts. <i>Journal of Bone and Mineral Research</i> , <b>2017</b> , 32, 872-881	.3	56
1358	Efficacy and safety of osteoporosis medications in a rat model of late-stage chronic kidney disease accompanied by secondary hyperparathyroidism and hyperphosphatemia. <b>2017</b> , 28, 1481-1490		12
1357	Hairy and Enhancer of Split-Related With YRPW Motif-Like (HeyL) Is Dispensable for Bone Remodeling in Mice. <b>2017</b> , 118, 1819-1826		7
1356	Bone loss at the distal femur and proximal tibia in persons with spinal cord injury: imaging approaches, risk of fracture, and potential treatment options. <b>2017</b> , 28, 747-765		38

1355	Syntaxin 4a Regulates Matrix Vesicle-Mediated Bone Matrix Production by Osteoblasts. <i>Journal of Bone and Mineral Research</i> , <b>2017</b> , 32, 440-448	6.3	3
1354	Bisphosphonate Withdrawal: Effects on Bone Formation and Bone Resorption in Maturing Male Mice. <i>Journal of Bone and Mineral Research</i> , <b>2017</b> , 32, 814-820	6.3	10
1353	Technical note: early post-mortem changes of human bone in taphonomy with IT. 2017, 131, 761-770		9
1352	Age-related periodontitis and alveolar bone loss in rice rats. <b>2017</b> , 73, 193-205		13
1351	Defective signaling, osteoblastogenesis and bone remodeling in a mouse model of connexin 43 C-terminal truncation. <b>2017</b> , 130, 531-540		42
1350	Retinoic acid receptor signalling directly regulates osteoblast and adipocyte differentiation from mesenchymal progenitor cells. <b>2017</b> , 350, 284-297		31
1349	Partial Protection by Dietary Antioxidants Against Ethanol-Induced Osteopenia and Changes in Bone Morphology in Female Mice. <b>2017</b> , 41, 46-56		13
1348	BMI-1 Mediates Estrogen-Deficiency-Induced Bone Loss by Inhibiting Reactive Oxygen Species Accumulation and T Cell Activation. <i>Journal of Bone and Mineral Research</i> , <b>2017</b> , 32, 962-973	6.3	30
1347	Time course of disassociation of bone formation signals with bone mass and bone strength in sclerostin antibody treated ovariectomized rats. <b>2017</b> , 97, 20-28		12
1346	Wnt10b and Dkk-1 gene therapy differentially influenced trabecular bone architecture, soft tissue integrity, and osteophytosis in a skeletally mature rat model of osteoarthritis. <b>2017</b> , 58, 542-552		8
1345	Administration of erythropoietin prevents bone loss in osteonecrosis of the femoral head in mice. <b>2017</b> , 16, 8755-8762		11
1344	WNT-activated bone grafts repair osteonecrotic lesions in aged animals. <b>2017</b> , 7, 14254		7
1343	Lack of Lrp5 Signaling in Osteoblasts Sensitizes Male Mice to Diet-Induced Disturbances in Glucose Metabolism. <b>2017</b> , 158, 3805-3816		3
1342	Mimicking the effects of spaceflight on bone: Combined effects of disuse and chronic low-dose rate radiation exposure on bone mass in mice. <b>2017</b> , 15, 62-68		12
1341	Comparison of the effects of once-weekly and once-daily rhPTH (1-34) injections on promoting fracture healing in rodents. <b>2018</b> , 36, 1145-1152		8
1340	Daily parathyroid hormone administration enhances bone turnover and preserves bone structure after severe immobilization-induced bone loss. <b>2017</b> , 5, e13446		11
1339	Semiautomated Longitudinal Microcomputed Tomography-based Quantitative Structural Analysis of a Nude Rat Osteoporosis-related Vertebral Fracture Model. <b>2017</b> ,		
1338	Thirty days of spaceflight does not alter murine calvariae structure despite increased expression. <b>2017</b> , 7, 57-62		13

1337	Accuracy, precision and inter-rater reliability of micro-CT analysis of false starts on bones. A preliminary validation study. <b>2017</b> , 29, 38-43	16
1336	Chronic psychosocial stress disturbs long-bone growth in adolescent mice. <b>2017</b> , 10, 1399-1409	13
1335	Animal Models in Bone Research. <b>2017</b> , 129-171	3
1334	Sost deficiency led to a greater cortical bone formation response to mechanical loading and altered gene expression. <b>2017</b> , 7, 9435	24
1333	Clcn7 as a new mouse model of Albers-Schfiberg disease. <b>2017</b> , 105, 253-261	6
1332	Comparison of Different Decalcification Methods Using Rat Mandibles as a Model. <b>2017</b> , 65, 705-722	41
1331	One-Step Fabrication of Bone Morphogenetic Protein-2 Gene-Activated Porous Poly-L-Lactide Scaffold for Bone Induction. <b>2017</b> , 7, 50-59	12
1330	Tissue viscoelasticity is related to tissue composition but may not fully predict the apparent-level viscoelasticity in human trabecular bone - An experimental and finite element study. <b>2017</b> , 65, 96-105	17
1329	Downregulation of miR-106b attenuates inflammatory responses and joint damage in collagen-induced arthritis. <b>2017</b> , 56, 1804-1813	32
1328	Effect of celastrol on bone structure and mechanics in arthritic rats. <b>2017</b> , 3, e000438	18
1327	Hibernating Little Pocket Mice Show Few Seasonal Changes in Bone Properties. 2017, 300, 2175-2183	1
1326	Spontaneous mutation of Dock7 results in lower trabecular bone mass and impaired periosteal expansion in aged female Misty mice. <b>2017</b> , 105, 103-114	9
1325	Boldine isolated from Litsea cubeba inhibits bone resorption by suppressing the osteoclast differentiation in collagen-induced arthritis. <b>2017</b> , 51, 114-123	15
1324	An Antibody to Notch2 Reverses the Osteopenic Phenotype of Hajdu-Cheney Mutant Male Mice. <b>2017</b> , 158, 730-742	23
1323	Effects of Tribulus terrestris on monosodium iodoacetate-induced osteoarthritis pain in rats. <b>2017</b> , 16, 5303-5311	7
1322	Role of subchondral bone properties and changes in development of load-induced osteoarthritis in mice. <b>2017</b> , 25, 2108-2118	31
1321	Obesity and type 2 diabetes, not a diet high in fat, sucrose, and cholesterol, negatively impacts bone outcomes in the hyperphagic Otsuka Long Evans Tokushima Fatty rat. <b>2017</b> , 105, 200-211	7
1320	Fabrication of Trabecular Bone-Templated Tissue-Engineered Constructs by 3D Inkjet Printing. <b>2017</b> , 6, 1700369	12

1319	Automatic registration of 2D histological sections to 3D microCT volumes: Trabecular bone. <b>2017</b> , 105, 173-183		3
1318	Development of new experimental platform 'MARS'-Multiple Artificial-gravity Research System-to elucidate the impacts of micro/partial gravity on mice. <b>2017</b> , 7, 10837		48
1317	Meniscal Ossicles as micro-CT Imaging Biomarker in a Rodent Model of Antigen-Induced Arthritis: a Synchrotron-Based X-ray Pilot Study. <b>2017</b> , 7, 7544		4
1316	Cortical and trabecular morphology is altered in the limb bones of mice artificially selected for faster skeletal growth. <b>2017</b> , 7, 10527		10
1315	Patient-specific in silico models can quantify primary implant stability in elderly human bone. <b>2018</b> , 36, 954-962		5
1314	Knockdown of SIRT7 enhances the osteogenic differentiation of human bone marrow mesenchymal stem cells partly via activation of the Wnt/L-catenin signaling pathway. <b>2017</b> , 8, e3042		34
1313	Evaluation of bone formation in calcium phosphate scaffolds with <b>I</b> IT-method validation using SEM. <b>2017</b> , 12, 065005		8
1312	In-situ tissue regeneration through SDF-1Edriven cell recruitment and stiffness-mediated bone regeneration in a critical-sized segmental femoral defect. <b>2017</b> , 60, 50-63		47
1311	Comparison of calcimimetic R568 and calcitriol in mineral homeostasis in the Hyp mouse, a murine homolog of X-linked hypophosphatemia. <b>2017</b> , 103, 224-232		7
1310	Neutron tomographic imaging of bone-implant interface: Comparison with X-ray tomography. <b>2017</b> , 103, 295-301		11
1309	Exogenous hedgehog antagonist delays but does not prevent fracture healing in young mice. <b>2017</b> , 103, 241-251		16
1308	Longitudinal effects of Parathyroid Hormone treatment on morphological, densitometric and mechanical properties of mouse tibia. <b>2017</b> , 75, 244-251		26
1307	Sclerostin Blockade and Zoledronic Acid Improve Bone Mass and Strength in Male Mice With Exogenous Hyperthyroidism. <b>2017</b> , 158, 3765-3777		10
1306	Micro-computed tomography characterization of tissue engineering scaffolds: effects of pixel size and rotation step. <b>2017</b> , 28, 129		19
1305	An Ectosteric Inhibitor of Cathepsin K Inhibits Bone Resorption in Ovariectomized Mice. <i>Journal of Bone and Mineral Research</i> , <b>2017</b> , 32, 2415-2430	6.3	28
1304	Low Doses of Simvastatin Potentiate the Effect of Sodium Alendronate in Inhibiting Bone Resorption and Restore Microstructural and Mechanical Bone Properties in Glucocorticoid-Induced Osteoporosis. <b>2017</b> , 23, 989-1001		10
1303	Comparative bone regeneration study of hardystonite and hydroxyapatite as filler in critical-sized defect of rat calvaria. <b>2017</b> , 7, 37522-37533		7
1302	Impact of Chiropractic Manipulation on Bone and Skeletal Muscle of Ovariectomized Rats. <b>2017</b> , 101, 519-529		2

1301	Commensal Gut Microbiota Immunomodulatory Actions in Bone Marrow and Liver have Catabolic Effects on Skeletal Homeostasis in Health. <b>2017</b> , 7, 5747		55
1300	Conditional knockdown of hyaluronidase 2 in articular cartilage stimulates osteoarthritic progression in a mice model. <b>2017</b> , 7, 7028		7
1299	Calcium and vitamin-D deficiency marginally impairs fracture healing but aggravates posttraumatic bone loss in osteoporotic mice. <b>2017</b> , 7, 7223		23
1298	Reduced bone loss in a murine model of postmenopausal osteoporosis lacking complement component 3. <b>2018</b> , 36, 118-128		11
1297	Tissue-specific mineralization defects in the periodontium of the Hyp mouse model of X-linked hypophosphatemia. <b>2017</b> , 103, 334-346		22
1296	Development of an efficient screening system to identify novel bone metabolism-related genes using the exchangeable gene trap mutagenesis mouse models. <b>2017</b> , 7, 40692		2
1295	Insulin-Stimulated Bone Blood Flow and Bone Biomechanical Properties Are Compromised in Obese, Type 2 Diabetic OLETF Rats. <b>2017</b> , 1, 116-126		2
1294	Treatment With a Soluble Bone Morphogenetic Protein Type 1A Receptor (BMPR1A) Fusion Protein Increases Bone Mass and Bone Formation in Mice Subjected to Hindlimb Unloading. <b>2017</b> , 1, 66-72		10
1293	Metformin Affects Cortical Bone Mass and Marrow Adiposity in Diet-Induced Obesity in Male Mice. <b>2017</b> , 158, 3369-3385		36
1292	Cross-sex testosterone therapy in ovariectomized mice: addition of low-dose estrogen preserves bone architecture. <b>2017</b> , 313, E540-E551		9
1291	Mast Cells Are Critical Regulators of Bone Fracture-Induced Inflammation and Osteoclast Formation and Activity. <i>Journal of Bone and Mineral Research</i> , <b>2017</b> , 32, 2431-2444	6.3	35
1290	Does a Treadmill Running Exercise Contribute to Preventing Deterioration of Bone Mineral Density and Bone Quality of the Femur in KK-Ay Mice, a Type 2 Diabetic Animal Model?. <b>2017</b> , 101, 631-640		5
1289	A kidney-specific genetic control module in mice governs endocrine regulation of the cytochrome P450 gene essential for vitamin D activation. <b>2017</b> , 292, 17541-17558		53
1288	A High-Fat Diet Decreases Bone Mass in Growing Mice with Systemic Chronic Inflammation Induced by Low-Dose, Slow-Release Lipopolysaccharide Pellets. <b>2017</b> , 147, 1909-1916		21
1287	Implanted Dental Pulp Cells Fail to Induce Regeneration in Partial Pulpotomies. 2017, 96, 1406-1413		23
1286	The impact of peripheral serotonin on leptin-brain serotonin axis, bone metabolism and strength in growing rats with experimental chronic kidney disease. <b>2017</b> , 105, 1-10		15
1285	Evidence-Based Advances in Rodent Medicine. <b>2017</b> , 20, 805-816		4
1284	Repeated irradiation from micro-computed tomography scanning at 2, 4 and 6 months of age does not induce damage to tibial bone microstructure in male and female CD-1 mice. <b>2017</b> , 6, 855		20

1283	A standardized Humulus lupulus (L.) ethanol extract partially prevents ovariectomy-induced bone loss in the rat without induction of adverse effects in the uterus. <b>2017</b> , 34, 50-58	19
1282	Gli1 identifies osteogenic progenitors for bone formation and fracture repair. <b>2017</b> , 8, 2043	126
1281	Osteoblasts remotely supply lung tumors with cancer-promoting SiglecF neutrophils. 2017, 358,	172
1280	DJ-1 controls bone homeostasis through the regulation of osteoclast differentiation. <b>2017</b> , 8, 1519	50
1279	Catabolic Effects of Human PTH (1-34) on Bone: Requirement of Monocyte Chemoattractant Protein-1 in Murine Model of Hyperparathyroidism. <b>2017</b> , 7, 15300	17
1278	Bone Mechanical Function and the Gut Microbiota. <b>2017</b> , 1033, 249-270	7
1277	Osteophytes and fracture calluses share developmental milestones and are diminished by unloading. <b>2018</b> , 36, 699-710	10
1276	Effects of strength training and raloxifene on femoral neck metabolism and microarchitecture of aging female Wistar rats. <b>2017</b> , 7, 14410	4
1275	ACVR2B/Fc counteracts chemotherapy-induced loss of muscle and bone mass. <b>2017</b> , 7, 14470	36
1274	Calcitonin-Loaded Thermosensitive Hydrogel for Long-Term Antiosteopenia Therapy. <b>2017</b> , 9, 23428-23440	48
1273	Inducible Activation of FGFR2 in Adult Mice Promotes Bone Formation After Bone Marrow Ablation. <i>Journal of Bone and Mineral Research</i> , <b>2017</b> , 32, 2194-2206	8
1272	DOK3 Modulates Bone Remodeling by Negatively Regulating Osteoclastogenesis and Positively Regulating Osteoblastogenesis. <i>Journal of Bone and Mineral Research</i> , <b>2017</b> , 32, 2207-2218	11
1271	Ecto-5'-nucleotidase (CD73) regulates bone formation and remodeling during intramembranous bone repair in aging mice. <b>2017</b> , 49, 545-551	11
1270	Activin receptor type 2A (ACVR2A) functions directly in osteoblasts as a negative regulator of bone mass. <b>2017</b> , 292, 13809-13822	37
1269	An Independent Active Contours Segmentation framework for bone micro-CT images. <b>2017</b> , 87, 358-370	8
1268	Characterization of the bone-metal implant interface by Digital Volume Correlation of in-situ loading using neutron tomography. <b>2017</b> , 75, 271-278	19
1267	Intermittent parathyroid hormone improve bone microarchitecture of the mandible and femoral head in ovariectomized rats. <b>2017</b> , 18, 171	3
1266	Cranial bone structure in children with sagittal craniosynostosis: Relationship with surgical outcomes. <b>2017</b> , 70, 1589-1597	6

1265	Endochondral Ossification in Critical-Sized Bone Defects via Readily Implantable Scaffold-Free Stem Cell Constructs. <b>2017</b> , 6, 1644-1659		42
1264	Optimally oriented grooves on dental implants improve bone quality around implants under repetitive mechanical loading. <b>2017</b> , 48, 433-444		34
1263	Effects of raloxifene against letrozole-induced bone loss in chemically-induced model of menopause in mice. <b>2017</b> , 440, 34-43		8
1262	Contribution of biomechanical forces to inflammation-induced bone resorption. <b>2017</b> , 44, 31-41		33
1261	Comparison of ex vivo and in vivo micro-computed tomography of rat tibia at different scanning settings. <b>2017</b> , 35, 1690-1698		7
1260	Subchondral bone scan uptake correlates with articular cartilage degeneration in osteoarthritic knees. <b>2017</b> , 20, 1393-1402		5
1259	Microarchitectural study of the augmented bone following ridge preservation with a porcine xenograft and a collagen membrane: preliminary report of a prospective clinical, histological, and micro-computed tomography analysis. <b>2017</b> , 46, 250-260		9
1258	Global molecular changes in a tibial compression induced ACL rupture model of post-traumatic osteoarthritis. <b>2017</b> , 35, 474-485		31
1257	Deletion of FoxO1, 3, and 4 in Osteoblast Progenitors Attenuates the Loss of Cancellous Bone Mass in a Mouse Model of Type 1 Diabetes. <i>Journal of Bone and Mineral Research</i> , <b>2017</b> , 32, 60-69	6.3	21
1256	Reduction of Longitudinal Vertebral Blood Perfusion and Its Likely Causes: A Quantitative Dynamic Contrast-enhanced MR Imaging Study of a Rat Osteoporosis Model. <b>2017</b> , 282, 369-380		20
1255	De novo bone formation underneath the sinus membrane supported by a bone patch: a pilot experiment in rabbit sinus model. <b>2017</b> , 28, 1175-1181		2
1254	IL-36 Induces Bisphosphonate-Related Osteonecrosis of the Jaw-Like Lesions in Mice by Inhibiting TGF-I-Mediated Collagen Expression. <i>Journal of Bone and Mineral Research</i> , <b>2017</b> , 32, 309-318	6.3	26
1253	Silk fibroin membrane used for guided bone tissue regeneration. <b>2017</b> , 70, 148-154		51
1252	Conditional Alpl Ablation Phenocopies Dental Defects of Hypophosphatasia. <b>2017</b> , 96, 81-91		29
1251	DDR2-CYR61-MMP1 Signaling Pathway Promotes Bone Erosion in Rheumatoid Arthritis Through Regulating Migration and Invasion of Fibroblast-Like Synoviocytes. <i>Journal of Bone and Mineral Research</i> , <b>2017</b> , 32, 407-418	6.3	15
1250	Micro-CT based finite element models of cancellous bone predict accurately displacement once the boundary condition is well replicated: A validation study. <b>2017</b> , 65, 644-651		60
1249	Beauty is more than skin deep: a non-invasive protocol for in vivo anatomical study using micro-CT. <b>2017</b> , 8, 358-369		8
1248	Boron supplementation improves bone health of non-obese diabetic mice. <b>2017</b> , 39, 169-175		22

1247	Autoimmune arthritis deteriorates bone quantity and quality of periarticular bone in a mouse model of rheumatoid arthritis. <b>2017</b> , 28, 709-718		7	
1246	Inhibition of SLC7A11 by Sulfasalazine Enhances Osteogenic Differentiation of Mesenchymal Stem Cells by Modulating BMP2/4 Expression and Suppresses Bone Loss in Ovariectomized Mice. <i>Journal of Bone and Mineral Research</i> , <b>2017</b> , 32, 508-521	6.3	17	
1245	Association between subchondral bone structure and osteoarthritis histopathological grade. <b>2017</b> , 35, 785-792		56	
1244	Time course of peri-implant bone regeneration around loaded and unloaded implants in a rat model. <b>2017</b> , 35, 997-1006		7	
1243	Histone deacetylase inhibition enhances in-vivo bone regeneration induced by human periodontal ligament cells. <b>2017</b> , 95, 76-84		20	
1242	Osteogenesis requires FAK-dependent collagen synthesis by fibroblasts and osteoblasts. <b>2017</b> , 31, 937-	953	20	
1241	The Circadian Gene Clock Regulates Bone Formation Via PDIA3. <i>Journal of Bone and Mineral Research</i> , <b>2017</b> , 32, 861-871	6.3	25	
1240	TET3 Mediates Alterations in the Epigenetic Marker 5hmC and Akt pathway in Steroid-Associated Osteonecrosis. <i>Journal of Bone and Mineral Research</i> , <b>2017</b> , 32, 319-332	6.3	19	
1239	Suppression of Sclerostin Alleviates Radiation-Induced Bone Loss by Protecting Bone-Forming Cells and Their Progenitors Through Distinct Mechanisms. <i>Journal of Bone and Mineral Research</i> , <b>2017</b> , 32, 360-372	6.3	65	
1238	Agreement and precision of periprosthetic bone density measurements in micro-CT, single and dual energy CT. <b>2017</b> , 35, 1470-1477		6	
1237	Suppressor of cytokine signaling 2 () deletion protects bone health of mice with DSS-induced inflammatory bowel disease. <b>2018</b> , 11,		8	
1236	Effect of integration time on the morphometric, densitometric and mechanical properties of the mouse tibia. <b>2017</b> , 65, 203-211		20	
1235	Homeostatic Expansion of CD4+ T Cells Promotes Cortical and Trabecular Bone Loss, Whereas CD8+ T Cells Induce Trabecular Bone Loss Only. <b>2017</b> , 216, 1070-1079		7	
1234	Reproduction Differentially Affects Trabecular Bone Depending on Its Mechanical Versus Metabolic Role. <b>2017</b> , 139,		13	
1233	Sanguinarine protects against ovariectomy-induced osteoporosis in mice. <b>2017</b> , 16, 288-294		1	
1232	. 2017,		4	
1231	Dihydromyricetin Protects against Bone Loss in Ovariectomized Mice by Suppressing Osteoclast		13	
	Activity. <b>2017</b> , 8, 928			

1229	Elevated Levels of Peripheral Kynurenine Decrease Bone Strength in Rats with Chronic Kidney Disease. <b>2017</b> , 8, 836	21
1228	Micro-Computed-Tomography-Guided Analysis of In Vitro Structural Modifications in Two Types of 45S5 Bioactive Glass Based Scaffolds. <b>2017</b> , 10,	11
1227	Imipramine Protects against Bone Loss by Inhibition of Osteoblast-Derived Microvesicles. 2017, 18,	26
1226	Three-dimensional structural analysis of the morphological condition of the alveolar bone before and after orthodontic treatment. <b>2017</b> , 47, 394-400	1
1225	Calcium Supplement Derived from Gallus gallus domesticus Promotes BMP-2/RUNX2/SMAD5 and Suppresses TRAP/RANK Expression through MAPK Signaling Activation. <b>2017</b> , 9,	17
1224	Beta Palmitate Improves Bone Length and Quality during Catch-Up Growth in Young Rats. 2017, 9,	1
1223	Quantification of Bone Fatty Acid Metabolism and Its Regulation by Adipocyte Lipoprotein Lipase. <b>2017</b> , 18,	21
1222	Marrow Adipose Tissue: Skeletal Location, Sexual Dimorphism, and Response to Sex Steroid Deficiency. <b>2017</b> , 8, 188	29
1221	Exenatide Improves Bone Quality in a Murine Model of Genetically Inherited Type 2 Diabetes Mellitus. <b>2017</b> , 8, 327	14
1220	3D Architecture of Trabecular Bone in the Pig Mandible and Femur: Inter-Trabecular Angle Distributions. <b>2017</b> , 4,	15
1219	Contrast-Enhanced Microtomographic Characterisation of Vessels in Native Bone and Engineered Vascularised Grafts Using Ink-Gelatin Perfusion and Phosphotungstic Acid. <b>2017</b> , 2017, 4035160	7
1218	Role of Periapical Diseases in Medication-Related Osteonecrosis of the Jaws. <b>2017</b> , 2017, 1560175	6
1217	Icariin Regulates the Bidirectional Differentiation of Bone Marrow Mesenchymal Stem Cells through Canonical Wnt Signaling Pathway. <b>2017</b> , 2017, 8085325	25
1216	Dose- and Ion-Dependent Effects in the Oxidative Stress Response to Space-Like Radiation Exposure in the Skeletal System. <b>2017</b> , 18,	15
1215	3.26 Imaging Mineralized Tissues in Vertebrates. <b>2017</b> , 549-578	1
1214	Effects of remote ischemic post-conditioning on fracture healing in rats. <b>2017</b> , 15, 3186-3192	6
1213	Recipient Glycemic Micro-environments Govern Therapeutic Effects of Mesenchymal Stem Cell Infusion on Osteopenia. <b>2017</b> , 7, 1225-1244	26
1212	Proper Positioning and Restraint of a Rat Hind Limb for Focused High Resolution Imaging of Bone Micro-architecture Using In Vivo Micro-computed Tomography. <b>2017</b> ,	4

1211	Repeated administration of mazindol reduces spontaneous pain-related behaviors without modifying bone density and microarchitecture in a mouse model of complete Freund's adjuvant-induced knee arthritis. <b>2017</b> , 10, 1777-1786	6
1210	Effects of Loading Duration and Short Rest Insertion on Cancellous and Cortical Bone Adaptation in the Mouse Tibia. <b>2017</b> , 12, e0169519	23
1209	Pulsed lavage cleansing of osteochondral grafts depends on lavage duration, flow intensity, and graft storage condition. <b>2017</b> , 12, e0176934	12
1208	Role of HTRA1 in bone formation and regeneration: In vitro and in vivo evaluation. <b>2017</b> , 12, e0181600	7
1207	Simulated space radiation sensitizes bone but not muscle to the catabolic effects of mechanical unloading. <b>2017</b> , 12, e0182403	20
1206	Model of hindlimb unloading in adult female rats: Characterizing bone physicochemical, microstructural, and biomechanical properties. <b>2017</b> , 12, e0189121	15
1205	Fully automated segmentation of callus by micro-CT compared to biomechanics. 2017, 12, 108	3
1204	Injectable and compression-resistant low-viscosity polymer/ceramic composite carriers for rhBMP-2 in a rabbit model of posterolateral fusion: a pilot study. <b>2017</b> , 12, 107	4
1203	Protein deubiquitinase USP7 is required for osteogenic differentiation of human adipose-derived stem cells. <b>2017</b> , 8, 186	19
1202	The inflammatory phase of fracture healing is influenced by oestrogen status in mice. <b>2017</b> , 22, 23	27
1201	A rodent model of caloric restriction using bone mass, microarchitecture, and stable isotope ratios: implications for revealing chronic food insufficiency in archaeological populations. <b>2017</b> , 3, 100-111	3
1200	Protective effect of Rhizoma Dioscoreae extract against alveolar bone loss in ovariectomized rats via regulation of IL-6/STAT3 signaling. <b>2017</b> , 40, 1602-1610	1
1199	Sustained intra-cartilage delivery of low dose dexamethasone using a cationic carrier for treatment of post traumatic osteoarthritis. <b>2017</b> , 34, 341-364	49
1198	Meloxicam as a Radiation-Protective Agent on Mandibles of Irradiated Rats. <b>2017</b> , 28, 249-255	6
1197	Knockin mouse with mutant G mimics human inherited hypocalcemia and is rescued by pharmacologic inhibitors. <b>2017</b> , 2, e91079	23
1196	MYC-dependent oxidative metabolism regulates osteoclastogenesis via nuclear receptor ERR⊞ <b>2017</b> , 127, 2555-2568	56
1195	A novel osteoporosis model with ascorbic acid deficiency in Akr1A1 gene knockout mice. <b>2017</b> , 8, 7357-7369	5
1194	Genetic Dissection of Trabecular Bone Structure with Mouse Intersubspecific Consomic Strains. <b>2017</b> , 7, 3449-3457	2

1193	Old age causes de novo intracortical bone remodeling and porosity in mice. 2017, 2,		91
1192	The high bone mass phenotype of Lrp5-mutant mice is not affected by megakaryocyte depletion. <b>2018</b> , 497, 659-666		
1191	Locomotor activity, growth hormones, and systemic robusticity: An investigation of cranial vault thickness in mouse lines bred for high endurance running. <b>2018</b> , 166, 442-458		9
1190	P2X7 receptor regulates osteoclast function and bone loss in a mouse model of osteoporosis. <b>2018</b> , 8, 3507		23
1189	Combining advantages: Direct correlation of two-dimensional microcomputed tomography datasets onto histomorphometric slides to quantify three-dimensional bone volume in scaffolds. <b>2018</b> , 106, 1812-1821		4
1188	Disease Duration and Stage Influence Bone Microstructure in Patients With Primary Biliary Cholangitis. <i>Journal of Bone and Mineral Research</i> , <b>2018</b> , 33, 1011-1019	6.3	14
1187	Neutralization of CD40 ligand costimulation promotes bone formation and accretion of vertebral bone mass in mice. <b>2018</b> , 57, 1105-1114		6
1186	The Advantages of Bilateral Osteotomy Over Unilateral Osteotomy for Osteoporotic Bone Healing. <b>2018</b> , 103, 80-94		7
1185	Pharmacological inhibition of IL-6 trans-signaling improves compromised fracture healing after severe trauma. <b>2018</b> , 391, 523-536		27
1184	Investigating the Longitudinal Effect of Ovariectomy on Bone Properties Using a Novel Spatiotemporal Approach. <b>2018</b> , 46, 749-761		6
1183	CTLA-4Ig (abatacept) balances bone anabolic effects of T cells and Wnt-10b with antianabolic effects of osteoblastic sclerostin. <b>2018</b> , 1415, 21-33		6
1182	PTH (1-34) and growth hormone in prevention of disuse osteopenia and sarcopenia in rats. <b>2018</b> , 110, 244-253		24
1181	Functional morphology in the pages of the AJPA. <b>2018</b> , 165, 688-704		2
1180	Targeting sphingosine-1-phosphate lyase as an anabolic therapy for bone loss. <b>2018</b> , 24, 667-678		62
1179	NOX4 Deletion in Male Mice Exacerbates the Effect of Ethanol on Trabecular Bone and Osteoblastogenesis. <b>2018</b> , 366, 46-57		12
1178	Microstructural properties of trabecular bone autografts: comparison of men and women with and without osteoporosis. <b>2018</b> , 13, 18		10
1177	Respective role of membrane and nuclear estrogen receptor (ER) In the mandible of growing mice: Implications for ERI modulation. <i>Journal of Bone and Mineral Research</i> , <b>2018</b> , 33, 1520-1531	6.3	6
1176	WAIF1 Is a Cell-Surface CTHRC1 Binding Protein Coupling Bone Resorption and Formation. <i>Journal of Bone and Mineral Research</i> , <b>2018</b> , 33, 1500-1512	6.3	11

1175	Regulation of Vascular Calcification by Growth Hormone-Releasing Hormone and Its Agonists. <b>2018</b> , 122, 1395-1408		23	
1174	Induction of the Hajdu-Cheney Syndrome Mutation in CD19 B Cells in Mice Alters B-Cell Allocation but Not Skeletal Homeostasis. <b>2018</b> , 188, 1430-1446		5	
1173	Alendronate induces osteoclast precursor apoptosis via peroxisomal dysfunction mediated ER stress. <b>2018</b> , 233, 7415-7423		17	
1172	Trabecular Anisotropy in the Primate Mandibular Condyle Is Associated with Dietary Toughness. <b>2018</b> , 301, 1342-1359		4	
1171	Superior cortical screw in osteoporotic lumbar vertebrae: A biomechanics and microstructure-based study. <b>2018</b> , 53, 14-21		4	
1170	Penalized-Likelihood Reconstruction With High-Fidelity Measurement Models for High-Resolution Cone-Beam Imaging. <b>2018</b> , 37, 988-999		15	
1169	Biomechanical, Histologic, and Molecular Evaluation of Tendon Healing in a New Murine Model of Rotator Cuff Repair. <b>2018</b> , 34, 1173-1183		27	
1168	Lactation induces increases in the RANK/RANKL/OPG system in maxillary bone. 2018, 110, 160-169		16	
1167	Galectin-3 is essential for proper bone cell differentiation and activity, bone remodeling and biomechanical competence in mice. <b>2018</b> , 83, 149-158		14	
1166	The p55TNFR-IKK2-Ripk3 axis orchestrates arthritis by regulating death and inflammatory pathways in synovial fibroblasts. <b>2018</b> , 9, 618		23	
1165	A Complex Role for Lipocalin 2 in Bone Metabolism: Global Ablation in Mice Induces Osteopenia Caused by an Altered Energy Metabolism. <i>Journal of Bone and Mineral Research</i> , <b>2018</b> , 33, 1141-1153	6.3	21	
1164	Tributyltin induces distinct effects on cortical and trabecular bone in female C57Bl/6J mice. <b>2018</b> , 233, 7007-7021		11	
1163	Characterization of bone morphology in CCN5/WISP5 knockout mice. 2018, 12, 265-270		4	
1162	CYR61/CCN1 Regulates Sclerostin Levels and Bone Maintenance. <i>Journal of Bone and Mineral Research</i> , <b>2018</b> , 33, 1076-1089	6.3	16	
1161	Electrodeless Reverse Electrodialysis Patches as an Ionic Power Source for Active Transdermal Drug Delivery. <b>2018</b> , 28, 1705952		9	
1160	Recent advances in articular cartilage evaluation using computed tomography and magnetic resonance imaging. <b>2018</b> , 50, 564-579		18	
1159	An effective delivery vehicle of demineralized bone matrix incorporated with engineered collagen-binding human bone morphogenetic protein-2 to accelerate spinal fusion at low dose. <b>2017</b> , 29, 2		9	
1158	Age-related changes of CD4 T cell migration and cytokine expression in germ-free and SPF mice periodontium. <b>2018</b> , 87, 72-78		7	

1157	Estrogen Deficiency-Mediated M2 Macrophage Osteoclastogenesis Contributes to M1/M2 Ratio Alteration in Ovariectomized Osteoporotic Mice. <i>Journal of Bone and Mineral Research</i> , <b>2018</b> , 33, 899-90	8.3	57	
1156	The effect of oral dabigatran etexilate on bone density, strength, and microstructure in healthy mice. <b>2018</b> , 8, 9-17		8	
1155	Impact of Temporomandibular Joint Discectomy on Condyle Morphology: An Animal Study. <b>2018</b> , 76, 955.e1-955.e5		4	
1154	Expression of an active G#mutant in skeletal stem cells is sufficient and necessary for fibrous dysplasia initiation and maintenance. <b>2018</b> , 115, E428-E437		23	
1153	Osteoporosis is associated with metabolic syndrome induced by high-carbohydrate high-fat diet in a rat model. <b>2018</b> , 98, 191-200		26	
1152	Effect of Strontium Ranelate on the Muscle and Vertebrae of Ovariectomized Rats. 2018, 102, 705-719		8	
1151	Comparative study of volumetric changes and trabecular microarchitecture in human maxillary sinus bone augmentation with bioactive glass and autogenous bone graft: a prospective and randomized assessment. <b>2018</b> , 47, 665-671		13	
1150	Genetic and Molecular Insights Into Genotype-Phenotype Relationships in Osteopathia Striata With Cranial Sclerosis (OSCS) Through the Analysis of Novel Mouse Wtx Mutant Alleles. <i>Journal of Bone and Mineral Research</i> , <b>2018</b> , 33, 875-887	6.3	5	
1149	Roles of Irisin in the Linkage from Muscle to Bone During Mechanical Unloading in Mice. <b>2018</b> , 103, 24-3	4	29	
1148	Skeletal Characterization of the Fgfr3 Mouse Model of Achondroplasia Using Micro-CT and MRI Volumetric Imaging. <b>2018</b> , 8, 469		6	
1147	Protein Kinase G Activation Reverses Oxidative Stress and Restores Osteoblast Function and Bone Formation in Male Mice With Type 1 Diabetes. <b>2018</b> , 67, 607-623		33	
1146	Effects of mechanical loading on cortical defect repair using a novel mechanobiological model of bone healing. <b>2018</b> , 108, 145-155		30	
1145	Cdc42 Is Essential for Both Articular Cartilage Degeneration and Subchondral Bone Deterioration in Experimental Osteoarthritis. <i>Journal of Bone and Mineral Research</i> , <b>2018</b> , 33, 945-958	6.3	20	
1144	High-fat/high-sucrose diet results in higher bone mass in aged rats. <b>2018</b> , 8, 18-24		6	
1143	A WNT protein therapeutic improves the bone-forming capacity of autografts from aged animals. <b>2018</b> , 8, 119		12	
1142	Simultaneous three-dimensional visualization of mineralized and soft skeletal tissues by a novel microCT contrast agent with polyoxometalate structure. <b>2018</b> , 159, 1-12		36	
1141	Ostm1 Bifunctional Roles in Osteoclast Maturation: Insights From a Mouse Model Mimicking a Human OSTM1 Mutation. <i>Journal of Bone and Mineral Research</i> , <b>2018</b> , 33, 888-898	6.3	12	
1140	Long-Term Quantitative Evaluation of Muscle and Bone Wasting Induced by Botulinum Toxin in Mice Using Microcomputed Tomography. <b>2018</b> , 102, 695-704		6	

1139	LRRC15 promotes osteogenic differentiation of mesenchymal stem cells by modulating p65 cytoplasmic/nuclear translocation. <b>2018</b> , 9, 65	11
1138	The Interaction of BMP2-Induced Defect Healing in Rat and Fixator Stiffness Modulates Matrix Alignment and Contraction. <b>2018</b> , 2, 174-186	5
1137	Cx43 overexpression in osteocytes prevents osteocyte apoptosis and preserves cortical bone quality in aging mice. <b>2018</b> , 2, 206-216	28
1136	Healing of fractures in osteoporotic bones in mice treated with bisphosphonates - A transcriptome analysis. <b>2018</b> , 112, 107-119	18
1135	Sclerostin Antibody Treatment Stimulates Bone Formation to Normalize Bone Mass in Male Down Syndrome Mice. <b>2018</b> , 2, 47-54	7
1134	Opioids delay healing of spinal fusion: a rabbit posterolateral lumbar fusion model. <b>2018</b> , 18, 1659-1668	21
1133	Type 2 diabetes impairs angiogenesis and osteogenesis in calvarial defects: MicroCT study in ZDF rats. <b>2018</b> , 112, 161-172	16
1132	An osteopenic/osteoporotic phenotype delays alveolar bone repair. <b>2018</b> , 112, 212-219	32
1131	Humanization of bone and bone marrow in an orthotopic site reveals new potential therapeutic targets in osteosarcoma. <b>2018</b> , 171, 230-246	27
1130	Temporary inhibition of the plasminogen activator inhibits periosteal chondrogenesis and promotes periosteal osteogenesis during appendicular bone fracture healing. <b>2018</b> , 112, 97-106	3
1129	Histone demethylase LSD1 regulates bone mass by controlling WNT7B and BMP2 signaling in osteoblasts. <b>2018</b> , 6, 14	29
1128	Soy Protein Isolate Suppresses Bone Resorption and Improves Trabecular Microarchitecture in Spontaneously Hyperphagic, Rapidly Growing Male OLETF Rats. <b>2018</b> , 2, nzy010	4
1127	A novel mouse model of intervertebral disc degeneration shows altered cell fate and matrix homeostasis. <b>2018</b> , 70, 102-122	53
1126	Inducible inactivation: WNT16 regulates cortical bone thickness in adult mice. <b>2018</b> , 237, 113-122	20
1125	Treatment with anti-Sclerostin antibody to stimulate mandibular bone formation. 2018, 40, 1453-1460	6
1124	Protein kinase D1 conditional null mice show minimal bone loss following ovariectomy. <b>2018</b> , 474, 176-183	1
1123	Outer-Boundary Assisted Segmentation and Quantification of Trabecular Bones by an Imagej Plugin. <b>2018</b> ,	
1122	Steroid-associated osteonecrosis animal model in rats. <b>2018</b> , 13, 13-24	26

1121	Adipose mesenchymal stem cells from osteoporotic donors preserve functionality and modulate systemic inflammatory microenvironment in osteoporotic cytotherapy. <b>2018</b> , 8, 5215	19
1120	Collagen and mPCL-TCP scaffolds induced differential bone regeneration in ovary-intact and ovariectomized rats. <b>2018</b> , 29, 389-399	1
1119	Beneficial effects of paeoniflorin on osteoporosis induced by high-carbohydrate, high-fat diet-associated hyperlipidemia in vivo. <b>2018</b> , 498, 981-987	8
1118	Structural and functional properties of bone are compromised in amyotrophic lateral sclerosis mice. <b>2018</b> , 19, 457-462	4
1117	A rat model of SHPT with bone abnormalities in CKD induced by adenine and a high phosphorus diet. <b>2018</b> , 498, 654-659	9
1116	RNA interference therapy for autosomal dominant osteopetrosis type 2. Towards the preclinical development. <b>2018</b> , 110, 343-354	15
1115	Contribution of metabolic disease to bone fragility in MAGP1-deficient mice. 2018, 67, 1-14	7
1114	Tristetraprolin Is Required for Alveolar Bone Homeostasis. <b>2018</b> , 97, 946-953	9
1113	Combination of hindlimb suspension and immobilization by casting exaggerates sarcopenia by stimulating autophagy but does not worsen osteopenia. <b>2018</b> , 110, 29-37	13
1112	A soluble activin type IIA receptor mitigates the loss of femoral neck bone strength and cancellous bone mass in a mouse model of disuse osteopenia. <b>2018</b> , 110, 326-334	12
1111	Local application of lactoferrin promotes bone regeneration in a rat critical-sized calvarial defect model as demonstrated by micro-CT and histological analysis. <b>2018</b> , 12, e620-e626	26
1110	Role of follistatin in muscle and bone alterations induced by gravity change in mice. <b>2018</b> , 233, 1191-1201	28
1109	Disuse osteopenia induced by botulinum toxin is similar in skeletally mature young and aged female C57BL/6J mice. <b>2018</b> , 36, 170-179	11
1108	Tubular open-porous Iltricalcium phosphate polycaprolactone scaffolds as guiding structure for segmental bone defect regeneration in a novel sheep model. <b>2018</b> , 12, 897-911	15
1107	Serum CTX levels and histomorphometric analysis in Src versus RANKL knockout mice. <b>2018</b> , 36, 264-273	6
1106	Sinus floor elevation using implants coated with recombinant human bone morphogenetic protein-2: micro-computed tomographic and histomorphometric analyses. <b>2018</b> , 22, 829-837	3
1105	Pharmacological inhibition of tankyrase induces bone loss in mice by increasing osteoclastogenesis. <b>2018</b> , 106, 156-166	23
1104	A Novel Diterpenoid Suppresses Osteoclastogenesis and Promotes Osteogenesis by Inhibiting Ifrd1-Mediated and IBHMediated p65 Nuclear Translocation. <i>Journal of Bone and Mineral Research</i> , 2018, 33, 667-678	38

1103	Animal models to explore the effects of glucocorticoids on skeletal growth and structure. <b>2018</b> , 236, R69-R91		23
1102	Modeling and evaluation of a high-resolution CMOS detector for cone-beam CT of the extremities. <b>2018</b> , 45, 114-130		16
1101	Quantitative imaging of peripheral trabecular bone microarchitecture using MDCT. <b>2018</b> , 45, 236-249		23
1100	I-Catenin Directs Long-Chain Fatty Acid Catabolism in the Osteoblasts of Male Mice. <b>2018</b> , 159, 272-284		20
1099	Understanding gene functions and disease mechanisms: Phenotyping pipelines in the German Mouse Clinic. <b>2018</b> , 352, 187-196		12
1098	Standardization of Small Animal Imaging-Current Status and Future Prospects. <b>2018</b> , 20, 716-731		16
1097	Is bone analysis with <code>©T</code> useful for short postmortem interval estimation?. <b>2018</b> , 132, 269-277		3
1096	Loss of the nutrient sensor TAS1R3 leads to reduced bone resorption. <b>2018</b> , 74, 3-8		6
1095	Loading-Induced Reduction in Sclerostin as a Mechanism of Subchondral Bone Plate Sclerosis in Mouse Knee Joints During Late-Stage Osteoarthritis. <b>2018</b> , 70, 230-241		31
1094	PFMG1 promotes osteoblast differentiation and prevents osteoporotic bone loss. <b>2018</b> , 32, 838-849		5
1093	Conductive gelatin methacrylate-poly(aniline) hydrogel for cell encapsulation. 2018, 4, 015005		11
1092	High Bone Turnover in Mice Carrying a Pathogenic Notch2 Mutation Causing Hajdu-Cheney Syndrome. <i>Journal of Bone and Mineral Research</i> , <b>2018</b> , 33, 70-83	-3	17
1091	Biomechanics and Microstructural Analysis of the Mouse Knee and Ligaments. 2018, 31, 520-527		4
1090	The mechanism of thoracolumbar burst fracture may be related to the basivertebral foramen. <b>2018</b> , 18, 472-481		5
1089	Reduced Serum IGF-1 Associated With Hepatic Osteodystrophy Is a Main Determinant of Low Cortical but Not Trabecular Bone Mass. <i>Journal of Bone and Mineral Research</i> , <b>2018</b> , 33, 123-136	.3	11
1088	Local delivery of strontium ranelate promotes regeneration of critical size bone defects filled with collagen sponge. <b>2018</b> , 106, 333-341		10
1087	Longitudinal Effects of Single Hindlimb Radiation Therapy on Bone Strength and Morphology at Local and Contralateral Sites. <i>Journal of Bone and Mineral Research</i> , <b>2018</b> , 33, 99-112	.3	16
1086	Impairment of Bone Remodeling in LIGHT/TNFSF14-Deficient Mice. <i>Journal of Bone and Mineral Research</i> , <b>2018</b> , 33, 704-719	.3	10

1085	IGFBP7 regulates the osteogenic differentiation of bone marrow-derived mesenchymal stem cells via Wnt/II-catenin signaling pathway. <b>2018</b> , 32, 2280-2291	33
1084	Strontium and bisphosphonate coated iron foam scaffolds for osteoporotic fracture defect healing. <b>2018</b> , 157, 1-16	55
1083	Metabolic Syndrome and Bone: Pharmacologically Induced Diabetes has Deleterious Effect on Bone in Growing Obese Rats. <b>2018</b> , 102, 683-694	7
1082	Distinct Effects of IL-6 Classic and Trans-Signaling in Bone Fracture Healing. <b>2018</b> , 188, 474-490	54
1081	LOX-related collagen crosslink changes act as an initiator of bone fragility in a ZDF rats model. <b>2018</b> , 495, 821-827	6
1080	Imbalanced Osteogenesis and Adipogenesis in Mice Deficient in the Chemokine Cxcl12/Sdf1 in the Bone Mesenchymal Stem/Progenitor Cells. <i>Journal of Bone and Mineral Research</i> , <b>2018</b> , 33, 679-690	15
1079	Kit Mutation Prevents Cancellous Bone Loss during Calcium Deprivation. 2018, 102, 93-104	1
1078	Forces associated with launch into space do not impact bone fracture healing. <b>2018</b> , 16, 52-62	10
1077	Neuronal Cell Adhesion Molecule 1 Regulates Leptin Sensitivity and Bone Mass. 2018, 102, 329-336	4
1076	Loss of PiT-2 results in abnormal bone development and decreased bone mineral density and length in mice. <b>2018</b> , 495, 553-559	13
1075	Neuropeptide Y Y2 antagonist treated ovariectomized mice exhibit greater bone mineral density. <b>2018</b> , 67, 45-55	7
1074	Effects of tofacitinib in early arthritis-induced bone loss in an adjuvant-induced arthritis rat model. <b>2018</b> , 57, 1461-1471	20
1073	Bone quality evaluation of experimental osteometabolic disease in Pantanal alligators (Caiman yacare) by High Resolution Computerized Microtomography (ITT). <b>2018</b> , 38, 981-990	1
1072	Microwave Sintering of Ti6Al4V: Optimization of Processing Parameters for Maximal Tensile Strength and Minimal Pore Size. <b>2018</b> , 8, 1086	3
1071	Inhibition of HIF-1H estrains fracture healing via regulation of autophagy in a rat model. <b>2019</b> , 17, 1884-1890	3
1070	X-ray microtomography in herpetological research: a review. <b>2018</b> , 39, 377-401	18
1069	Effects of strontium ranelate on wear particle-induced aseptic loosening in female ovariectomized mice. <b>2018</b> , 18, 1849-1857	3
1068	Bone Healing in Rabbit Calvaria Defects Using a Synthetic Bone Substitute: A Histological and Micro-CT Comparative Study. <b>2018</b> , 11,	10

1067	The Polyphenolic Compound Hesperidin and Bone Protection. <b>2018</b> , 431-440	3
1066	Optimizing bone wound healing using BMP2 with absorbable collagen sponge and Talymed nanofiber scaffold. <b>2018</b> , 16, 321	15
1065	Can repeated in vivo micro-CT irradiation during adolescence alter bone microstructure, histomorphometry and longitudinal growth in a rodent model?. <b>2018</b> , 13, e0207323	15
1064	Raman Spectroscopic Analysis to Detect Reduced Bone Quality after Sciatic Neurectomy in Mice. <b>2018</b> , 23,	14
1063	Iron-enriched diet contributes to early onset of osteoporotic phenotype in a mouse model of hereditary hemochromatosis. <b>2018</b> , 13, e0207441	11
1062	Masseter muscle atrophy impairs bone quality of the mandibular condyle but not the alveolar process early after induction. <b>2019</b> , 46, 233-241	10
1061	In-Line X-Ray Phase Tomography of Bone and Biomaterials for Regenerative Medicine. 2018, 91-109	
1060	Influences of donor and host age on human muscle-derived stem cell-mediated bone regeneration. <b>2018</b> , 9, 316	7
1059	The Microbial Metabolite Butyrate Stimulates Bone Formation via T Regulatory Cell-Mediated Regulation of WNT10B Expression. <b>2018</b> , 49, 1116-1131.e7	144
1058	Mettl3-mediated mA RNA methylation regulates the fate of bone marrow mesenchymal stem cells and osteoporosis. <b>2018</b> , 9, 4772	153
1057	Blackcurrant Supplementation Improves Trabecular Bone Mass in Young but Not Aged Mice. <b>2018</b> , 10,	9
1056	Error introduced by common reorientation algorithms in the assessment of rodent trabecular morphometry using micro-computed tomography. <b>2018</b> , 36, 2762-2770	
1055	Prevalence of glucocorticoid induced osteonecrosis in the mouse is not affected by treatments that maintain bone vascularity. <b>2018</b> , 9, 181-187	6
1054	Self-assembled micro-computed tomography for dental education. <b>2018</b> , 13, e0209698	5
1053	Effect of anti-angiogenesis induced by chemotherapeutic monotherapy, chemotherapeutic/bisphosphonate combination therapy and anti-VEGFA mAb therapy on tooth extraction socket healing in mice. <b>2018</b> , 36, 547-559	19
1052	Histological and micro-computed tomography evaluations of newly formed bone after maxillary sinus augmentation using a xenograft with similar density and mineral content of bone: An experimental study in rabbits. <b>2018</b> , 4, 284-290	11
1051	ALK5 transfection of bone marrow mesenchymal stem cells to repair osteoarthritis of knee joint. <b>2018</b> , 1, 135-145	1
1050	Differential effects of type 1 diabetes mellitus and subsequent osteoblastic I-catenin activation on trabecular and cortical bone in a mouse model. <b>2018</b> , 50, 1-14	11

1049	Gender-independent efficacy of mesenchymal stem cell therapy in sex hormone-deficient bone loss via immunosuppression and resident stem cell recovery. <b>2018</b> , 50, 1-14	25
1048	Relationships of Ultrasonic Backscatter With Bone Densities and Microstructure in Bovine Cancellous Bone. <b>2018</b> , 65, 2311-2321	15
1047	The Contribution of Alcohol Dehydrogenase 3 to the Development of Alcoholic Osteoporosis in Mice. <b>2018</b> , 85, 322-329	6
1046	A multi-factorial analysis of bone morphology and fracture strength of rat femur in response to ovariectomy. <b>2018</b> , 13, 318	12
1045	Irisin Mediates Effects on Bone and Fat via ₩ Integrin Receptors. 2018, 175, 1756-1768.e17	207
1044	Gelatin coating increases in vivo bone formation capacity of three-dimensional 45S5 bioactive glass-based crystalline scaffolds. <b>2019</b> , 13, 179-190	5
1043	Identifying animal taxa used to manufacture bone tools during the Middle Stone Age at Sibudu, South Africa: Results of a CT-rendered histological analysis. <b>2018</b> , 13, e0208319	5
1042	FasL Modulates Expression of in Osteoblasts. <b>2018</b> , 9, 1314	7
1041	Bone protection by inhibition of microRNA-182. <b>2018</b> , 9, 4108	45
1040	Hesperetin Prevents Bone Resorption by Inhibiting RANKL-Induced Osteoclastogenesis and Jnk Mediated Irf-3/c-Jun Activation. <b>2018</b> , 9, 1028	21
1039	Novel magnetic resonance technique for characterizing mesoscale structure of trabecular bone. <b>2018</b> , 5, 180563	3
1038	Intrauterine Programming of Glucocorticoid-Insulin-Like Growth Factor-1 Axis-Mediated Developmental Origin of Osteoporosis Susceptibility in Female Offspring Rats with Prenatal Caffeine Exposure. <b>2018</b> , 188, 2863-2876	14
1037	Studying Osteoarthritis Pathogenesis in Mice. <b>2018</b> , 8, e50	6
1036	Micro-CT - a digital 3D microstructural voyage into scaffolds: a systematic review of the reported methods and results. <b>2018</b> , 22, 26	39
1035	Quantification of the mandibular defect healing by micro-CT morphometric analysis in rats. <b>2018</b> , 46, 2203-2213	12
1034	Bisphosphonates reduce biomaterial turnover in healing of critical-size rat femoral defects. <b>2018</b> , 26, 2309499018802487	6
1033	Parathyroid Hormone (PTH) Increases Skeletal Tumour Growth and Alters Tumour Distribution in an In Vivo Model of Breast Cancer. <b>2018</b> , 19,	6
1032	The Antiosteoporosis Effects of Zhuanggu Guanjie Pill and. <b>2018</b> , 2018, 9075318	4

1031	FOXO1 Deletion Reverses the Effect of Diabetic-Induced Impaired Fracture Healing. 2018, 67, 2682-2694	21
1030	Loss of Gs∄n osteocytes leads to osteopenia due to sclerostin induced suppression of osteoblast activity. <b>2018</b> , 117, 138-148	11
1029	Microbubble-Mediated Ultrasound Outweighs Low-Intensity Pulsed Ultrasound on Osteogenesis and Neovascularization in a Rabbit Model of Steroid-Associated Osteonecrosis. <b>2018</b> , 2018, 4606791	3
1028	Glucocorticoids cause mandibular bone fragility and suppress osteocyte perilacunar-canalicular remodeling. <b>2018</b> , 9, 145-153	11
1027	Dose of alendronate directly increases trabeculae expansivity without altering bone volume in rat femurs. <b>2018</b> , 9, 190-197	3
1026	Antiresorptive Agents are More Effective in Preventing Titanium Particle-Induced Calvarial Osteolysis in Ovariectomized Mice Than Anabolic Agents in Short-Term Administration. <b>2018</b> , 42, E259-E271	7
1025	Different bone sites-specific response to diabetes rat models: Bone density, histology and microarchitecture. <b>2018</b> , 13, e0205503	7
1024	Diosgenin protects against alveolar bone loss in ovariectomized rats via regulating long non-coding RNAs. <b>2018</b> , 16, 3939-3950	7
1023	Synthetic Peptide CK2.3 Enhances Bone Mineral Density in Senile Mice. <b>2018</b> , 6,	5
1022	Assessment of Bone Mass, Structure, and Quality in Rodents. <b>2018</b> , 93-100	2
1021	Bone-Fracture-Targeted Dasatinib-Oligoaspartic Acid Conjugate Potently Accelerates Fracture Repair. <b>2018</b> , 29, 3800-3809	15
1020	Comparative Transcriptomics Identifies Novel Genes and Pathways Involved in Post-Traumatic Osteoarthritis Development and Progression. <b>2018</b> , 19,	18
1019	Computer-based automatic classification of trabecular bone pattern can assist radiographic bone quality assessment at dental implant site. <b>2018</b> , 91, 20180437	5
1018	Low temperature decreases bone mass in mice: Implications for humans. <b>2018</b> , 167, 557-568	13
1017	Plastin 3 influences bone homeostasis through regulation of osteoclast activity. <b>2018</b> , 27, 4249-4262	27
1016	A bone mineralization defect in the Pah model of classical phenylketonuria involves compromised mesenchymal stem cell differentiation. <b>2018</b> , 125, 193-199	11
1015	Combination therapy with BMP-2 and psoralen enhances fracture healing in ovariectomized mice. <b>2018</b> , 16, 1655-1662	7
1014	Expression of vitamin D hydroxylases and bone quality in obese mice consuming saturated or monounsaturated enriched high-fat diets. <b>2018</b> , 60, 106-115	4

1013	The lateral meningocele syndrome mutation causes marked osteopenia in mice. <b>2018</b> , 293, 14165-1417	7	23
1012	Selective serotonin re-uptake inhibitor sertraline inhibits bone healing in a calvarial defect model. <b>2018</b> , 10, 25		9
1011	CCR2 Contributes to F4/80+ Cells Migration Along Intramembranous Bone Healing in Maxilla, but Its Deficiency Does Not Critically Affect the Healing Outcome. <b>2018</b> , 9, 1804		11
1010	Microarchitecture of the Augmented Bone Following Sinus Elevation with an Albumin Impregnated Demineralized Freeze-Dried Bone Allograft (BoneAlbumin) versus Anorganic Bovine Bone Mineral: A Randomized Prospective Clinical, Histomorphometric, and Micro-Computed Tomography Study.		10
1009	Iterative and discrete reconstruction in the evaluation of the rabbit model of osteoarthritis. <b>2018</b> , 8, 12051		4
1008	Investigation of Lake HvØ Mineral Water Balneotherapy and HvØ Mud Treatment in Murine Osteoarthritis and Rheumatoid Arthritis Models. <b>2018</b> , 2018, 4816905		7
1007	Ubiquitin-specific protease USP34 controls osteogenic differentiation and bone formation by regulating BMP2 signaling. <b>2018</b> , 37,		36
1006	Absence of complement factor H alters bone architecture and dynamics. <b>2018</b> , 223, 761-771		3
1005	Porcine induced pluripotent stem cell-derived osteoblast-like cells prevent glucocorticoid-induced bone loss in Lanyu pigs. <b>2018</b> , 13, e0202155		7
1004	Collagen-induced arthritis in Dark Agouti rats as a model for study of immunological sexual dimorphisms in the human disease. <b>2018</b> , 105, 10-22		7
1003	Extracellular matrix protein DMP1 suppresses osteogenic differentiation of Mesenchymal Stem Cells. <b>2018</b> , 501, 968-973		10
1002	Soy protein improves tibial whole-bone and tissue-level biomechanical properties in ovariectomized and ovary-intact, low-fit female rats. <b>2018</b> , 8, 244-254		4
1001	Micro-computed tomography reconstructions of tibiae of stem cell transplanted osteogenesis imperfecta mice. <b>2018</b> , 5, 180100		2
1000	Resorption of the mandibular residual ridge: A micro-CT and histomorphometrical analysis. <b>2018</b> , 35, 221		2
999	Skeletal Response to Soluble Activin Receptor Type IIB in Mouse Models of Osteogenesis Imperfecta. <i>Journal of Bone and Mineral Research</i> , <b>2018</b> , 33, 1760-1772	6.3	18
998	Increased H3K27ac level of ACE mediates the intergenerational effect of low peak bone mass induced by prenatal dexamethasone exposure in male offspring rats. <b>2018</b> , 9, 638		26
997	Magnetic resonance imaging based assessment of bone microstructure as a non-invasive alternative to histomorphometry in patients with chronic kidney disease. <b>2018</b> , 114, 14-21		18
996	The reproducibility of measuring trabecular bone parameters using a commercially available high-resolution magnetic resonance imaging approach: A pilot study. <b>2018</b> , 8, 180-186		1

995 offspring of high (C3H/HeJ) and low (C57BL/6J) bone mass phenotype mice. 2018, 8, 239-243 Validation of finite element models of the mouse tibia using digital volume correlation. 2018, 86, 172-184 994 33 Enabling three-dimensional densitometric measurements using laboratory source X-ray 993 5 micro-computed tomography. 2018, 7, 115-121 Atlases with Arcuate Foramen Present Cortical Bone Thickening That May Contribute to Lower 992 Fracture Risk. 2018, 117, e162-e166 Mice harboring a Hajdu Cheney Syndrome mutation are sensitized to osteoarthritis. 2018, 114, 198-205 991 14 Retrospective Analysis of the Outcome of Ridge Preservation with Anorganic Bovine Bone Minerals: Microcomputed Tomographic Assessment of Wound Healing in Grafted Extraction Sockets. 2018, 38, 103-111 989 Effects of reproduction on sexual dimorphisms in rat bone mechanics. 2018, 77, 40-47 11 988 Osteocytic oxygen sensing controls bone mass through epigenetic regulation of sclerostin. 2018, 9, 2557 54 Differential effects of high fat diet and diet-induced obesity on skeletal acquisition in female 987 17 C57BL/6J vs. FVB/NJ Mice. 2018, 8, 204-214 3D MicroCT spatial and temporal characterization of thoracic aorta perivascular adipose tissue and 986 7 plague volumes in the ApoE-/- mouse model. 2018, 7, 156-165 ARQ-197, a small-molecule inhibitor of c-Met, reduces tumour burden and prevents 985 7 myeloma-induced bone disease in vivo. 2018, 13, e0199517 cGMP-dependent protein kinase-2 regulates bone mass and prevents diabetic bone loss. 2018, 238, 203-219 984 9 Serum vitamin C levels modulate the lifespan and endoplasmic reticulum stress response pathways 983 3 in mice synthesizing a nonfunctional mutant WRN protein. 2018, 32, 3623-3640 Involvement of calvarial stem cells in healing: A regional analysis of large cranial defects. 2018, 26, 359-365 982 6 Use of Micro-Computed Tomography for Bone Evaluation in Dentistry. 2018, 29, 227-238 981 30 Bone-borne accelerated sutural expansion: A microcomputed tomography study in rabbits. 2018, 980 154, 260-269 Probing the influence of post-processing on microstructure and in situ compression failure with in 979 4 silico modeling of 3D-printed scaffolds. 2018, 33, 2062-2076 Alveolar bone healing in rats: micro-CT, immunohistochemical and molecular analysis. 2018, 26, e20170326 978 23

Evaluation of the long-term skeletal effect induced by teratogen 5-aza-2'deoxycytidine on

977	Osseointegration of ultrafine-grained titanium with a hydrophilic nano-patterned surface: an in vivo examination in miniature pigs. <b>2018</b> , 6, 2448-2459	15
976	A bone-targeting delivery system carrying osteogenic phytomolecule icaritin prevents osteoporosis in mice. <b>2018</b> , 182, 58-71	40
975	Eight Days of Earth Reambulation Worsen Bone Loss Induced by 1-Month Spaceflight in the Major Weight-Bearing Ankle Bones of Mature Mice. <b>2018</b> , 9, 746	11
974	Nuclear factor of activated T cells 2 is required for osteoclast differentiation and function in vitro but not in vivo. <b>2018</b> , 119, 9334-9345	7
973	Effect of Multilaminate Small Intestinal Submucosa as a Barrier Membrane on Bone Formation in a Rabbit Mandible Defect Model. <b>2018</b> , 2018, 3270293	12
972	Isosteviol Derivative Inhibits Osteoclast Differentiation and Ameliorates Ovariectomy-Induced Osteoporosis. <b>2018</b> , 8, 11190	4
971	Resveratrol counteracts bone loss via mitofilin-mediated osteogenic improvement of mesenchymal stem cells in senescence-accelerated mice. <b>2018</b> , 8, 2387-2406	60
970	Testing a novel nanofibre scaffold for utility in bone tissue regeneration. <b>2018</b> , 12, 2055-2066	6
969	Annatto-extracted tocotrienols improve glucose homeostasis and bone properties in high-fat diet-induced type 2 diabetic mice by decreasing the inflammatory response. <b>2018</b> , 8, 11377	17
968	Maternal obesity impairs skeletal development in adult offspring. <b>2018</b> , 239, 33-47	20
967	The Effects of Indian Hedgehog Deletion on Mesenchyme Cells: Inducing Intermediate Cartilage Scaffold Ossification to Cause Growth Plate and Phalange Joint Absence, Short Limb, and Dwarfish Phenotypes. <b>2018</b> , 27, 1412-1425	8
966	INFLUENCE OF THE BONE MORPHOLOGY ON MECHANICAL BEHAVIOR OF HUMAN SKULL FOR TWO STRAIN RATE CASES. <b>2018</b> , 18, 1850046	
965	Evaluation of the sealing ability of different root canal sealers: a combined SEM and micro-CT study. <b>2018</b> , 26, e20160584	18
964	Retinoic Acid Receptor l'Activity in Mesenchymal Stem Cells Regulates Endochondral Bone, Angiogenesis, and B Lymphopoiesis. <i>Journal of Bone and Mineral Research</i> , <b>2018</b> , 33, 2202-2213	17
963	Structural Adaptations in the Rat Tibia Bone Induced by Pregnancy and Lactation Confer Protective Effects Against Future Estrogen Deficiency. <i>Journal of Bone and Mineral Research</i> , <b>2018</b> , 33, 2165-2176	10
962	High-Resolution Imaging Techniques for Bone Quality Assessment. 2018, 1007-1041	2
961	Incorporating BMP-2 and skeletal muscle to a semitendinosus autograft in an oversized tunnel yields robust bone tunnel ossification in rabbits: Toward single-step revision of failed anterior cruciate ligament reconstruction. <b>2018</b> , 25, 765-773	3
960	Evidence for Ongoing Modeling-Based Bone Formation in Human Femoral Head Trabeculae Forming Minimodeling Structures: A Study in Patients with Fractures and Arthritis. <b>2018</b> , 9, 88	6

959	An Automated Step-Wise Micro-Compression Device for 3D Dynamic Image-Guided Failure Assessment of Bone Tissue on a Microstructural Level Using Time-Lapsed Tomography. <b>2018</b> , 5,		6	
958	The effect of ovariectomy and 2 antiresorptive therapeutic agents on bone response in rats: A 3-dimensional imaging analysis. <b>2018</b> , 126, 218-225		3	
957	Bone Toolbox: Biomarkers, Imaging Tools, Biomechanics, and Histomorphometry. <b>2018</b> , 46, 511-529		13	
956	Effect of biodegradable magnesium-copper coatings on bone integration based on the porous structures in a rabbit model <b>2018</b> , 8, 25127-25132		1	
955	Growth of ovarian cancer xenografts causes loss of muscle and bone mass: a new model for the study of cancer cachexia. <b>2018</b> , 9, 685-700		52	
954	Intestinal Inflammation and Tumor Burden as Determinants for Bone Fragility in APC-Driven Tumorigenesis. <b>2018</b> , 24, 2386-2393		4	
953	Can the contralateral limb be used as a control during the growing period in a rodent model?. <b>2018</b> , 58, 31-31		5	
952	Oral implant osseointegration model in C57Bl/6 mice: microtomographic, histological, histomorphometric and molecular characterization. <b>2018</b> , 26, e20170601		23	
951	Deletion of the Fanconi Anemia C Gene in Mice Leads to Skeletal Anomalies and Defective Bone Mineralization and Microarchitecture. <i>Journal of Bone and Mineral Research</i> , <b>2018</b> , 33, 2007-2020	6.3	3	
950	FoxO1 expression in osteoblasts modulates bone formation through resistance to oxidative stress in mice. <b>2018</b> , 503, 1401-1408		19	
949	Differential effects of high-fat diet and exercise training on bone and energy metabolism. <b>2018</b> , 116, 120-134		24	
948	Acemannan increased bone surface, bone volume, and bone density in a calvarial defect model in skeletally-mature rats. <b>2018</b> , 13, 334-341		12	
947	Tiludronate and clodronate do not affect bone structure or remodeling kinetics over a 60´day randomized trial. <b>2018</b> , 14, 105		9	
946	The degree of peri-implant osteolysis induced by PEEK, CoCrMo, and HXLPE wear particles: a study based on a porous Ti6Al4V implant in a rabbit model. <b>2018</b> , 13, 23		12	
945	A comparative analysis of the avian skull: Woodpeckers and chickens. <b>2018</b> , 84, 273-280		8	
944	Prevalence of bisphosphonate-related osteonecrosis of the jaw-like lesions is increased in a chemotherapeutic dose-dependent manner in mice. <b>2018</b> , 112, 177-186		17	
943	Age-related changes in female mouse cortical bone microporosity. 2018, 113, 1-8		28	
942	Conditional Deletion of Sost in MSC-Derived Lineages Identifies Specific Cell-Type Contributions to Bone Mass and B-Cell Development. <i>Journal of Bone and Mineral Research</i> , <b>2018</b> , 33, 1748-1759	6.3	28	

941	LRP1 Suppresses Bone Resorption in Mice by Inhibiting the RANKL-Stimulated NF- <b>B</b> and p38 Pathways During Osteoclastogenesis. <i>Journal of Bone and Mineral Research</i> , <b>2018</b> , 33, 1773-1784	15
940	A SERM increasing the expression of the osteoblastogenesis and mineralization-related proteins and improving quality of bone tissue in an experimental model of osteoporosis. <b>2018</b> , 26, e20170329	11
939	BIOMECHANICAL ANALYSES OF ARCHAEOLOGICAL HUMAN SKELETONS. 2018, 189-224	5
938	Inflammatory bone loss associated with MFG-E8 deficiency is rescued by teriparatide. <b>2018</b> , 32, 3730-3741	8
937	Analysis of short-term treatment with the phosphodiesterase type 5 inhibitor tadalafil on long bone development in young rats. <b>2018</b> , 315, E446-E453	5
936	Polyethylene particles inserted over calvarium induce cancellous bone loss in femur in female mice. <b>2018</b> , 9, 84-92	2
935	Paravertebral injection of botulinum toxin-A reduces lumbar vertebral bone quality. <b>2018</b> , 36, 2664-2670	1
934	Continuing Challenges in Advancing Preclinical Science in Skeletal Cell-Based Therapies and Tissue Regeneration. <i>Journal of Bone and Mineral Research</i> , <b>2018</b> , 33, 1721-1728	5
933	Loss of Intestinal Alkaline Phosphatase Leads to Distinct Chronic Changes in Bone Phenotype. <b>2018</b> , 232, 325-331	5
932	Inhibition of Histone Deacetylases Attenuates Morphine Tolerance and Restores MOR Expression in the DRG of BCP Rats. <b>2018</b> , 9, 509	8
931	Loss of RANKL in osteocytes dramatically increases cancellous bone mass in the osteogenesis imperfecta mouse (oim). <b>2018</b> , 9, 61-73	18
930	Marked alterations in the structure, dynamics and maturation of growth plate likely explain growth retardation and bone deformities of young Hyp mice. <b>2018</b> , 116, 187-195	12
929	Knockdown of FOXA2 enhances the osteogenic differentiation of bone marrow-derived mesenchymal stem cells partly via activation of the ERK signalling pathway. <b>2018</b> , 9, 836	21
928	Caloric restriction combined with exercise is effective in reducing adiposity and mitigating bone structural deterioration in obese rats. <b>2018</b> , 1433, 41-52	4
927	Thy-1 (CD90) promotes bone formation and protects against obesity. <b>2018</b> , 10,	51
926	Non-thermal plasma reduces periodontitis-induced alveolar bone loss in rats. <b>2018</b> , 503, 2040-2046	6
925	Efficacy of targeting bone-specific GIP receptor in ovariectomy-induced bone loss. 2018,	11
924	R-spondin-2 is a Wnt agonist that regulates osteoblast activity and bone mass. <b>2018</b> , 6, 24	22

923	Effect of deriving periosteal and endosteal contours from microCT scans on computation of cross-sectional properties in non-adults: the femur. <b>2018</b> , 233, 381	4
922	RNA interfering molecule delivery from in situ forming biodegradable hydrogels for enhancement of bone formation in rat calvarial bone defects. <b>2018</b> , 75, 105-114	51
921	Laser-induced alteration of microstructural and microscopic transport properties in porous materials: Experiment, modeling and analysis. <b>2018</b> , 155, 307-316	2
920	Effects of standardized quassinoid-rich Eurycoma longifolia extract in a rat model of osteoporosis due to testosterone deficiency: A densitometric, morphometric and biomechanical study. <b>2018</b> , 26, 643-656	7
919	Mucin 1 (Muc1) Deficiency in Female Mice Leads to Temporal Skeletal Changes During Aging. <b>2018</b> , 2, 341-350	1
918	Early life vitamin D depletion alters the postnatal response to skeletal loading in growing and mature bone. <b>2018</b> , 13, e0190675	6
917	Impaired bone healing at tooth extraction sites in CD24-deficient mice: A pilot study. <b>2018</b> , 13, e0191665	4
916	Folliculin Regulates Osteoclastogenesis Through Metabolic Regulation. <i>Journal of Bone and Mineral Research</i> , <b>2018</b> , 33, 1785-1798	15
915	The Effect of 🛮 Aminopropionitrile on Skeletal Micromorphology and Osteogenesis. 2018, 103, 411-421	3
914	Iron overload involved in the enhancement of unloading-induced bone loss by hypomagnetic field. <b>2018</b> , 114, 235-245	22
913	Influence of Vitamin D Status and Mechanical Loading on the Morphometric and Mechanical Properties of the Mouse Tibia. <b>2019</b> , 39, 523-531	1
912	Finite-element analysis of the mouse proximal ulna in response to elbow loading. <b>2019</b> , 37, 419-429	
911	Bone regeneration with bovine bone impairs orthodontic tooth movement despite proper osseous wound healing in a novel mouse model. <b>2019</b> , 90, 189-199	6
910	An Automatic Regularization Method: An Application for 3-D X-Ray Micro-CT Reconstruction Using Sparse Data. <b>2019</b> , 38, 417-425	4
909	Archeological bone injuries by lithic backed projectiles: new evidence on bear hunting from the Late Epigravettian site of Cornafessa rock shelter (Italy). <b>2019</b> , 11, 2249-2270	8
908	Hormone-Independent Sexual Dimorphism in the Regulation of Bone Resorption by Krox20. <i>Journal of Bone and Mineral Research</i> , <b>2019</b> , 34, 2277-2286	4
907	The effects of myokines on osteoclasts and osteoblasts. <b>2019</b> , 517, 749-754	5
906	Chitosan/Dextran Hydrogel Constructs Containing Strontium-Doped Hydroxyapatite with Enhanced Osteogenic Potential in Rat Cranium. <b>2019</b> , 5, 4574-4586	17

905	Bone healing with niobium-containing bioactive glass composition in rat femur model: A micro-CT study. <b>2019</b> , 35, 1490-1497		11
904	Effect of micro-computed tomography reconstruction protocols on bone fractal dimension analysis. <b>2019</b> , 48, 20190235		1
903	Persistent Activation of Calcium-Sensing Receptor Suppresses Bone Turnover, Increases Microcracks, and Decreases Bone Strength. <b>2019</b> , 3, e10182		1
902	Stimulation of bone formation by monocyte-activator functionalized graphene oxide in vivo. <b>2019</b> , 11, 19408-19421		18
901	Lattice Boltzmann Methods for Industrial Applications. <b>2019</b> , 58, 16205-16234		14
900	Nanocomposite-coated porous templates for engineered bone scaffolds: a parametric study of layer-by-layer assembly conditions. <b>2019</b> , 14, 065008		3
899	Asiatic Acid Attenuates Bone Loss by Regulating Osteoclastic Differentiation. 2019, 105, 531-545		6
898	Sclerostin inhibition alleviates breast cancer-induced bone metastases and muscle weakness. <b>2019</b> , 5,		40
897	GG attenuates tenofovir disoproxil fumarate-induced bone loss in male mice gut-microbiota-dependent anti-inflammation. <b>2019</b> , 10, 2040622319860653		10
896	Error in the estimation of periosteal and endosteal contours from micro-CT scans for nonadult tibiae and humeri. <b>2019</b> , 170, 275-294		1
895	PSTPIP2 attenuates joint damage and suppresses inflammation in adjuvant-induced arthritis. <b>2019</b> , 859, 172558		8
894	The L-type amino acid transporter LAT1 inhibits osteoclastogenesis and maintains bone homeostasis through the mTORC1 pathway. <b>2019</b> , 12,		5
893	Absence of Dipeptidyl Peptidase 3 Increases Oxidative Stress and Causes Bone Loss. <i>Journal of Bone and Mineral Research</i> , <b>2019</b> , 34, 2133-2148	6.3	14
892	Effect of parathyroid hormone on the structural, densitometric and failure behaviors of mouse tibia in the spatiotemporal space. <b>2019</b> , 14, e0219575		2
891	Radioprotective Effect of Sodium Selenite on Mandible of Irradiated Rats. <b>2019</b> , 30, 232-237		
890	Changes in Musculoskeletal System and Metabolism in Osteoporotic Rats Treated With Urocortin. <b>2019</b> , 10, 400		3
889	Acute Changes in NADPH Oxidase 4 in Early Post-Traumatic Osteoarthritis. 2019, 37, 2429-2436		6
888	In vivo contrast-enhanced microCT for the monitoring of mouse thoracic, lumbar, and coccygeal intervertebral discs. <b>2019</b> , 2, e1058		2

887	Developmental low-dose exposure to bisphenol A induces chronic inflammation, bone marrow fibrosis and reduces bone stiffness in female rat offspring only. <b>2019</b> , 177, 108584	16
886	Microstructure, mineral and mechanical properties of teleost intermuscular bones. <b>2019</b> , 94, 59-66	8
885	Osteocyte numbers decrease only in postcranial but not in cranial bones in humans of advanced age. <b>2019</b> , 226, 57-63	4
884	Effect of the software binning and averaging data during microcomputed tomography image acquisition. <b>2019</b> , 9, 10562	1
883	Stachydrine prevents LPS-induced bone loss by inhibiting osteoclastogenesis via NF- <b>B</b> and Akt signalling. <b>2019</b> , 23, 6730-6743	10
882	A new method to monitor bone geometry changes at different spatial scales in the longitudinal in vivo <b>I</b> T studies of mice bones. <b>2019</b> , 14, e0219404	2
881	WNT3A accelerates delayed alveolar bone repair in ovariectomized mice. <b>2019</b> , 30, 1873-1885	14
880	Profilin 1 Negatively Regulates Osteoclast Migration in Postnatal Skeletal Growth, Remodeling, and Homeostasis in Mice. <b>2019</b> , 3, e10130	5
879	Assessment of the elastic properties of human vertebral trabecular bone using computational mechanical tests and x-ray microtomographyâ subvolume analysis. <b>2019</b> , 5, 045031	1
878	Deficiency of sphingosine-1-phosphate receptor 3 does not affect the skeletal phenotype of mice lacking sphingosine-1-phosphate lyase. <b>2019</b> , 14, e0219734	2
877	Low-Frequency Electrical Stimulation of Denervated Skeletal Muscle Retards Muscle and Trabecular Bone Loss in Aged Rats. <b>2019</b> , 16, 822-830	3
876	Apelin enhances the osteogenic differentiation of human bone marrow mesenchymal stem cells partly through Wnt/I-catenin signaling pathway. <b>2019</b> , 10, 189	15
875	Impaired Gastric Hormone Regulation of Osteoblasts and Lysyl Oxidase Drives Bone Disease in Diabetes Mellitus. <b>2019</b> , 3, e10212	6
874	Conditional Activation of NF- <b>B</b> Inducing Kinase (NIK) in the Osteolineage Enhances Both Basal and Loading-Induced Bone Formation. <i>Journal of Bone and Mineral Research</i> , <b>2019</b> , 34, 2087-2100	4
873	KLF4 as a rheostat of osteolysis and osteogenesis in prostate tumors in the bone. <b>2019</b> , 38, 5766-5777	3
872	Extraction of gray-scale intensity distributions from micro computed tomography imaging for femoral cortical bone differentiation between low-magnesium and normal diets in a laboratory mouse model. <b>2019</b> , 9, 8135	3
871	High-resolution contrast-enhanced microCT reveals the true three-dimensional morphology of the murine placenta. <b>2019</b> , 116, 13927-13936	28
870	Glucocorticoid-Induced Bone Fragility Is Prevented in Female Mice by Blocking Pyk2/Anoikis Signaling. <b>2019</b> , 160, 1659-1673	10

869	Positive impact of low-dose, high-energy radiation on bone in partial- and/or full-weightbearing mice. <b>2019</b> , 5, 13	4
868	Microarchitectural changes in the mandibles of ovariectomized rats: a systematic review and meta-analysis. <b>2019</b> , 19, 128	7
867	Regulation of the Bone Vascular Network is Sexually Dimorphic. <i>Journal of Bone and Mineral Research</i> , <b>2019</b> , 34, 2117-2132	7
866	The longitudinal effects of ovariectomy on the morphometric, densitometric and mechanical properties in the murine tibia: A comparison between two mouse strains. <b>2019</b> , 127, 260-270	21
865	Micro-CT Scanning to Examine Soil Clogging Behavior of Natural Fiber Drains. <b>2019</b> , 145, 04019037	9
864	Skeletal response to whole body vibration and dietary calcium and phosphorus in growing pigs. <b>2019</b> , 97, 3369-3378	1
863	Histone Lys demethylase KDM3C demonstrates anti-inflammatory effects by suppressing NF- <b>B</b> signaling and osteoclastogenesis. <b>2019</b> , 33, 10515-10527	10
862	Literature review and micro-computed tomography analysis of natal teeth: A pilot study. <b>2019</b> , 10, e12466	1
861	Micro-CT imaging analysis for the effects of ibandronate and eldecalcitol on secondary osteoporosis and arthritis in adjuvant-induced arthritis rats. <b>2019</b> , 40, 197-205	2
860	Differential Modulation of Cancellous and Cortical Distal Femur by Fructose and Natural Mineral-Rich Water Consumption in Ovariectomized Female Sprague Dawley Rats. <b>2019</b> , 11,	5
859	Exercise reduces inflammatory cell production and cardiovascular inflammation via instruction of hematopoietic progenitor cells. <b>2019</b> , 25, 1761-1771	90
858	Let-7f-5p regulates TGFBR1 in glucocorticoid-inhibited osteoblast differentiation and ameliorates glucocorticoid-induced bone loss. <b>2019</b> , 15, 2182-2197	15
857	Effects of injection parameters on heat extraction performance of supercritical CO2 in enhanced geothermal systems. <b>2019</b> , 7, 3076-3094	5
856	3-(3-Hydroxyphenyl)-Propionic Acid (PPA) Suppresses Osteoblastic Cell Senescence to Promote Bone Accretion in Mice. <b>2019</b> , 3, e10201	8
855	FAM20A is essential for amelogenesis, but is dispensable for dentinogenesis. <b>2019</b> , 50, 581-591	8
854	Site-Specific Load-Induced Expansion of Sca-1Prrx1 and Sca-1Prrx1 Cells in Adult Mouse Long Bone Is Attenuated With Age. <b>2019</b> , 3, e10199	7
853	Shifts in bacterial community composition increase with depth in three soil types from paddy fields in China. <b>2019</b> , 77, 150589	9
852	Age-related changes in size, bone microarchitecture and volumetric bone mineral density of the mandible in the harbor seal (Phoca vitulina). <b>2019</b> , 14, e0224480	O

851	Potential therapeutic use of relaxin in accelerating closure of cranial bone defects in mice. 2019, 7, e14	106	2
850	Abaloparatide exhibits greater osteoanabolic response and higher cAMP stimulation and Darrestin recruitment than teriparatide. <b>2019</b> , 7, e14225		13
849	A benchtop system to assess the feasibility of a fully independent and implantable brain-machine interface. <b>2019</b> , 16, 066043		9
848	Effect of platelet-rich plasma on peri-implant trabecular bone volume and architecture: A preclinical micro-CT study in beagle dogs. <b>2019</b> , 30, 1190-1199		10
847	A preclinical model links osseo-densification due to misfit and osseo-destruction due to stress/strain. <b>2019</b> , 30, 1238-1249		6
846	Myosin 1a Regulates Osteoblast Differentiation Independent of Intestinal Calcium Transport. <b>2019</b> , 3, 1993-2011		2
845	-Deficiency Impacts Body Composition, Skeleton, and Bone Microstructure in a Mouse Model of Fragile X Syndrome. <b>2019</b> , 10, 678		6
844	HU-671, a Novel Oleoyl Serine Derivative, Exhibits Enhanced Efficacy in Reversing Ovariectomy-Induced Osteoporosis and Bone Marrow Adiposity. <b>2019</b> , 24,		2
843	Improving intraoperative storage conditions for autologous bone grafts: An experimental investigation in mice. <b>2019</b> , 13, 2169-2180		3
842	Roles of leptin in the recovery of muscle and bone by reloading after mechanical unloading in high fat diet-fed obese mice. <b>2019</b> , 14, e0224403		3
841	Relative contributions of adipose-resident CD146 pericytes and CD34 adventitial progenitor cells in bone tissue engineering. <b>2019</b> , 4, 1		37
840	Calcium Phosphate Bone Graft Substitutes with High Mechanical Load Capacity and High Degree of Interconnecting Porosity. <b>2019</b> , 12,		6
839	Clumps of Mesenchymal Stem Cell/Extracellular Matrix Complexes Generated with Xeno-Free Conditions Facilitate Bone Regeneration via Direct and Indirect Osteogenesis. <b>2019</b> , 20,		9
838	Combinatorial morphogenetic and mechanical cues to mimic bone development for defect repair. <b>2019</b> , 5, eaax2476		23
837	Quantitative CT-based bone strength parameters for the prediction of novel spinal implant stability using resonance frequency analysis: a cadaveric study involving experimental micro-CT and clinical multislice CT. <b>2019</b> , 3, 1		14
836	TGFIInhibition Stimulates Collagen Maturation to Enhance Bone Repair and Fracture Resistance in a Murine Myeloma Model. <i>Journal of Bone and Mineral Research</i> , <b>2019</b> , 34, 2311-2326	6.3	10
835	Analysis on Channel Deposition and Erosion in Liaohe River. <b>2019</b> , 252, 052041		
834	Synergistic Enhancement Effect of Palladium-Silver Alloy Nanoparticle Catalysts Towards High-Sensitive Hydrogen Detection. <b>2019</b> ,		

833	Individual Effector/Regulator T Cell Ratios Impact Bone Regeneration. 2019, 10, 1954	25
832	Associations of Health-Related Quality of Life, Fear of Falling and Objective Measures of Physical Function with Bone Health in Postmenopausal Women with Low Bone Mass. <b>2019</b> , 8,	O
831	Growth factor-mediated augmentation of long bones: evaluation of a BMP-7 loaded thermoresponsive hydrogel in a murine femoral intramedullary injection model. <b>2019</b> , 14, 297	2
830	Jump Exercise and Food Restriction on Bone Parameters in Young Female Rats. <b>2019</b> , 105, 557-566	3
829	Effect of alendronate or 8-prenylnaringenin applied as a single therapy or in combination with vibration on muscle structure and bone healing in ovariectomized rats. <b>2019</b> , 11, 100224	6
828	TRPV6 and Ca1.3 Mediate Distal Small Intestine Calcium Absorption Before Weaning. <b>2019</b> , 8, 625-642	13
827	Disturbed bone remodelling activity varies in different stages of experimental, gradually progressive apical periodontitis in rats. <b>2019</b> , 11, 27	5
826	Conditional disruption of the gene in chondrocytes during early postnatal growth impairs secondary ossification in the mouse tibial epiphysis. <b>2019</b> , 7, 24	13
825	The emerging role of IMD 0354 on bone homeostasis by suppressing osteoclastogenesis and bone resorption, but without affecting bone formation. <b>2019</b> , 10, 654	4
824	Mechanical properties of replicated cellular Zn and Zn1.5Mg in uniaxial compression. <b>2019</b> , 157, 109895	2
823	High Impact Exercise Improves Bone Microstructure and Strength in Growing Rats. 2019, 9, 13128	8
822	Lung tumor cells inhibit bone mineralization and osteoblast activity. <b>2019</b> , 519, 566-571	6
821	Dual-Purpose Magnesium-Incorporated Titanium Nanotubes for Combating Bacterial Infection and Ameliorating Osteolysis to Realize Better Osseointegration. <b>2019</b> , 5, 5368-5383	17
820	A Delphinidin-Enriched Maqui Berry Extract Improves Bone Metabolism and Protects against Bone Loss in Osteopenic Mouse Models. <b>2019</b> , 8,	13
819	Twist1 Inactivation in Dmp1-Expressing Cells Increases Bone Mass but Does Not Affect the Anabolic Response to Sclerostin Neutralization. <b>2019</b> , 20,	3
818	Arachidonic acid exacerbates diet-induced obesity and reduces bone mineral content without impacting bone strength in growing male rats. <b>2019</b> , 73, 108226	4
817	Cell Therapy: Effect of Locally Injected Mesenchymal Stromal Cells Derived from Bone Marrow or Adipose Tissue on Bone Regeneration of Rat Calvarial Defects. <b>2019</b> , 9, 13476	13
816	Influence of Social Isolation During Prolonged Simulated Weightlessness by Hindlimb Unloading. <b>2019</b> , 10, 1147	23

815	Bone loss caused by dopaminergic degeneration and levodopa treatment in Parkinson's disease model mice. <b>2019</b> , 9, 13768	16
814	Age- and sex-dependent role of osteocytic pannexin1 on bone and muscle mass and strength. <b>2019</b> , 9, 13903	4
813	In Vivo Bone Regeneration Induced by a Scaffold of Chitosan/Dicarboxylic Acid Seeded with Human Periodontal Ligament Cells. <b>2019</b> , 20,	13
812	Vdr expression in osteoclast precursors is not critical in bone homeostasis. <b>2019</b> , 195, 105478	7
811	BK ablation attenuates osteoblast bone formation via integrin pathway. <b>2019</b> , 10, 738	5
810	Early Alterations of Subchondral Bone in the Rat Anterior Cruciate Ligament Transection Model of Osteoarthritis. <b>2019</b> , 1947603519878479	7
809	Consumption of sheep milk compared to cow milk can affect trabecular bone ultrastructure in a rat model. <b>2019</b> , 10, 163-171	2
808	Non-bone metastatic cancers promote osteocyte-induced bone destruction. <b>2021</b> , 520, 80-90	3
807	Large-scale quantification of human osteocyte lacunar morphological biomarkers as assessed by ultra-high-resolution desktop micro-computed tomography. <b>2021</b> , 152, 116094	5
806	Low bone mass resulting from impaired estrogen signaling in bone increases severity of load-induced osteoarthritis in female mice. <b>2021</b> , 152, 116071	3
805	Implantable blood clot loaded with BMP-2 for regulation of osteoimmunology and enhancement of bone repair. <b>2021</b> , 6, 4014-4026	6
804	A technique for improving dispersion within polymer-glass composites using polymer precipitation. <b>2021</b> , 123, 104767	1
803	3D-printed multisampling holder for microcomputed tomography applied to life and materials science research. <b>2021</b> , 150, 103142	1
802	Biodegradable magnesium pins enhanced the healing of transverse patellar fracture in rabbits. <b>2021</b> , 6, 4176-4185	5
801	Osteocyte Wnt/I-catenin pathway activation upon mechanical loading is altered in ovariectomized mice. <b>2021</b> , 15, 101129	О
800	Microstructure and mechanical behaviors of tibia for collagen-induced arthritic mice treated with gingiva-derived mesenchymal stem cells. <b>2021</b> , 124, 104719	
799	Resistance to disuse-induced iron overload in Daurian ground squirrels (Spermophilus dauricus) during extended hibernation inactivity. <b>2022</b> , 257, 110650	О
798	Sclerostin antibody improves phosphate metabolism hormones, bone formation rates, and bone mass in adult Hyp mice. <b>2022</b> , 154, 116201	2

797	GPR109A mediates the effects of hippuric acid on regulating osteoclastogenesis and bone resorption in mice. <b>2021</b> , 4, 53	1
796	Scaffold-free human mesenchymal stem cell construct geometry regulates long bone regeneration. <b>2021</b> , 4, 89	1
795	Accelerating functional gene discovery in osteoarthritis. <b>2021</b> , 12, 467	12
794	Activation of Notch3 in osteoblasts/osteocytes causes compartment-specific changes in bone remodeling. <b>2021</b> , 296, 100583	1
793	Investigation of Mechanical, Material, and Compositional Determinants of Human Trabecular Bone Quality in Type 2 Diabetes. <b>2021</b> , 106, e2271-e2289	18
79 <sup>2</sup>	Exosomes derived from osteogenic tumor activate osteoclast differentiation and concurrently inhibit osteogenesis by transferring COL1A1-targeting miRNA-92a-1-5p. <b>2021</b> , 10, e12056	21
791	Application of subject-specific adaptive mechanical loading for bone healing in a mouse tail vertebral defect. <b>2021</b> , 11, 1861	55
790	Alveolar Preservation with Albumin and Gentamycin-Coated Allograft after Third Molar Tooth Removal: A Randomized Clinical Trial. <b>2021</b> , 11, 586	O
789	Gene-metabolite networks associated with impediment of bone fracture repair in spaceflight. <b>2021</b> , 19, 3507-3520	1
788	BMP-2 delivery strategy modulates local bone regeneration and systemic immune responses to complex extremity trauma. <b>2021</b> , 9, 1668-1682	6
787	Application of machine learning classifiers for microcomputed tomography data assessment of mouse bone microarchitecture. <b>2021</b> , 8, 101497	0
786	Preclinical models for orthopedic research and bone tissue engineering. <b>2018</b> , 36, 832-840	14
7 <sup>8</sup> 5	Induction of fully stabilized cortical bone defects to study intramembranous bone regeneration. <b>2015</b> , 1226, 183-92	2
784	Overview of skeletal repair (fracture healing and its assessment). <b>2014</b> , 1130, 13-31	33
783	Microcomputed Tomography. <b>2019</b> , 1205-1236	2
782	Local Binary Patterns to Evaluate Trabecular Bone Structure from Micro-CT Data: Application to Studies of Human Osteoarthritis. <b>2015</b> , 63-79	4
781	Bone Physiology and Biology. <b>2017</b> , 27-94	10
780	Skeletal Imaging. <b>2017</b> , 203-228	3

779	Feature Space Clustering for Trabecular Bone Segmentation. <b>2017</b> , 65-75	6
778	Synchrotron X-Ray Phase Nanotomography for Bone Tissue Characterization. <b>2016</b> , 1-42	2
777	Registered Micro-Computed Tomography Data as a Four-Dimensional Imaging Biomarker of Bone Formation and Resorption. <b>2017</b> , 557-586	1
776	Volumetric Assessment of Bone Microstructures by a 3D Local Binary Patterns â <b>B</b> ased Method: Bone Changes with Osteoarthritis. <b>2018</b> , 900-903	1
775	Aberrant structure of fibrillar collagen and elevated levels of advanced glycation end products typify delayed fracture healing in the diet-induced obesity mouse model. <b>2020</b> , 137, 115436	7
774	Genetic correlations between cartilage regeneration and degeneration reveal an inverse relationship. <b>2020</b> , 28, 1111-1120	4
773	Trabecular bone deterioration at the greater trochanter of mice with unilateral obstructive nephropathy. <b>2013</b> , 15, 564-6	1
772	Intramembranous bone regeneration and implant placement using mechanical femoral marrow ablation: rodent models. <b>2016</b> , 5, 837	6
771	Kindlin-2 regulates skeletal homeostasis by modulating PTH1R in mice. <b>2020</b> , 5, 297	14
770	Focal adhesion protein Kindlin-2 regulates bone homeostasis in mice. <b>2020</b> , 8, 2	26
77° 769	Focal adhesion protein Kindlin-2 regulates bone homeostasis in mice. <b>2020</b> , 8, 2  Arylsulfatase K inactivation causes mucopolysaccharidosis due to deficient glucuronate desulfation of heparan and chondroitin sulfate. <b>2020</b> , 477, 3433-3451	26 4
	Arylsulfatase K inactivation causes mucopolysaccharidosis due to deficient glucuronate desulfation	
769	Arylsulfatase K inactivation causes mucopolysaccharidosis due to deficient glucuronate desulfation of heparan and chondroitin sulfate. <b>2020</b> , 477, 3433-3451  Microstructure and mechanical properties of subchondral bone are negatively regulated by	4
769 768	Arylsulfatase K inactivation causes mucopolysaccharidosis due to deficient glucuronate desulfation of heparan and chondroitin sulfate. 2020, 477, 3433-3451  Microstructure and mechanical properties of subchondral bone are negatively regulated by tramadol in osteoarthritis in mice. 2020, 40,  Dried and free flowing granules of Spinacia oleracea accelerate bone regeneration and alleviate	3
769 768 767	Arylsulfatase K inactivation causes mucopolysaccharidosis due to deficient glucuronate desulfation of heparan and chondroitin sulfate. 2020, 477, 3433-3451  Microstructure and mechanical properties of subchondral bone are negatively regulated by tramadol in osteoarthritis in mice. 2020, 40,  Dried and free flowing granules of Spinacia oleracea accelerate bone regeneration and alleviate postmenopausal osteoporosis. 2017, 24, 686-698  Mimicking high strength lightweight novel structures inspired from the trabecular bone	4 3 9
769 768 767 766	Arylsulfatase K inactivation causes mucopolysaccharidosis due to deficient glucuronate desulfation of heparan and chondroitin sulfate. 2020, 477, 3433-3451  Microstructure and mechanical properties of subchondral bone are negatively regulated by tramadol in osteoarthritis in mice. 2020, 40,  Dried and free flowing granules of Spinacia oleracea accelerate bone regeneration and alleviate postmenopausal osteoporosis. 2017, 24, 686-698  Mimicking high strength lightweight novel structures inspired from the trabecular bone microarchitecture. 2020, 378, 20190448  The microbiome mediates subchondral bone loss and metabolomic changes after acute joint	4 3 9 4
769 768 767 766 765	Arylsulfatase K inactivation causes mucopolysaccharidosis due to deficient glucuronate desulfation of heparan and chondroitin sulfate. 2020, 477, 3433-3451  Microstructure and mechanical properties of subchondral bone are negatively regulated by tramadol in osteoarthritis in mice. 2020, 40,  Dried and free flowing granules of Spinacia oleracea accelerate bone regeneration and alleviate postmenopausal osteoporosis. 2017, 24, 686-698  Mimicking high strength lightweight novel structures inspired from the trabecular bone microarchitecture. 2020, 378, 20190448  The microbiome mediates subchondral bone loss and metabolomic changes after acute joint trauma.	4 3 9 4

761	Reconstitution of the host holobiont in germ-free rats acutely increases bone growth and affects marrow cellular content.	1
760	Bone marrow adipogenic lineage precursors (MALPs) promote osteoclastogenesis in bone remodeling and pathologic bone loss.	2
759	COPB2haploinsufficiency causes a coatopathy with osteoporosis and developmental delay.	1
758	Age dependence of systemic bone loss and recovery following femur fracture in mice.	1
757	Zoledronate treatment duration is linked to bisphosphonate-related osteonecrosis of the jaw prevalence in rice rats with generalized periodontitis. <b>2019</b> , 25, 1116-1135	15
756	MicroCT Bone Densitometry: Context Sensitivity, Beam Hardening Correction and the Effect of Surrounding Media. <b>2014</b> , 2, 1-25	9
755	Deep Learning Based High-Resolution Reconstruction of Trabecular Bone Microstructures from Low-Resolution CT Scans using GAN-CIRCLE. <b>2020</b> , 11317,	11
754	Global estrogen receptor-knockout has differential effects on cortical and cancellous bone in aged male mice. <b>2020</b> , 5, 328-348	3
753	Lipoatrophy and metabolic disturbance in mice with adipose-specific deletion of kindlin-2. 2019, 4,	24
75 <sup>2</sup>	Precocious chondrocyte differentiation disrupts skeletal growth in Kabuki syndrome mice. <b>2019</b> , 4,	10
751	Focal adhesion proteins Pinch1 and Pinch2 regulate bone homeostasis in mice. 2019, 4,	14
75°	Osteoclast-derived IGF1 is required for pagetic lesion formation in vivo. <b>2020</b> , 5,	2
749	Osteocyte RANKL is required for cortical bone loss with age and is induced by senescence. <b>2020</b> , 5,	12
748	Fatty acid oxidation by the osteoblast is required for normal bone acquisition in a sex- and diet-dependent manner. <b>2017</b> , 2,	44
747	Sclerostin neutralization unleashes the osteoanabolic effects of Dkk1 inhibition. 2018, 3,	39
746	Cathepsin K-deficient osteocytes prevent lactation-induced bone loss and parathyroid hormone suppression. <b>2019</b> , 129, 3058-3071	26
745	Fracture repair requires TrkA signaling by skeletal sensory nerves. <b>2019</b> , 129, 5137-5150	50
744	Salt-inducible kinases dictate parathyroid hormone 1 receptor action in bone development and remodeling. <b>2019</b> , 129, 5187-5203	14

## (2014-2020)

743	Parathyroid hormone-dependent bone formation requires butyrate production by intestinal microbiota. <b>2020</b> , 130, 1767-1781	44
742	Gsænhances commitment of mesenchymal progenitors to the osteoblast lineage but restrains osteoblast differentiation in mice. <b>2011</b> , 121, 3492-504	80
741	Osteoclast-specific cathepsin K deletion stimulates S1P-dependent bone formation. <b>2013</b> , 123, 666-81	203
740	Osteoclast-secreted CTHRC1 in the coupling of bone resorption to formation. <b>2013</b> , 123, 3914-24	143
739	The visible skeleton 2.0: phenotyping of cartilage and bone in fixed vertebrate embryos and foetuses based on X-ray microCT. <b>2020</b> , 147,	3
738	Spatially-offset Raman spectroscopy for monitoring mineralization of bone tissue engineering scaffolds: feasibility study based on phantom samples. <b>2019</b> , 10, 1678-1690	10
737	Decreased bone formation and osteopenia in lamin a/c-deficient mice. <b>2011</b> , 6, e19313	53
736	Age-related skeletal dynamics and decrease in bone strength in DNA repair deficient male trichothiodystrophy mice. <b>2012</b> , 7, e35246	13
735	Regulation of lean mass, bone mass, and exercise tolerance by the central melanocortin system. <b>2012</b> , 7, e42183	12
734	Quantification of lung fibrosis and emphysema in mice using automated micro-computed tomography. <b>2012</b> , 7, e43123	74
733	Synchrotron ultraviolet microspectroscopy on rat cortical bone: involvement of tyrosine and tryptophan in the osteocyte and its environment. <b>2012</b> , 7, e43930	16
732	Local mechanical stimuli regulate bone formation and resorption in mice at the tissue level. <b>2013</b> , 8, e62172	141
731	Lrp5 and Lrp6 exert overlapping functions in osteoblasts during postnatal bone acquisition. <b>2013</b> , 8, e63323	82
730	Mice with hypomorphic expression of the sodium-phosphate cotransporter PiT1/Slc20a1 have an unexpected normal bone mineralization. <b>2013</b> , 8, e65979	29
729	Transgenic overexpression of ephrin b1 in bone cells promotes bone formation and an anabolic response to mechanical loading in mice. <b>2013</b> , 8, e69051	18
728	Total water, phosphorus relaxation and inter-atomic organic to inorganic interface are new determinants of trabecular bone integrity. <b>2013</b> , 8, e83478	20
727	Trabecular bone adaptation to low-magnitude high-frequency loading in microgravity. <b>2014</b> , 9, e93527	4
726	Effect of low-magnitude whole-body vibration combined with alendronate in ovariectomized rats: a random controlled osteoporosis prevention study. <b>2014</b> , 9, e96181	25

725	Midkine-deficiency delays chondrogenesis during the early phase of fracture healing in mice. <b>2014</b> , 9, e116282	27
724	Bone mass and bone quality are altered by hypoactivity in the chicken. <b>2015</b> , 10, e0116763	29
723	Impact of long-term exposure to the tyrosine kinase inhibitor imatinib on the skeleton of growing rats. <b>2015</b> , 10, e0131192	27
722	Glucagon-like peptide-1 receptor agonist Liraglutide has anabolic bone effects in ovariectomized rats without diabetes. <b>2015</b> , 10, e0132744	49
721	Fracture Healing Is Delayed in Immunodeficient NOD/scid- IL2R@null Mice. 2016, 11, e0147465	27
720	Three-Dimensional Quantitative Morphometric Analysis (QMA) for In Situ Joint and Tissue Assessment of Osteoarthritis in a Preclinical Rabbit Disease Model. <b>2016</b> , 11, e0147564	12
719	Novel Lesions of Bones and Joints Associated with Chikungunya Virus Infection in Two Mouse Models of Disease: New Insights into Disease Pathogenesis. <b>2016</b> , 11, e0155243	23
718	Trabecular and Cortical Bone of Growing C3H Mice Is Highly Responsive to the Removal of Weightbearing. <b>2016</b> , 11, e0156222	4
717	Beta-Catenin Haplo Insufficient Male Mice Do Not Lose Bone in Response to Hindlimb Unloading. <b>2016</b> , 11, e0158381	13
716	Predicting Trabecular Bone Stiffness from Clinical Cone-Beam CT and HR-pQCT Data; an In Vitro Study Using Finite Element Analysis. <b>2016</b> , 11, e0161101	18
715	Variation in Lateral Plate Quality in Threespine Stickleback from Fresh, Brackish and Marine Water: A Micro-Computed Tomography Study. <b>2016</b> , 11, e0164578	4
714	Micro-CT vs. Whole Body Multirow Detector CT for Analysing Bone Regeneration in an Animal Model. <b>2016</b> , 11, e0166540	7
713	A Convenient In Vivo Model Using Small Interfering RNA Silencing to Rapidly Assess Skeletal Gene Function. <b>2016</b> , 11, e0167222	4
712	Mechanical Loading Attenuates Radiation-Induced Bone Loss in Bone Marrow Transplanted Mice. <b>2016</b> , 11, e0167673	9
711	Reduced bone formation markers, and altered trabecular and cortical bone mineral densities of non-paretic femurs observed in rats with ischemic stroke: A randomized controlled pilot study. <b>2017</b> , 12, e0172889	3
710	Automated assessment of bone changes in cross-sectional micro-CT studies of murine experimental osteoarthritis. <b>2017</b> , 12, e0174294	23
709	Attenuating trabecular morphology associated with low magnesium diet evaluated using micro computed tomography. <b>2017</b> , 12, e0174806	8
708	Osteoblast-specific overexpression of complement receptor C5aR1 impairs fracture healing. <b>2017</b> , 12, e0179512	16

## (2015-2017)

707	Effects of combination treatment with alendronate and raloxifene on skeletal properties in a beagle dog model. <b>2017</b> , 12, e0181750	4
706	Impaired bone formation in ovariectomized mice reduces implant integration as indicated by longitudinal in vivo micro-computed tomography. <b>2017</b> , 12, e0184835	11
705	Trabecular bone in the calcaneus of runners. <b>2017</b> , 12, e0188200	18
704	Adiponectin receptor 1 resists the decline of serum osteocalcin and GPRC6A expression in ovariectomized mice. <b>2017</b> , 12, e0189063	4
703	Early arthritis induces disturbances at bone nanostructural level reflected in decreased tissue hardness in an animal model of arthritis. <b>2018</b> , 13, e0190920	7
702	Clinically relevant doses of vitamin A decrease cortical bone mass in mice. <b>2018</b> , 239, 389-402	13
701	Fibrin biopolymer as scaffold candidate to treat bone defects in rats. <b>2019</b> , 25, e20190027	15
700	Degeneration of the osteocyte network in the C57BL/6 mouse model of aging. <b>2017</b> , 9, 2190-2208	66
699	PPARlagonists promote differentiation of cancer stem cells by restraining YAP transcriptional activity. <b>2016</b> , 7, 60954-60970	31
698	Aromatase inhibitor-induced bone loss increases the progression of estrogen receptor-negative breast cancer in bone and exacerbates muscle weakness in vivo. <b>2017</b> , 8, 8406-8419	25
697	Monocyte chemotactic protein-1 deficiency attenuates and high-fat diet exacerbates bone loss in mice with Lewis lung carcinoma. <b>2017</b> , 8, 23303-23311	6
696	Cyclophosphamide causes osteoporosis in C57BL/6 male mice: suppressive effects of cyclophosphamide on osteoblastogenesis and osteoclastogenesis. <b>2017</b> , 8, 98163-98183	11
695	FK506 prevented bone loss in streptozotocin-induced diabetic rats via enhancing osteogenesis and inhibiting adipogenesis. <b>2019</b> , 7, 265	1
694	Cinacalcet attenuated bone loss via inhibiting parathyroid hormone-induced endothelial-to-adipocyte transition in chronic kidney disease rats. <b>2019</b> , 7, 312	2
693	B Cell Production of Both OPG and RANKL is Significantly Increased in Aged Mice. <b>2014</b> , 6, 8-17	16
692	Daily Acute Bouts of Weight-bearing During Hindlimb Unloading Mitigate Disuse-Induced Deficits in Cancellous Bone. <b>2018</b> , 6, 2-11	3
691	Assessment of Trabecular Bone Architecture and Intrinsic Properties of Cortical bone Tissue in a Mouse Model of Chronic Kidney Disease. <b>2011</b> , 20, 79-86	5
690	Histochemical and Radiological Study of Bone Regeneration by the Combinatorial Use of Tetrapod-Shaped Artificial Bone and Collagen. <b>2015</b> , 24, 199-210	2

689	Intra-observer error of mouse long bone cross section digitization. <b>2012</b> , 61, 340-349	1
688	Difference in Spinal Fusion Process in Osteopenic and Nonosteopenic Living Rat Models Using Serial Microcomputed Tomography. <b>2017</b> , 60, 348-354	2
687	IDH2-deficient mice develop spinal deformities with aging. <b>2018</b> , 67, 487-494	3
686	Multiscale Characterisation of Cortical Bone Tissue. <b>2019</b> , 9, 5228	1
685	Biomechanical Interfaces of Corticotomies on Periodontal Tissue Remodeling during Orthodontic Tooth Movement. <b>2021</b> , 11, 1	39
684	Marantodes pumilum Leaves Promote Repair of Osteoporotic fracture In Postmenopausal Sprague-Dawley Rats. <b>2018</b> , 14, 973-980	2
683	Predictors of midpalatal suture expansion by miniscrew-assisted rapid palatal expansion in young adults: A preliminary study. <b>2019</b> , 49, 360-371	13
682	Microcomputed Tomography Applications in Bone and Mineral Research. <b>2013</b> , 02, 121-127	4
681	Micro-computed tomography assessment of human femoral trabecular bone for two disease groups (fragility fracture and coxarthrosis): Age and gender related effects on the microstructure. <b>2013</b> , 06, 175-184	4
680	Vav1 inhibits RANKL-induced osteoclast differentiation and bone resorption. <b>2019</b> , 52, 659-664	2
679	Influence of reconstruction parameters of micro-computed tomography on the analysis of bone mineral density. <b>2020</b> , 50, 153-159	4
678	How image-processing parameters can influence the assessment of dental materials using micro-CT. <b>2020</b> , 50, 161-168	4
677	Clec11a/osteolectin is an osteogenic growth factor that promotes the maintenance of the adult skeleton. <b>2016</b> , 5,	51
676	MicroCT-based phenomics in the zebrafish skeleton reveals virtues of deep phenotyping in a distributed organ system. <b>2017</b> , 6,	37
675	Integrin alpha11 is an Osteolectin receptor and is required for the maintenance of adult skeletal bone mass. <b>2019</b> , 8,	35
674	Cortical bone maturation in mice requires SOCS3 suppression of gp130/STAT3 signalling in osteocytes. <b>2020</b> , 9,	11
673	Structural strength of cancellous specimens from bovine femur under cyclic compression. <b>2016</b> , 4, e1562	11
672	Diversification along a benthic to pelagic gradient contributes to fish diversity in the world's largest lake (Lake Baikal, Russia). <b>2021</b> ,	O

671	An X-ray micro-computer tomography study of the Malpighian tubules of the Blue Bottle Blow Fly (Calliphora vomitoria) Diptera: Calliphoridae. <b>2021</b> , 149, 125972	0
670	Bone-derived sclerostin and Wnt/II-catenin signaling regulate PDGFR dipoprogenitor cell differentiation. <b>2021</b> , 35, e21957	1
669	Study of Sexual Dimorphism in Metatarsal Bones: Geometric and Inertial Analysis of the Three-Dimensional Reconstructed Models. <b>2021</b> , 12, 734362	0
668	Brd4 is required for chondrocyte differentiation and endochondral ossification. <b>2022</b> , 154, 116234	O
667	Experimental evidence that physical activity inhibits osteoarthritis: Implications for inferring activity patterns from osteoarthritis in archeological human skeletons.	2
666	Anti-Friction MSCs Delivery System Improves the Therapy for Severe Osteoarthritis. <b>2021</b> , e2104758	7
665	Posttraumatic Osteoarthritis Damage in Mice: From Histological and Micro-Computed Tomodensitometric Changes to Gait Disturbance. <b>2021</b> , 19476035211053821	1
664	Transcriptome-wide Association Study and eQTL colocalization identify potentially causal genes responsible for bone mineral density GWAS associations.	Ο
663	A Three-Dimensional Mechanical Loading Model of Human Osteocytes in Their Native Matrix. <b>2021</b> , 110, 367	1
662	Genetic variability affects the skeletal response to immobilization in founder strains of the diversity outbred mouse population. <b>2021</b> , 15, 101140	0
661	Chronic exposure to lead acetate promotes changes in the alveolar bone of rats: microstructural and physical-chemical characterization. <b>2021</b> ,	
660	Post-traumatic osteoarthritis progression is diminished by early mechanical unloading and anti-inflammatory treatment in mice. <b>2021</b> ,	2
659	Antimicrobial-induced oral dysbiosis exacerbates naturally occurring alveolar bone loss. <b>2021</b> , 35, e22015	
658	Mast Cells Trigger Disturbed Bone Healing in Osteoporotic Mice. <i>Journal of Bone and Mineral Research</i> , <b>2021</b> ,	3
657	Spatial transcriptomics reveals a role for sensory nerves in preserving cranial suture patency through modulation of BMP/TGF-Dsignaling. <b>2021</b> , 118,	3
656	Systemic Administration of Recombinant Irisin Accelerates Fracture Healing in Mice. <b>2021</b> , 22,	5
655	Tributyltin protects against ovariectomy-induced trabecular bone loss in C57BL/6J mice with an attenuated effect in high fat fed mice. <b>2021</b> , 431, 115736	0
654	Timing of orthodontic tooth movement in bone defects repaired with synthetic scaffolds: A scoping review of animal studies. <b>2021</b> , 132, 105278	O

653	Effect of continuous and intermittent sodium alendronate oral dosing on post-extraction alveoli healing in rats. <b>2021</b> , 132, 105291	1
652	Hallmarks of frailty and osteosarcopenia in prematurely aged PolgAD257A/D257A mice.	
651	Registered Micro-Computed Tomography Data as a Four-Dimensional Imaging Biomarker of Bone Formation and Resorption. <b>2015</b> , 1-30	
650	Development of Self-Diagnosis Linearity Quality Assurance Technique in Computed Tomography by Using Iodic Contrast Media. <b>2015</b> , 15, 436-443	
649	Quantification of Implant Osseointegration by Means of a Reconstruction Algorithm on Micro-computed Tomography Images. <b>2016</b> , 111-122	
648	The Reproductive System. <b>2015</b> , 206-227	
647	Acute hypothalamic suppression significantly affects trabecular bone but not cortical bone following recovery and ovariectomy surgery in a rat model. <b>2016</b> , 4, e1575	0
646	Osteoporosis. <b>2016</b> , 569-578	
645	13. Analysis of mineral composition in osteoporosis. <b>2016</b> , 277-304	
644	Lifelong challenge of calcium homeostasis in male mice lacking TRPV5 leads to changes in bone and calcium metabolism. <b>2016</b> , 7, 24928-41	1
643	Genome-wide association study in Collaborative Cross mice reveals a role for Rhbdf2 in skeletal homeostasis.	
642	Low Dose Marantodes pumilum Leaf and Roots Extracts Preserved Bone Structure in Ovariectomized Rats. <b>2016</b> , 10, 1-9	1
641	Granulometry-Based Trabecular Bone Segmentation. 2017, 100-108	
640	microCT-Based Phenomics in the Zebrafish Skeleton Reveals Virtues of Deep Phenotyping in a Distributed Organ System.	
639	Direct biomechanical modeling of trabecular bone using a nonlinear manifold-based volumetric representation. <b>2017</b> ,	
638	Hepatic Osteodystrophy: The Mechanism of Bone Loss in Hepatocellular Disease and the Effects of Pamidronate Treatment. <b>2017</b> , 72, 231-237	2
637	Effects of mechanical loading on cortical defect repair using a novel mechanobiological model of bone healing.	
636	Micro-CT analysis of trabecular parameters gradients in femurs of mice affected by chronic kidney disease. <b>2018</b> ,	

635	ATRAID regulates the action of nitrogen-containing bisphosphonates on bone.	O
634	Integrin alpha11 is an Osteolectin receptor and is required for the maintenance of adult skeletal bone mass.	
633	Mouse Genome-Wide Association and Systems Genetics Identifies Lhfp as a Regulator of Bone Mass.	
632	Freshwater influence is associated with differences in bone mineral density and armour configuration in threespine stickleback (Gasterosteus aculeatus). <b>2018</b> , 3, 665-681	O
631	Osteocyte death and bone overgrowth in mice lacking Fibroblast Growth Factor Receptors 1 and 2 in mature osteoblasts and osteocytes.	
630	Genetic dissection of femoral and tibial microarchitecture.	
629	Effects of the secondhand smoking exposure in the early stages of the bone development.	
628	Combinatorial morphogenetic and mechanical cues to mimic bone development for defect repair.	
627	Medication-related osteonecrosis of the jaws after tooth extraction in senescent female mice treated with zoledronic acid: microtomographic, histological and immunohistochemical characterization.	1
626	Methods for quantitative characterization of bone injury from computed-tomography images. <b>2019</b> , 10953,	
625	Precocious Chondrocyte Differentiation Disrupts Skeletal Growth in Kabuki Syndrome Mice.	
624	Membrane-type 1 matrix metalloproteinase (MMP-14) modulates tissue homeostasis by a non-proteolytic mechanism.	
623	Novos mtodos de imagem em osteoporose: tomografia computadorizada quantitativa periftica de alta resolu <b>b</b> (HR-pQCT) e escore de osso trabecular (TBS). <b>2019</b> , 6-14	
622	Stroke prevents exercise-induced gains in bone microstructure but not composition in mice.	O
621	High Fat Diet-Induced Obesity Negatively Affects Whole Bone Bending Strength but not Cortical Structure in the Femur.	
620	MACF1 Facilitates SMAD7 Nuclear Translocation to Drive Bone Formation in Mice.	O
619	An Osteocalcin-deficient mouse strain without endocrine abnormalities.	
618	Stroke Prevents Exercise-induced Gains in Bone Microstructure But Not Composition in Mice. 2019,	

617	The heparan sulfate proteoglycan Syndecan-1 influences local bone cell communication via the RANKL/OPG axis.	
616	Etoricoxib decreases mouse subchondral bone mass and biomechanical properties in early osteoarthritis.	
615	Systemic Bone Loss Following Myocardial Infarction in Mice is Mitigated by Treatment with a $\ensuremath{\mathbb{B}}$ Adrenergic Receptor Antagonist.	
614	Characterizing Trabecular Bone Properties near the Glenohumeral Joint Following Brachial Plexus Birth Injury.	
613	Osteoking improves OP rat by enhancing HSP90-🛘 expression. <b>2020</b> , 45, 1543-1553	3
612	A new pipeline to automatically segment and semi-automatically measure bone length on 3D models obtained by Computed Tomography.	
611	Genetic Variability affects the Skeletal Response to Unloading.	
610	Monocyte Subsets with High Osteoclastogenic Potential and Their Epigenetic Regulation Orchestrated by IRF8.	
609	Effects of N-methyl-d-aspartate receptor antagonist MK-801 (dizocilpine) on bone homeostasis in mice. <b>2020</b> , 62, 131-138	O
608	Effects of early life stress on bone homeostasis in mice and humans.	O
607	Lactobacillus rhamnosus attenuates bone loss and maintains bone health by skewing Tregs-Th17 cell balance in Ovx mice.	O
606	Reconstitution of the host holobiont in germ-free born male rats acutely increases bone growth and affects marrow cellular content. <b>2021</b> , 53, 518-533	
605	Syrbactin-class dual constitutive- and immuno-proteasome inhibitor TIR-199 impedes myeloma-mediated bone degeneration in vivo.	
604	3D-Printed Porous Tantalum Coated with Antitubercular Drugs Achieving Antibacterial Properties and Good Biocompatibility. <b>2021</b> , e2100338	4
603	A novel therapeutic strategy for skeletal disorders: Proof of concept of gene therapy for X-linked hypophosphatemia. <b>2021</b> , 7, eabj5018	
602	Mechanical and morphological properties of parietal bone in patients with sagittal craniosynostosis. <b>2022</b> , 125, 104929	Ο
601	Subchondral Bone Microarchitectural and Mineral Properties and Expression of Key Degradative Proteinases by Chondrocytes in Human Hip Osteoarthritis. <b>2021</b> , 9,	
600	LRP5-Mediated Lipid Uptake Modulates Osteogenic Differentiation of Bone Marrow Mesenchymal Stromal Cells. <b>2021</b> , 9, 766815	O

599	The local and global geometry of trabecular bone.	
598	Feeding intervention potentiates the effect of mechanical loading to induce new bone formation in mice.	
597	PH domain and leucine rich repeat phosphatase 1 (Phlpp1) suppresses parathyroid hormone receptor 1 (Pth1r) expression and signaling during bone growth.	
596	The combination of aging and chronic kidney disease leads to an exacerbated cortical porosity phenotype. <b>2022</b> , 154, 116228	
595	Visualization of woven bone structure through analysis of biopsy specimens using synchrotron radiation and conventional X-ray microcomputed tomography. <b>2020</b> , 27, 199-206	
594	Validation of a rabbit model of irradiated bone healing: preliminary report. <b>2020</b> , 26, 24	
593	High-throughput microCT scanning of small specimens: preparation, packing, parameters and post-processing.	
592	Effects of C-peptide replacement therapy on bone microarchitecture parameters in streptozotocin-diabetic rats.	
591	Propranolol promotes bone formation and limits resorption through novel mechanisms during anabolic parathyroid hormone treatment in female C57BL/6J mice.	
590	A Method for the Quantification of Architectural Anisotropy in Cancellous Bone Samples Using CT Images. <b>2020</b> , 153-162	
589	Obesity-linked PPARI\$273 phosphorylation promotes insulin resistance through Growth Differentiation Factor 3.	
588	Pharmacological inhibition of longevity regulator PAPP-A restrains mesenchymal stromal cell activity.	
587	Trpm8 modulates thermogenesis in a sex-dependent manner without influencing cold-induced bone loss.	
586	The Thyroid Hormone Transporter MCT10 Is a Novel Regulator of Trabecular Bone Mass and Bone Turnover in Male Mice. <b>2022</b> , 163,	o
585	Gestational and lactational exposure to BPA, but not BPS, negatively impacts trabecular microarchitecture and cortical geometry in adult male offspring. <b>2021</b> , 15, 101147	О
584	Hairy and enhancer of split 1 is a primary effector of NOTCH2 signaling and induces osteoclast differentiation and function. <b>2021</b> , 297, 101376	1
583	Imatinib has minimal effects on inflammatory and osteopenic phenotypes in a murine cherubism model. <b>2021</b> ,	О
582	Decreased Trabecular Bone Mass in -Deficient Mice. <b>2021</b> , 10,	O

581	Harnessing Thor's Hammer: Experimentally induced lightning trauma to human bone by high impulse current <b>2021</b> , 3, 100206	О
580	A robust, semi-automated approach for counting cementum increments imaged with synchrotron X-ray computed tomography. <b>2021</b> , 16, e0249743	3
579	PPARI/Daccelerates bone regeneration in diabetic mellitus by enhancing AMPK/mTOR pathway-mediated autophagy. <b>2021</b> , 12, 566	2
578	Establishment of a Novel Method for Spinal Discectomy Surgery in Elderly Rats in an In Vivo Spinal Fusion Model. <b>2021</b> , 4,	O
577	Bone microstructure in healthy men measured by HR-pQCT: Age-related changes and their relationships with DXA parameters and biochemical markers. <b>2022</b> , 154, 116252	1
576	Inhibition of acid sphingomyelinase by imipramine abolishes the synergy between metabolic syndrome and periodontitis on alveolar bone loss. <b>2021</b> ,	O
575	Regional differences in microarchitecture and mineralization of the atrophic edentulous mandible: A microcomputed tomography study. <b>2022</b> , 133, 105302	O
574	Temporal and Quantitative Transcriptomic Differences Define Sexual Dimorphism in Murine Postnatal Bone Aging <b>2022</b> , 6, e10579	2
573	Skeletal Phenotype and Mechanisms of Bone Loss in Winnie Mice as a Model for Inflammatory Bowel Disease.	
572	Ablation of Proliferating Osteoblast Lineage Cells After Fracture Leads to Atrophic Nonunion in a Mouse Model.	
571	Soluble RANKL exaggerates hindlimb suspension-induced osteopenia but not muscle protein balance.	
570	Generation and Characterization of Mouse Models for Skeletal Disease. <b>2021</b> , 2221, 165-191	O
569	Nondestructive Assessment of Growing Rat Tibial Mechanical Properties Under Three-Point Bending: A Microcomputed Tomography Based Finite Element Study. <b>2020</b> , 142,	
568	APPL1 negatively regulates bone mass, possibly by controlling the fate of bone marrow mesenchymal progenitor cells. <b>2020</b> , 96, 364-371	O
567	PPARG in osteocytes is essential for sclerostin expression, bone mass, marrow adiposity and TZD-induced bone loss.	
566	Application of subject-specific adaptive mechanical loading for bone healing in a mouse tail vertebral defect.	
565	A comparative study of trabecular bone micro-structural measurements using different CT modalities. <b>2020</b> ,	4
564	Sclerostin depletion induces inflammation in the bone marrow of mice.	

563	MicroCT for Scanning and Analysis of Mouse Bones. <b>2021</b> , 2230, 169-198	2
562	Overview of Skeletal Repair (Fracture Healing and Its Assessment). <b>2021</b> , 2230, 17-37	O
561	Three-dimensional bone modeling of forelimb joints in New Zealand Rabbit: A Micro-Computed Tomography study.	
560	Atypical antipsychotic drugs inhibit trabecular bone accrual in C57BL/6J mice. <b>2013</b> , 11, 21-24	2
559	Bone loss from high repetitive high force loading is prevented by ibuprofen treatment. <b>2014</b> , 14, 78-94	28
558	Exercise protocol induces muscle, tendon, and bone adaptations in the rat shoulder. <b>2014</b> , 4, 413-9	19
557	Combined micro CT and histopathology for evaluation of skeletal metastasis in live animals. <b>2015</b> , 7, 348-55	5
556	Local delivery of a selective androgen receptor modulator failed as an anabolic agent in a rat bone marrow ablation model. <b>2015</b> , 86, 751-9	1
555	Osteocytic connexin 43 is not required for the increase in bone mass induced by intermittent PTH administration in male mice. <b>2016</b> , 16, 45-57	10
554	In vivo dynamic compression has less detrimental effect than static compression on newly formed bone of a rat caudal vertebra. <b>2016</b> , 16, 211-20	5
553	Alterations in gene expression precede sarcopenia and osteopenia in botulinum toxin immobilized mice. <b>2016</b> , 16, 355-368	11
552	Effect of electrical stimulation-induced muscle force and streptomycin treatment on muscle and trabecular bone mass in early-stage disuse musculoskeletal atrophy. <b>2015</b> , 15, 270-8	6
551	Pantoprazole, a proton pump inhibitor, does not prevent botulinum toxin induced disuse osteopenia in mice. <b>2017</b> , 17, 162-175	4
550	Alterations to maternal cortical and trabecular bone in multiparous middle-aged mice. 2017, 17, 312-318	1
549	Zoledronic acid prevents disuse osteopenia and augments gene expression of osteoclastic differentiation markers in mice. <b>2018</b> , 18, 165-175	5
548	Neuromuscular dysfunction, independent of gait dysfunction, modulates trabecular bone homeostasis in mice. <b>2019</b> , 19, 79-93	4
547	Advanced oxidation protein products accelerated the bone loss and weakened bone strength in ovariectomised rats. <b>2017</b> , 10, 8402-8413	
546	Gender differences in tibial fractures healing in normal and muscular dystrophic mice. <b>2020</b> , 12, 2640-2651	4

Recombinant Human Bone Morphogenetic Protein-2 Improves Spine Fusion in a Vitamin D-Deficient Rat Model, 2020, 14, 694-705  1 Efficient Rat Model, 2020, 14, 694-705  1 Influence of incomputed tomographic study in dogs], 2021, 53, 364-370  1 Three dimensional modeling and quantitative analysis of long bone parameters of rabbit using inextraction sockets: A micro-computed tomography, 2021, 22, 140-145  1 Influence of fixation on CA4+ contrast enhanced micro-CT of articular cartilage and subsequent feasibility for histological evaluation, 2021, 13, 921-8937  1 Influence of fixation on CA4+ contrast enhanced micro-CT of articular cartilage and subsequent feasibility for histological evaluation, 2021, 13, 921-8937  1 Discontinuation of PTH therapy amplifies bone loss by increasing oxidative stress: An event ameliorated by sequential IL-17 neutralizing antibody therapy, 2021, 145, 112390  2 Discontinuation of PTH therapy amplifies bone loss by increasing oxidative stress: An event ameliorated by sequential IL-17 neutralizing antibody therapy, 2021, 145, 112390  2 Discontinuation of PTH therapy amplifies bone loss by increasing oxidative stress: An event ameliorated by sequential IL-17 neutralizing antibody therapy, 2021, 145, 112390  3 Discontinuation of PTH therapy amplifies bone loss burners in a protect the femoral head against tobaccos smoke exposure-induced osteonecrosis in spontaneously hypertensive rats, 2021, 465, 153045  3 Hematopoiletic stem cell-derived functional oxteoblasts exhibit therapeutic efficacy in a murine model of osteogenesis imperfecta, 2021, 39, 1457-1477  3 Hematopoiletic stem cell-derived functional oxteoblasts exhibit therapeutic efficacy in a murine model of osteogenesis imperfecta and submit and protects and protects are submit and submit and protects and protects are submit and submit and protects are submit and s	545	Impaired bone defect and fracture healing in dystrophin/utrophin double-knockout mice and the mechanism. <b>2020</b> , 12, 5269-5282	
Three dimensional modeling and quantitative analysis of long bone parameters of rabbit using micro-computed tomography, 2021, 22, 140-145  Influence of fixation on CA4+ contrast enhanced microCT of articular cartilage and subsequent feasibility for histological evaluation. 2021, 13, 8921-8937  Discontinuation of PTH therapy amplifies bone loss by increasing oxidative stress: An event ameliorated by sequential IL-17 neutralizing antibody therapy, 2021, 145, 112390  Soluble epoxide hydrolase inhibitor can protect the femoral head against tobacco smoke exposure-induced osteonecrosis in spontaneously hypertensive rats. 2021, 465, 153045  Hematopoietic stem cell-derived functional osteoblasts exhibit therapeutic efficacy in a murine model of osteogenesis imperfecta. 2021, 39, 1457-1477  High-resolution analysis of the degradation and osseointegration of Mg-xGd implant screws in 3D 2022, 13, 37-52  The Use of Mushrooms and Spirulina Algae as Supplements to Prevent Growth Inhibition in a Pre-Clinical Model for an Unbalanced Diet. 2021, 13, 13, 13, 14, 14, 14, 14, 14, 14, 14, 14, 14, 14	544		1
influence of fixation on CA4+ contrast enhanced microCT of articular cartilage and subsequent feasibility for histological evaluation. 2021, 13, 8921-8937  biscontinuation of PTH therapy amplifies bone loss by increasing oxidative stress: An event ameliorated by sequential IL-17 neutralizing antibody therapy. 2021, 145, 112390  50 Discontinuation of PTH therapy amplifies bone loss by increasing oxidative stress: An event ameliorated by sequential IL-17 neutralizing antibody therapy. 2021, 145, 112390  50 Discontinuation of PTH therapy amplifies bone loss by increasing oxidative stress: An event ameliorated by sequential IL-17 neutralizing antibody therapy. 2021, 145, 112390  50 Discontinuation of PTH therapy amplifies bone loss by increasing oxidative stress: An event ameliorated by sequential IL-17 neutralizing antibody therapy. 2021, 145, 112390  50 Discontinuation of PTH therapy amplifies bone loss by increasing oxidative stress: An event ameliorated by sequential IL-17 neutralizing antibody therapy. 2021, 146, 112390  50 Discontinuation of purple and protects the femoral head against tobacco smoke exposure-induced steepore-tiss, 2021, 1465, 112390  51 Hematopoietic stem cell-derived functional osteoblasts exhibit therapeutic efficacy in a murine model of osteogenesis in 3D.  51 Discontinuation analysis of the degradation alosteoblasts exhibit therapeutic efficacy in a murine model of osteogenesis in 3D.  52 Discontinuation analysis of the degradation and osseointegration of Mg-xGd implant screws in 3D.  53 Discontinuation analysis of the degradation and osseointegration of Mg-xGd implant screws in 3D.  53 Discontinuation analysis of the degradation and osseointegration of Mg-xGd implant screws in 3D.  53 Discontinuation analysis of the degradation and osseointegrates bone morphology and exacerbates bone loss during aging. 2021, 20, e13505  53 Discontinuation of Sumatopause in adult mice compromises bone morphology and exacerbates bone loss during aging. 2021, 20, e13505  54 Discontinuation of analysis of th	543		
Discontinuation of PTH therapy amplifies bone loss by increasing oxidative stress: An event ameliorated by sequential IL-17 neutralizing antibody therapy. 2021, 145, 112390 o  Soluble epoxide hydrolase inhibitor can protect the femoral head against tobacco smoke exposure-induced osteonecrosis in spontaneously hypertensive rats. 2021, 465, 153045 o  Hematopoietic stem cell-derived functional osteoblasts exhibit therapeutic efficacy in a murine model of osteogenesis imperfecta. 2021, 39, 1457-1477 3  High-resolution analysis of the degradation and osseointegration of Mg-xGd implant screws in 3D 2022, 13, 37-52  The Use of Mushrooms and Spirulina Algae as Supplements to Prevent Growth Inhibition in a Pre-Clinical Model for an Unbalanced Diet 2021, 13, 130-1535 during aging. 2021, 20, e13505 1  Induction of somatopause in adult mice compromises bone morphology and exacerbates bone loss during aging. 2021, 20, e13505 1  Challenge Tooth Regeneration in Adult Dogs with Dental Pulp Stem Cells on 3D-Printed Hydroxyapatite/Polylactic Acid Scaffolds 2021, 10, 1  Non-Obese MKR Mouse Model of Type 2 Diabetes Reveals Skeletal Alterations in Mineralization and Material Properties 2022, 6, e10583 1  Activation of canonical Wnt signaling accelerates intramembranous bone regeneration in male mice. 2021, 1  Mouse LGR6 regulates osteogenesis in vitro and in vivo through differential ligand use. 2021, 155, 116267 2  Inhibition of TGF-Disignaling attenuates disuse-induced trabecular bone loss after spinal cord injury in male mice. 2021, 1  The WNT1 mutation specifically affects skeletal integrity in a mouse model of osteogenesis	542		1
Soluble epoxide hydrolase inhibitor can protect the femoral head against tobacco smoke exposure-induced osteonecrosis in spontaneously hypertensive rats. 2021, 465, 153045  38 Hematopoietic stem cell-derived functional osteoblasts exhibit therapeutic efficacy in a murine model of osteogenesis imperfecta. 2021, 39, 1457-1477  39 High-resolution analysis of the degradation and osseointegration of Mg-xGd implant screws in 3D 2022, 13, 37-52  30 The Use of Mushrooms and Spirulina Algae as Supplements to Prevent Growth Inhibition in a Pre-Clinical Model for an Unbalanced Diet 2021, 13, 10 Induction of somatopause in adult mice compromises bone morphology and exacerbates bone loss during aging. 2021, 20, e13505  30 Challenge Tooth Regeneration in Adult Dogs with Dental Pulp Stem Cells on 3D-Printed Hydroxyapatite/Polylactic Acid Scaffolds 2021, 10, 10 Non-Obese MKR Mouse Model of Type 2 Diabetes Reveals Skeletal Alterations in Mineralization and Material Properties 2022, 6, e10583  31 Activation of canonical Wnt signaling accelerates intramembranous bone regeneration in male mice. 2021,  32 Partial prevention of glucocorticoid-induced osteocyte deterioration with osteocrin gene therapy.  33 Mouse LGR6 regulates osteogenesis in vitro and in vivo through differential ligand use. 2021, 155, 116267  34 Inhibition of TGF-Dsignaling attenuates disuse-induced trabecular bone loss after spinal cord injury in male mice. 2021,  35 The WNT1 mutation specifically affects skeletal integrity in a mouse model of osteogenesis	541		
exposure-induced osteonecrosis in spontaneously hypertensive rats. 2021, 465, 153045  Hematopoietic stem cell-derived functional osteoblasts exhibit therapeutic efficacy in a murine model of osteogenesis imperfecta. 2021, 39, 1457-1477  High-resolution analysis of the degradation and osseointegration of Mg-xGd implant screws in 3D 2022, 13, 37-52  The Use of Mushrooms and Spirulina Algae as Supplements to Prevent Growth Inhibition in a Pre-Clinical Model for an Unbalanced Diet 2021, 13, 10  Induction of somatopause in adult mice compromises bone morphology and exacerbates bone loss during aging. 2021, 20, e13505  Challenge Tooth Regeneration in Adult Dogs with Dental Pulp Stem Cells on 3D-Printed Hydroxyapatite/Polylactic Acid Scaffolds 2021, 10, 10  Non-Obese MKR Mouse Model of Type 2 Diabetes Reveals Skeletal Alterations in Mineralization and Material Properties 2022, 6, e10583  Activation of canonical Wnt signaling accelerates intramembranous bone regeneration in male mice. 2021,  Partial prevention of glucocorticoid-induced osteocyte deterioration with osteocrin gene therapy.  Mouse LGR6 regulates osteogenesis in vitro and in vivo through differential ligand use. 2021, 155, 116267  Inhibition of TGF-Usignaling attenuates disuse-induced trabecular bone loss after spinal cord injury in male mice. 2021,  The WNT1 mutation specifically affects skeletal integrity in a mouse model of osteogenesis	540		O
model of osteogenesis imperfecta. 2021, 39, 1457-1477  High-resolution analysis of the degradation and osseointegration of Mg-xGd implant screws in 3D 2022, 13, 37-52  The Use of Mushrooms and Spirulina Algae as Supplements to Prevent Growth Inhibition in a Pre-Clinical Model for an Unbalanced Diet 2021, 13,  Induction of somatopause in adult mice compromises bone morphology and exacerbates bone loss during aging. 2021, 20, e13505  Challenge Tooth Regeneration in Adult Dogs with Dental Pulp Stem Cells on 3D-Printed Hydroxyapatite/Polylactic Acid Scaffolds 2021, 10,  Non-Obese MKR Mouse Model of Type 2 Diabetes Reveals Skeletal Alterations in Mineralization and Material Properties 2022, 6, e10583  Activation of canonical Wnt signaling accelerates intramembranous bone regeneration in male mice. 2021,  Partial prevention of glucocorticoid-induced osteocyte deterioration with osteocrin gene therapy.  Mouse LGR6 regulates osteogenesis in vitro and in vivo through differential ligand use. 2021, 155, 116267  Inhibition of TGF-Usignaling attenuates disuse-induced trabecular bone loss after spinal cord injury in male mice. 2021,  The WNT1 mutation specifically affects skeletal integrity in a mouse model of osteogenesis	539		О
The Use of Mushrooms and Spirulina Algae as Supplements to Prevent Growth Inhibition in a Pre-Clinical Model for an Unbalanced Diet 2021, 13,  Induction of somatopause in adult mice compromises bone morphology and exacerbates bone loss during aging. 2021, 20, e13505  Challenge Tooth Regeneration in Adult Dogs with Dental Pulp Stem Cells on 3D-Printed Hydroxyapatite/Polylactic Acid Scaffolds 2021, 10,  Non-Obese MKR Mouse Model of Type 2 Diabetes Reveals Skeletal Alterations in Mineralization and Material Properties 2022, 6, e10583  Activation of canonical Wnt signaling accelerates intramembranous bone regeneration in male mice. 2021,  Partial prevention of glucocorticoid-induced osteocyte deterioration with osteocrin gene therapy.  Mouse LGR6 regulates osteogenesis in vitro and in vivo through differential ligand use. 2021, 155, 116267  Inhibition of TGF-II signaling attenuates disuse-induced trabecular bone loss after spinal cord injury in male mice. 2021,  The WNT1 mutation specifically affects skeletal integrity in a mouse model of osteogenesis	538		3
Pre-Clinical Model for an Unbalanced Diet 2021, 13,  Induction of somatopause in adult mice compromises bone morphology and exacerbates bone loss during aging. 2021, 20, e13505  Challenge Tooth Regeneration in Adult Dogs with Dental Pulp Stem Cells on 3D-Printed Hydroxyapatite/Polylactic Acid Scaffolds 2021, 10,  Non-Obese MKR Mouse Model of Type 2 Diabetes Reveals Skeletal Alterations in Mineralization and Material Properties 2022, 6, e10583  Activation of canonical Wnt signaling accelerates intramembranous bone regeneration in male mice. 2021,  Partial prevention of glucocorticoid-induced osteocyte deterioration with osteocrin gene therapy.  Mouse LGR6 regulates osteogenesis in vitro and in vivo through differential ligand use. 2021, 155, 116267  Inhibition of TGF-IJsignaling attenuates disuse-induced trabecular bone loss after spinal cord injury in male mice. 2021,  The WNT1 mutation specifically affects skeletal integrity in a mouse model of osteogenesis	537		3
Challenge Tooth Regeneration in Adult Dogs with Dental Pulp Stem Cells on 3D-Printed Hydroxyapatite/Polylactic Acid Scaffolds 2021, 10,  Non-Obese MKR Mouse Model of Type 2 Diabetes Reveals Skeletal Alterations in Mineralization and Material Properties 2022, 6, e10583  Activation of canonical Wnt signaling accelerates intramembranous bone regeneration in male mice. 2021,  Partial prevention of glucocorticoid-induced osteocyte deterioration with osteocrin gene therapy.  Mouse LGR6 regulates osteogenesis in vitro and in vivo through differential ligand use. 2021, 155, 116267  Inhibition of TGF-Dsignaling attenuates disuse-induced trabecular bone loss after spinal cord injury in male mice. 2021,  The WNT1 mutation specifically affects skeletal integrity in a mouse model of osteogenesis	536		O
Hydroxyapatite/Polylactic Acid Scaffolds 2021, 10,  Non-Obese MKR Mouse Model of Type 2 Diabetes Reveals Skeletal Alterations in Mineralization and Material Properties 2022, 6, e10583  Activation of canonical Wnt signaling accelerates intramembranous bone regeneration in male mice. 2021,  Partial prevention of glucocorticoid-induced osteocyte deterioration with osteocrin gene therapy.  Mouse LGR6 regulates osteogenesis in vitro and in vivo through differential ligand use. 2021, 155, 116267  Inhibition of TGF-Ilsignaling attenuates disuse-induced trabecular bone loss after spinal cord injury in male mice. 2021,  The WNT1 mutation specifically affects skeletal integrity in a mouse model of osteogenesis	535		1
and Material Properties 2022, 6, e10583  Activation of canonical Wnt signaling accelerates intramembranous bone regeneration in male mice. 2021,  Partial prevention of glucocorticoid-induced osteocyte deterioration with osteocrin gene therapy.  Mouse LGR6 regulates osteogenesis in vitro and in vivo through differential ligand use. 2021, 155, 116267  Inhibition of TGF-Dsignaling attenuates disuse-induced trabecular bone loss after spinal cord injury in male mice. 2021,  The WNT1 mutation specifically affects skeletal integrity in a mouse model of osteogenesis	534		4
Partial prevention of glucocorticoid-induced osteocyte deterioration with osteocrin gene therapy.  Mouse LGR6 regulates osteogenesis in vitro and in vivo through differential ligand use. 2021, 155, 116267  Inhibition of TGF-Dsignaling attenuates disuse-induced trabecular bone loss after spinal cord injury in male mice. 2021,  The WNT1 mutation specifically affects skeletal integrity in a mouse model of osteogenesis	533	_ ·	1
Mouse LGR6 regulates osteogenesis in vitro and in vivo through differential ligand use. <b>2021</b> , 155, 116267  Inhibition of TGF-D signaling attenuates disuse-induced trabecular bone loss after spinal cord injury in male mice. <b>2021</b> ,  The WNT1 mutation specifically affects skeletal integrity in a mouse model of osteogenesis	532		O
Inhibition of TGF-Disignaling attenuates disuse-induced trabecular bone loss after spinal cord injury in male mice. <b>2021</b> ,  The WNT1 mutation specifically affects skeletal integrity in a mouse model of osteogenesis	531	Partial prevention of glucocorticoid-induced osteocyte deterioration with osteocrin gene therapy.	
in male mice. <b>2021</b> ,  The WNT1 mutation specifically affects skeletal integrity in a mouse model of osteogenesis	530	Mouse LGR6 regulates osteogenesis in vitro and in vivo through differential ligand use. <b>2021</b> , 155, 116267	2
	529		0
	528		2

527	Silk Fibroin Scaffolds as Biomaterials for 3D Mesenchymal Stromal Cells Cultures. <b>2021</b> , 11, 11345	1
526	Osteoblast-specific inactivation of p53 results in locally increased bone formation. <b>2021</b> , 16, e0249894	O
525	Injectable Erythrocyte Gel Loaded with Bulleyaconitine A for the Treatment of Rheumatoid Arthritis. <b>2021</b> ,	1
524	On the human vertebra computational modeling: a literature review. 1	1
523	Transcriptional responses of skeletal stem/progenitor cells to hindlimb unloading and recovery correlate with localized but not systemic multi-systems impacts. <b>2021</b> , 7, 49	2
522	Perspective of the GEMSTONE Consortium on Current and Future Approaches to Functional Validation for Skeletal Genetic Disease Using Cellular, Molecular and Animal-Modeling Techniques <b>2021</b> , 12, 731217	1
521	PPARI/Dagonist Alleviates Diabetic Osteoporosis Regulating M1/M2 Macrophage Polarization <b>2021</b> , 9, 753194	O
520	Micro-angiogenic patterns around orthodontic implants migrating in bone: A micro-CT study in the rat tail model. <b>2021</b> ,	
519	Refining the mandibular osteoradionecrosis rat model by in vivo longitudinal µCT analysis. <b>2021</b> , 11, 22241	O
518	Heterogeneous Tissue Modulus Improved Prediction of Mechanical Behavior in Osteoporotic Vertebral Cancellous Bone.	O
517	Effects of Once-Weekly Teriparatide Treatment on Trabecular Bone Microdamage Accumulation and Cortical Structure in the Lumbar Vertebrae of Ovariectomized Cynomolgus Monkeys. <b>2022</b> , 361-376	
516	Assessment of Osteoporosis by QCT, HR-pQCT, and MRI. <b>2022</b> , 177-185	Ο
515	Bone Phenotyping Approaches in Human, Mice and Zebrafish - Expert Overview of the EU Cost Action GEMSTONE ("GEnomics of MusculoSkeletal traits TranslatiOnal NEtwork") <b>2021</b> , 12, 720728	O
514	Three-Dimensional Microstructural Measurement for Predicting the Risk of Osteoporotic Fracture. <b>2022</b> , 129-160	
513	P2RX7 inhibition reduces breast cancer induced osteolytic lesions - implications for bone metastasis.	0
512	Effect of Swell1 on regulating chondrocyte hypertrophy during the condylar osteochondral development process in mice <b>2021</b> , 590, 42-48	
511	RANKL inhibition halts lesion progression and promotes bone remineralization in mice with fibrous dysplasia <b>2021</b> , 156, 116301	О
510	Induction and rescue of skeletal fragility in a high-fat diet mouse model of type 2 diabetes: An in vivo and in vitro approach <b>2021</b> , 116302	3

509	Effects of organic macro and trace minerals in fast and slower growing broiler breeders' diet on offspring growth performance and tibia characteristics <b>2021</b> , 101, 101647		O
508	Deletion of IL-17ra in osteoclast precursors increases bone mass by decreasing osteoclast precursor abundance <b>2021</b> , 157, 116310		O
507	Modulating the systemic and local adaptive immune response after fracture improves bone regeneration during aging <b>2022</b> , 116324		1
506	Sex-specific differences in direct osteoclastic indirect osteoblastic effects underlay the low bone mass of Pannexin1 deletion in TRAP-expressing cells in mice <b>2022</b> , 16, 101164		O
505	Housing in the Animal Enclosure Module Spaceflight Hardware Increases Trabecular Bone Mass in Ground-Control Mice. <b>2013</b> , 1, 2-19		3
504	Recombinant Human Bone Morphogenetic Proteinâl Improves Spine Fusion in a Vitamin DâlDeficient Rat Model. <b>2020</b> , 14, 694-705		1
503	Alterations of Bone Material Properties in Growing  Ifitm5/Bril p.S42 Knock-In Mice, a New Model for Atypical  Type VI Osteogenesis Imperfecta.		
502	Macrophages in epididymal adipose tissue secrete osteopontin to regulate bone homeostasis <b>2022</b> , 13, 427		2
501	Short Cyclic Regimen with Parathyroid Hormone (PTH) Results in Prolonged Anabolic Effect Relative to Continuous Treatment Followed by Discontinuation in Ovariectomized Rats <i>Journal of Bone and Mineral Research</i> , <b>2021</b> ,	6.3	1
500	Alcohol and Circadian Disruption Minimally Impact Bone Properties in Two Cohorts of Male Mice While Between-Cohort Differences Predominate: Association With Season of Birth?. <b>2022</b> , 6, e10591		
499	Loss of Vlk in Prx1 cells delays the initial steps of endochondral bone formation and fracture repair in the limb <i>Journal of Bone and Mineral Research</i> , <b>2022</b> ,	6.3	
498	Hao1 Is Not a Pathogenic Factor for Ectopic Ossifications but Functions to Regulate the TCA Cycle In Vivo <b>2022</b> , 12,		
497	Degradation of the NOTCH intracellular domain by elevated autophagy in osteoblasts promotes osteoblast differentiation and alleviates osteoporosis <b>2022</b> , 1-10		3
496	Bone microarchitecture and strength in long-standing type 1 diabetes <i>Journal of Bone and Mineral Research</i> , <b>2022</b> ,	6.3	O
495	How do imaging protocols affect the assessment of root-end fillings?. <b>2022</b> , 47, e2		
494	The Ability and Mechanism of nHAC/CGF in Promoting Osteogenesis and Repairing Mandibular Defects <b>2022</b> , 12,		1
493	Osteopenia in a Mouse Model of Spinal Cord Injury: Effects of Age, Sex and Motor Function <b>2022</b> , 11,		0
492	Lipocalin 2 Influences Bone and Muscle Phenotype in the Mouse Model of Duchenne Muscular Dystrophy <b>2022</b> , 23,		3

491	Histone H3K27 demethylase, Utx, regulates osteoblast-to-osteocyte differentiation <b>2021</b> , 590, 132-138	1
490	Intermittent parathyroid hormone treatment affects the bone structural parameters and mechanical strength of the femoral neck after ovariectomy-induced osteoporosis in rats <b>2022</b> , 21, 6	O
489	Treatment with Soluble Activin Type IIB Receptor Ameliorates Ovariectomy-Induced Bone Loss and Fat Gain in Mice <b>2022</b> ,	
488	Commensal oral microbiota induces osteoimmunomodulatory effects separate from systemic microbiome in mice <b>2022</b> ,	O
487	Syrbactin-class dual constitutive- and immuno-proteasome inhibitor TIR-199 impedes myeloma-mediated bone degeneration in vivo <b>2022</b> ,	4
486	Effects of masticatory loading on bone remodeling around teeth vs. implants: insights from a preclinical model <b>2022</b> ,	1
485	Technical note: Mapping of trabecular bone anisotropy and volume fraction in 3D using $\Omega T$ images of the human calcaneus.	
484	The impact of weight cycling on health outcomes in animal models: A systematic review and meta-analysis <b>2022</b> , e13416	O
483	GDF15 promotes prostate cancer bone metastasis and colonization through osteoblastic CCL2 and RANKL activation <b>2022</b> , 10, 6	2
482	☑-Adrenoceptor Deficiency Results in Increased Calcified Cartilage Thickness and Subchondral Bone Remodeling in Murine Experimental Osteoarthritis <b>2021</b> , 12, 801505	O
481	Myeloid-derived growth factor (MYDGF) protects bone mass through inhibiting osteoclastogenesis and promoting osteoblast differentiation <b>2022</b> , e53509	2
480	Effect of data binning and frame averaging for micro-CT image acquisition on the morphometric outcome of bone repair assessment <b>2022</b> , 12, 1424	1
479	Imaging Study on Acupuncture Inhibiting Inflammation and Bone Destruction in Knee Osteoarthritis Induced by Monosodium Iodoacetate in Rat Model <b>2022</b> , 15, 93-103	
478	Nutritional Approaches as a Treatment for Impaired Bone Growth and Quality Following the Consumption of Ultra-Processed Food <b>2022</b> , 23,	O
477	Ibandronate Suppresses Changes in Apatite Orientation and Young's Modulus Caused by Estrogen Deficiency in Rat Vertebrae <b>2022</b> , 1	
476	Loss of phosphatidylinositol-4-phosphate 5-kinase type-1 gamma (Pip5k1c) in mesenchymal stem cells leads to osteopenia by impairing bone remodeling <b>2022</b> , 101639	O
475	Activation of osteoblast ferroptosis via the METTL3/ASK1-p38 signaling pathway in high glucose and high fat (HGHF)-induced diabetic bone loss <b>2022</b> , 36, e22147	6
474	Characterization of pain-related behaviors, changes in bone microarchitecture and sensory innervation induced by chronic cadmium exposure in adult mice <b>2022</b> , 89, 99-99	O

473	Injectable hydrogels with high drug loading through B-N coordination and ROS-triggered drug release for efficient treatment of chronic periodontitis in diabetic rats <b>2022</b> , 282, 121387		7
472	Cortical porosity development and progression is mitigated after etelcalcetide treatment in an animal model of chronic kidney disease <b>2022</b> , 116340		O
471	MRI-based mechanical competence assessment of bone using micro finite element analysis (micro-FEA): Review <b>2022</b> , 88, 9-9		O
470	A high-throughput semi-automated bone segmentation workflow for murine hindpaw micro-CT datasets <b>2022</b> , 16, 101167		2
469	Propranolol promotes bone formation and limits resorption through novel mechanisms during anabolic parathyroid hormone treatment in female C57BL/6J mice <i>Journal of Bone and Mineral Research</i> , <b>2022</b> ,	6.3	O
468	Prediction of Cortical Bone Thickness Variations in the Tibial Diaphysis of Running Rats <b>2022</b> , 12,		
467	Inhibition of Cdk5 Ameliorates Skeletal Bone Loss in Glucocorticoid-Treated Mice <b>2022</b> , 10,		O
466	Cortical porosity is elevated after a single dose of zoledronate in two rodent models of chronic kidney disease <b>2022</b> , 16, 101174		
465	Role of Autonomous Neuropathy in Diabetic Bone Regeneration 2022, 11,		O
464	O-fucosylation of thrombospondin type 1 repeats is essential for ECM remodeling and signaling during bone development <b>2022</b> , 107, 77-77		2
463	Microstructural and histomorphological features of osteophytes in late-stage human knee osteoarthritis with varus deformity <b>2022</b> , 89, 105353		О
462	Combining sclerostin neutralization with tissue engineering: an improved strategy for craniofacial bone repair. <b>2021</b> , 140, 178-178		2
461	Large-scale osteocyte lacunar morphological analysis of transiliac bone in normal and osteoporotic premenopausal women.		
460	Ultra-Processed Food Impairs Bone Quality, Increases Marrow Adiposity and Alters Gut Microbiome in Mice <b>2021</b> , 10,		O
459	<i>FLNA</i> -Filaminopathy Skeletal Phenotypes are Not Due to an Osteoblast Autonomous Loss-of-Function.		
45 <sup>8</sup>	Individual Trabecular Bone Demonstrate a Linear Relation between Deteriorated Volume Fraction and Mechanical Properties - a Discovery Come from 3D Printing Combining Finite Element Method.		
457	Juvenile toxicology testing. <b>2022</b> , 75-92		
456	Specific overexpression of SIRT1 in mesenchymal stem cells rescues hematopoiesis niche in BMI1 knockout mice through promoting CXCL12 expression <b>2022</b> , 18, 2091-2103		O

455	Bisphenol A-Related Effects on Bone Morphology and Biomechanical Properties in an Animal Model <b>2022</b> , 10,	0
454	Quantitative in vivo micro-computed tomography for monitoring disease activity and treatment response in a collagen-induced arthritis mouse model <b>2022</b> , 12, 2863	1
453	The Role of Bone Muscle Ring Finger-1 (MuRF1), MuRF2, MuRF3, and Atrogin-1 on Microarchitecture In Vivo <b>2022</b> , 1	
452	Insulin-like growth factor binding protein 2 null mice (Igfbp2-/-) are protected against trabecular bone loss after vertical sleeve gastrectomy <b>2022</b> ,	
451	Focal osteoporosis defect is associated with vertebral compression fracture prevalence in a bone mineral density-independent manner <b>2022</b> , 5, e1195	
450	NLRP3 Is Involved in Neutrophil Mobilization in Experimental Periodontitis <b>2022</b> , 13, 839929	O
449	Lycopene Improves Bone Quality and Regulates AGE/RAGE/NF- <del>B</del> -Signaling Pathway in High-Fat Diet-Induced Obese Mice <b>2022</b> , 2022, 3697067	1
448	Growth and development of trabecular structure in the calcaneus of Japanese macaques (Macaca fuscata) reflects locomotor behavior, life history, and neuromuscular development <b>2022</b> ,	O
447	Regulation of sclerostin by the SIRT1 stabilization pathway in osteocytes 2022,	1
446	A computational framework for canonical holistic morphometric analysis of trabecular bone <b>2022</b> , 12, 5187	O
445	Bone biopsy findings in patients receiving long-term bisphosphonate therapy for glucocorticoid-induced osteoporosis <b>2022</b> , 1	O
444	Peripartal treatment with low-dose sertraline accelerates mammary gland involution and has minimal effects on maternal and offspring bone <b>2022</b> , 10, e15204	1
443	Selection of animal bone surrogate samples for orthopaedic screw testing based on human radius CT-derived bone morphology <b>2022</b> , 103, 103786	
442	Effects of Channels and Micropores in Honeycomb Scaffolds on the Reconstruction of Segmental Bone Defects <b>2022</b> , 10, 825831	1
441	Intravenous Transplantation of Human Hair Follicle-Derived Mesenchymal Stem Cells Ameliorates Trabecular Bone Loss in Osteoporotic Mice <b>2022</b> , 10, 814949	0
440	Role of nuclear factor of activated T cells in chondrogenesis osteogenesis and osteochondroma formation <b>2022</b> , 1	
439	Quantifying vascularity in the frontoparietal dome of Stegoceras validum (Dinosauria: Pachycephalosauridae) from high resolution CT scans.	О
438	Lonafarnib Inhibits Farnesyltransferase via Suppressing ERK Signaling Pathway to Prevent Osteoclastogenesis in Titanium Particle-Induced Osteolysis <b>2022</b> , 13, 848152	

437	Functional replacement of myostatin with GDF-11 in the germline of mice 2022, 12, 7	1
436	Bone Mass and Osteoblast Activity Are Sex-Dependent in Mice Lacking the Estrogen Receptor <del>I</del> n Chondrocytes and Osteoblast Progenitor Cells <b>2022</b> , 23,	1
435	Role of Neural (N)-Cadherin in Breast Cancer Cell Stemness and Dormancy in the Bone Microenvironment <b>2022</b> , 14,	O
434	Mice with Targeted Knockout of Tetraspanin 3 Exhibit Reduced Trabecular Bone Mass Caused by Decreased Osteoblast Functions <b>2022</b> , 11,	O
433	Human periodontal ligament stem cells with distinct osteogenic potential induce bone formation in rat calvaria defects <b>2022</b> ,	1
432	PTH-Induced Bone Regeneration and Vascular Modulation Are Both Dependent on Endothelial Signaling <b>2022</b> , 11,	
431	Low-carbohydrate, high-fat diet and running exercise influence bone parameters in old mice 2022,	
430	The miR-98-3p/JAG1/Notch1 axis mediates the multigenerational inheritance of osteopenia caused by maternal dexamethasone exposure in female rat offspring <b>2022</b> ,	1
429	Effects of testosterone and exercise training on bone microstructure of rats 2022, 15, 627-633	O
428	Development and CHARACTERIZATION of a humanized mouse model of osteoarthritis 2022,	O
427	Hypomorphic expression of parathyroid Bmal1 disrupts the internal parathyroid circadian clock and increases parathyroid cell proliferation in response to uremia <b>2022</b> ,	2
426	Puerarin specifically disrupts osteoclast activation via blocking integrin-IB Pyk2/Src/Cbl signaling pathway <b>2022</b> , 33, 55-69	1
425	Indigenous microbiota protects development of medication-related osteonecrosis induced by periapical disease in mice <b>2022</b> , 14, 16	1
424	The role of TGF□signaling in Gli1+ tendon and enthesis cells.	
423	Plumbagin is a NF- <b>B</b> -Inducing Kinase Inhibitor with Dual Anabolic and Anti-Resorptive Effects that Prevents Menopausal-Related Osteoporosis in Mice <b>2022</b> , 101767	О
422	Exercised accelerated the production of muscle-derived kynurenic acid in skeletal muscle and alleviated the postmenopausal osteoporosis through the Gpr35/NFB p65 pathway. 2022,	2
421	Morphologic and histologic characterization of sheep and porcine TMJ as large animal models for tissue engineering applications <b>2022</b> , 1	
420	Osteoblast lineage Sod2 deficiency leads to an osteoporosis-like phenotype in mice 2022,	3

419	Randomized controlled trial of daily teriparatide, weekly high-dose teriparatide, or bisphosphonate in patients with postmenopausal osteoporosis: The TERABIT study <b>2022</b> , 116416	O
418	3D-Printed Hydroxyapatite and Tricalcium Phosphates-Based Scaffolds for Alveolar Bone Regeneration in Animal Models: A Scoping Review <b>2022</b> , 15,	3
417	Genetic Deletion of Menin in Mouse Mesenchymal Stem Cells: An Experimental and Computational Analysis <b>2022</b> , 6, e10622	0
416	Finite element analysis of trabecular bone microstructure using CT imaging and continuum mechanical modelling <b>2022</b> ,	Ο
415	Acod1 negatively impacts osteoclastogenesis via GPR91-mediated NFATc1 activation.	
414	Anti-sclerostin antibodies and abaloparatide have additive effects when used as a countermeasure against disuse osteopenia in female rats <b>2022</b> , 116417	О
413	The CMS19 disease model specifies a pivotal role for collagen XIII in bone homeostasis <b>2022</b> , 12, 5866	1
412	A cholinergic neuroskeletal interface promotes bone formation during postnatal growth and exercise <b>2022</b> ,	1
411	Early effects of ovariectomy on bone microstructure, bone turnover markers and mechanical properties in rats <b>2022</b> , 23, 316	1
410	GIRK3 deletion facilitates kappa opioid signaling in chondrocytes, delays vascularization and promotes bone lengthening in mice <b>2022</b> , 116391	
409	Estrogen Receptor Bignaling in Osteoblasts is Required for Mechanotransduction in Bone Fracture Healing <b>2021</b> , 9, 782355	1
408	Pulsed electromagnetic fields attenuate glucocorticoid-induced bone loss by targeting senescent LepR bone marrow mesenchymal stromal cells <b>2021</b> , 112635	Ο
407	Scaling the U-net: segmentation of biodegradable bone implants in high-resolution synchrotron radiation microtomograms <b>2021</b> , 11, 24237	1
406	Rosiglitazone induces adipogenesis of both marrow and periosteum derived mesenchymal stem cells during endochondral fracture healing. <b>2021</b> ,	O
405	Frequent, quantitative bone planar scintigraphy for determination of bone anabolism in growing mice <b>2021</b> , 9, e12355	1
404	Commensal gut bacterium critically regulates alveolar bone homeostasis 2021,	1
403	Animal Model for Glucocorticoid Induced Osteoporosis: A Systematic Review from 2011 to 2021 <b>2021</b> , 23,	1
402	Micro-CT Study of Mongolian Gerbil Humeral Bone After Prolonged Spaceflight Based on a New Algorithm for Delimitation of Long-Bone Regions <b>2021</b> , 12, 752893	О

401	Administration of High-Dose Methylprednisolone Worsens Bone Loss after Acute Spinal Cord Injury in Rats <b>2021</b> , 2, 592-602	1
400	Bones and Teeth. <b>2021</b> , 520-540	
399	Evaluation of the effect of vitamin D3 on mandibular condyles in an ovariectomized mouse model: a micro-CT study. <b>2021</b> , 21, 627	
398	Jintiange Capsule Alleviates Rheumatoid Arthritis and Reverses Changes of Serum Metabolic Profile in Collagen-Induced Arthritic Rats <b>2021</b> , 14, 6685-6706	O
397	Macrophage Polarization and Alveolar Bone Healing Outcome: Despite a Significant M2 Polarizing Effect, VIP and PACAP Treatments Present a Minor Impact in Alveolar Bone Healing in Homeostatic Conditions <b>2021</b> , 12, 782566	1
396	Hmga2 deficiency is associated with allometric growth retardation, infertility, and behavioral abnormalities in mice. <b>2021</b> ,	1
395	Secreted frizzled related-protein 2 (Sfrp2) deficiency decreases adult skeletal stem cell function in mice. <b>2021</b> , 9, 49	2
394	Reduced Osteogenic Differentiation Potential in Acute Myeloid Leukaemia Patients Correlates with Decreased Expression in Mesenchymal Stromal Cells <b>2021</b> ,	
393	Micro-CT-Based Bone Microarchitecture Analysis of the Murine Skull <b>2022</b> , 2403, 129-145	2
392	Negative pressure wound therapy improves bone regeneration by promoting osteogenic differentiation via the AMPK-ULK1-autophagy axis <b>2021</b> , 1-17	4
391	Effect of Topical PTH 1-34 Functionalized to Biogran in the Process of Alveolar Repair in Rats Submitted to Orchiectomy <b>2021</b> , 15,	2
390	Effect of verapamil on bone mass, microstructure and mechanical properties in type 2 diabetes mellitus rats <b>2022</b> , 23, 363	o
389	Subchondral bone and synovial fluid metabolomic profiles are altered in injured and contralateral limbs 7 days after non-invasive joint injury in skeletally-mature C57BL/6 mice.	
388	Reduced bone mass in collagen prolyl 4-hydroxylase P4ha1 +/-; P4ha2 -/- compound mutant mice.	О
387	CHD7 regulates bone-fat balance by suppressing PPAR-laignaling 2022, 13, 1989	0
386	Identification and Characterization of a Novel Long Noncoding RNA that Regulates Osteogenesis in Diet-Induced Obesity Mice <b>2022</b> , 10, 832460	o
385	3D-Printed Double-Helical Biodegradable Iron Suture Anchor: A Rabbit Rotator Cuff Tear Model <b>2022</b> , 15,	1
384	Soluble CD13 induces inflammatory arthritis by activating the bradykinin receptor B1 2022,	1

## (2018-)

Sustained morphine delivery suppresses bone formation and alters metabolic and circulating 383 miRNA profiles in male C57BL/6J mice. Transporting Hydrogel via Chinese Acupuncture Needles for Lesion Positioning Therapy.. 2022, e2200079 382 Large-scale osteocyte lacunar morphological analysis of transiliac bone in normal and osteoporotic 381 2 premenopausal women.. 2022, 116424 380 Table\_1.DOCX. 2020, Table\_1.DOCX. 2019, 379 Presentation\_1.pdf. 2020, 378 Data\_Sheet\_1.ZIP. 2019, 377 Data\_Sheet\_2.ZIP. 2019, 376 Data\_Sheet\_1.PDF. 2019, 375 Data\_Sheet\_3.ZIP. 2019, 374 Data\_Sheet\_4.ZIP. 2019, 373 Data\_Sheet\_5.ZIP. 2019, 372 Data\_Sheet\_6.ZIP. 2019, 371 Image\_1.TIF. **2019**, 370 Presentation\_1.PPTX. 2018, 369 368 Data\_Sheet\_1.docx. 2019, 367 Image\_1.pdf. 2019, image\_1.tif. 2018, 366

365 video\_1.mp4. 2018, Data\_Sheet\_1.docx. 2020, 364 Data\_Sheet\_1.docx. 2019, 363 362 Image\_1.JPEG. 2017, Image\_2.JPEG. 2017, 361 360 Image\_3.JPEG. **2017**, Presentation\_1.pdf. 2017, 359 Data\_Sheet\_1.pdf. 2019, 358 Image\_1.JPEG. 2019, 357 356 Image\_2.jpg. 2019, Image\_3.JPEG. 2019, 355 Image\_4.jpg. **2019**, 354 Image\_5.JPEG. 2019, 353 Image\_6.JPEG. 2019, 352 Image\_7.JPEG. 2019, 351 350 Image\_8.JPEG. **2019**, Table\_1.DOCX. 2019, 349 348 Table\_2.DOCX. **2019**,

347 Table\_3.DOCX. **2019**,

346	Table_4.DOCX. <b>2019</b> ,	
345	Volumetric analysis of the periodontal microstructure under antiresorptive therapy: an experimental study in rabbits <b>2022</b> , 1	О
344	Alveolar Bone Remodeling with or without Collagen Filling of the Extraction Socket: A High-Resolution X-ray Tomography Animal Study <b>2022</b> , 11,	1
343	Mast Cells Drive Systemic Inflammation and Compromised Bone Repair After Trauma <b>2022</b> , 13, 883707	О
342	Effects of ferric citrate and intravenous iron sucrose on markers of mineral, bone, and iron homeostasis in a rat model of CKD-MBD <b>2022</b> ,	1
341	An Osteotomy Tool That Preserves Bone Viability: Evaluation in Preclinical and Clinical Settings <b>2022</b> , 11,	О
340	Use of antisense oligonucleotides to target Notch3 in skeletal cells <b>2022</b> , 17, e0268225	O
339	In vivo microCT-based time-lapse morphometry reveals anatomical site-specific differences in bone (re)modeling serving as baseline parameters to detect early pathological events <b>2022</b> , 116432	0
338	Spaceflight-Associated Vascular Remodeling and Gene Expression in Mouse Calvaria. 2022, 13,	
337	Wheel-Running Exercise Protects Ovariectomized Mice from Bone Loss via IFN-EMediated Suppression of the NF-B and MAPK Pathways. <b>2022</b> , 2022, 1-17	О
336	The prostacyclin analogue iloprost promotes cementum formation and collagen reattachment of replanted molars and upregulates mineralization by human periodontal ligament cells <b>2022</b> ,	O
335	The microbiome restrains melanoma bone growth by promoting intestinal NK and Th1 cells homing to bone <b>2022</b> ,	1
334	SARS-CoV-2 infection induces inflammatory bone loss in golden Syrian hamsters <b>2022</b> , 13, 2539	2
333	Thiazide use and skeletal microstructure: Results from a multi-ethnic study. <b>2022</b> , 101589	
332	IL-10 inhibits osteoclast differentiation and osteolysis through MEG3/IRF8 pathway <b>2022</b> , 110353	O
331	cAMP-Dependent Phosphodiesterase Inhibition Promotes Bone Anabolism Through CD8 + T-cell Wnt-10b Production in Mice.	О
330	Temporal changes in cortical microporosity during estrogen deficiency associated with perilacunar resorption and osteocyte apoptosis: A pilot study. <b>2022</b> , 101590	O

329	Micro-computed tomography assessment of bone structure in aging mice 2022, 12, 8117	1
328	LY450139 Inhibited Ti-Particle-Induced Bone Dissolution via Suppressing Notch and NF- <b>B</b> Signaling Pathways <b>2022</b> ,	
327	Open-porous magnesium-based scaffolds withstand corrosion under cyclic loading: A mechanistic study <b>2023</b> , 19, 406-417	0
326	Reversing the imbalance in bone homeostasis via sustained release of SIRT-1 agonist to promote bone healing under osteoporotic condition <b>2023</b> , 19, 429-443	Ο
325	BHLHE40 promotes osteoclastogenesis and abnormal bone resorption via c-Fos/NFATc1. <b>2022</b> , 12,	1
324	Osteogenic growth peptide is a potent anti-inflammatory and bone preserving hormone via cannabinoid receptor type 2. 11,	1
323	Roxadustat promotes osteoblast differentiation and prevents estrogen deficiency-induced bone loss by stabilizing HIF-1 activating the Wnt/I-catenin signaling pathway. <b>2022</b> , 17,	1
322	Tissue-Level Regeneration and Remodeling Dynamics are Driven by Mechanical Stimuli in the Microenvironment in a Post-Bridging Loaded Femur Defect Healing Model in Mice. <b>2022</b> , 10,	
321	Spatiotemporal responses of trabecular and cortical bone to complete spinal cord injury in skeletally mature rats. <b>2022</b> , 16, 101592	0
320	High phosphate intake induces bone loss in nephrectomized thalassemic mice. <b>2022</b> , 17, e0268732	O
319	Alterations of bone material properties in growing Ifitm5/BRIL p.S42 knock-in mice, a new model for atypical type VI osteogenesis imperfecta. <b>2022</b> , 116451	O
318	ERBignaling in a subset of CXCL12-abundant reticular cells regulates trabecular bone in mice.	
317	Effects of Dietary Protein Source and Quantity on Bone Morphology and Body Composition Following a High-Protein Weight-Loss Diet in a Rat Model for Postmenopausal Obesity. <b>2022</b> , 14, 2262	
316	Inactivation of AR or ERIIn extrahypothalamic neurons does not affect osteogenic response to loading in male mice.	
315	Absence of P2Y2 Receptor Does Not Prevent Bone Destruction in a Murine Model of Muscle Paralysis-Induced Bone Loss. <b>2022</b> , 13,	
314	Analysis of the femoral neck from rats in the periestropause treated with oxytocin and submitted to strength training. <b>2022</b> , 116452	O
313	The cortical bone metabolome of C57BL / 6J mice is sexually dimorphic.	0
312	Providing organic macro minerals and an elevated platform improved tibia characteristics, and increased locomotion and performance of fast- and slower-growing broilers. <b>2022</b> , 101973	O

311	Novel Therapeutic Strategy for Bacteria-Contaminated Bone Defects: Reconstruction with Multi-Biofunctional GO/Cu-Incorporated 3D Scaffolds. 2200043	O
310	Bone Quality in Patients with Osteoporosis undergoing Lumbar Fusion Surgery-Analysis of the MRI-based Vertebral Bone Quality Score and the Bone Microstructure derived from Microcomputed Tomography. <b>2022</b> ,	O
309	Effect of resistance training combined with 🛭 glucan ingestion on bone of ovariectomized mice. 1-8	
308	The role of geometrical features of the microarchitecture in the cancellous stiffness of the bovine femoral bone. <b>2022</b> , 105, 103823	
307	Crocin attenuates osteoclastogenesis and enhances bone health by skewing the immunoporotic âllreg-Th17âlæell axis in post-menopausal osteoporotic mice model. <b>2022</b> , 2, 100302	O
306	Mechanical loading attenuated negative effects of nucleotide analogue reverse-transcriptase inhibitor TDF on bone repair via Wnt/I-catenin pathway. <b>2022</b> , 161, 116449	O
305	X-ray computed microtomography datasets for osteogenic nanofibrous coated titanium implants. <b>2022</b> , 9,	
304	Cannabidiol-Treated Ovariectomized Mice Show Improved Glucose, Energy, and Bone Metabolism With a Bloom in Lactobacillus. 13,	O
303	Comparison of the 3D-Microstructure Between Alveolar and Iliac Bone for Enhanced Bioinspired Bone Graft Substitutes. 10,	0
302	Atom probe tomography for biomaterials and biomineralization. <b>2022</b> ,	4
		1
301	Glucocorticoid-induced expansion of classical monocytes contributes to bone loss.	0
301	Glucocorticoid-induced expansion of classical monocytes contributes to bone loss.  Small laboratory animal models of anterior cruciate ligament reconstruction.	
300	Small laboratory animal models of anterior cruciate ligament reconstruction.  Quantifying the Human Subchondral Trabecular Bone Microstructure in Osteoarthritis with Clinical	0
300	Small laboratory animal models of anterior cruciate ligament reconstruction.  Quantifying the Human Subchondral Trabecular Bone Microstructure in Osteoarthritis with Clinical CT. 2201692  Echinacoside Inhibits Osteoclast Function by Down-Regulating PI3K/Akt/C-Fos to Alleviate	0
300 299 298	Small laboratory animal models of anterior cruciate ligament reconstruction.  Quantifying the Human Subchondral Trabecular Bone Microstructure in Osteoarthritis with Clinical CT. 2201692  Echinacoside Inhibits Osteoclast Function by Down-Regulating PI3K/Akt/C-Fos to Alleviate Osteolysis Caused by Periprosthetic Joint Infection. 13,  Mmp13 deletion in mesenchymal cells increases bone mass and may attenuate the cortical bone	0
300 299 298 297	Small laboratory animal models of anterior cruciate ligament reconstruction.  Quantifying the Human Subchondral Trabecular Bone Microstructure in Osteoarthritis with Clinical CT. 2201692  Echinacoside Inhibits Osteoclast Function by Down-Regulating PI3K/Akt/C-Fos to Alleviate Osteolysis Caused by Periprosthetic Joint Infection. 13,  Mmp13 deletion in mesenchymal cells increases bone mass and may attenuate the cortical bone loss caused by estrogen deficiency. 2022, 12,  Utility of micro-CT for dating post-cranial fractures of known post-traumatic ages through 3D	0

293	Three-dimensional radiological anatomy of condyle trabecular bone based on a Volume-of-Interest analysis.	
292	Nox4 expression in osteo-progenitors controls bone development in mice during early life. <b>2022</b> , 5,	Ο
291	An integrated micro-extracting system facilitates lesion-free biomacromolecules enrichment and detection. <b>2022</b> , 219, 110812	
290	Mesobiliverdin IX meliorates osteoporosis via promoting osteogenic differentiation of mesenchymal stem cells. <b>2022</b> , 619, 56-61	
289	Low bone mass and impaired fracture healing in mouse models of Trisomy21 (Down syndrome). <b>2022</b> , 162, 116471	О
288	Temporal and spatial changes in bone mineral content and mechanical properties during breast-cancer bone metastases. <b>2022</b> , 17, 101597	O
287	Intrauterine alcohol exposure delays growth and disturbs trabecular morphology in 3-week-old Sprague âlDawley rat femur. <b>2022</b> , 71, 93	
286	On the Use of Micro-Computed Tomography for Pre-Clinical Testing of Cardiovascular Devices that Treat Intravascular Calcium. <b>2022</b> , 110, 383-388	
285	Micro-CT in Dentistry. <b>2022</b> , 215-225	
284	Systemic Dietary Hesperidin Modulation of Osteoclastogenesis, Bone Homeostasis and Periodontal Disease in Mice. <b>2022</b> , 23, 7100	1
283	Reproducibility of Densitometric and Biomechanical Assessment of the Mouse Tibia From In Vivo Micro-CT Images. 13,	
282	CD137 Regulates Bone Loss via the p53 Wnt/I-Catenin Signaling Pathways in Aged Mice. 13,	1
281	Intestinal inflammation promotes MDL-1+ osteoclast precursor expansion to trigger osteoclastogenesis and bone loss. <b>2022</b> ,	O
280	A Novel Inhibitor INF 39 Promotes Osteogenesis via Blocking the NLRP3/IL-1 Axis. <b>2022</b> , 2022, 1-12	
279	Impaired bone strength and bone microstructure in a novel early-onset osteoporotic rat model with a clinically relevant PLS3 mutation.	
278	A preliminary study exploring the mechanical properties of normal and Mgp-deficient mouse femurs during early growth. 095441192211090	
277	Micro-scale assessment of bone quality changes in adult cadaveric men with congestive hepatopathy.	O
276	Long Bone Mineral Loss, Bone Microstructural Changes and Oxidative Stress After Eimeria Challenge in Broilers. 13,	O

275	Effect of chronic lithium on mechanical sensitivity and trabecular bone loss induced by type-1 diabetes mellitus in mice.	
274	Contrast-enhanced micro-computed tomography of compartment and time-dependent changes in femoral cartilage and subchondral plate in a murine model of osteoarthritis.	
273	Ontogenetic Patterning of Human Subchondral Bone Microarchitecture in the Proximal Tibia. <b>2022</b> , 11, 1002	1
272	Linagliptin in Combination With Metformin Ameliorates Diabetic Osteoporosis Through Modulating BMP-2 and Sclerostin in the High-Fat Diet Fed C57BL/6 Mice. 13,	O
271	Di-(2-ethylhexyl) phthalate exposure links to inflammation and low bone mass in premenopausal and postmenopausal females: Evidence from ovariectomized mice and humans.	O
270	Conditioned medium of amniotic fluid-derived stromal cells exerts a bone anabolic effect by enhancing progenitor population and angiogenesis.	
269	An optimized workflow for microCT imaging of formalin-fixed and paraffin-embedded (FFPE) early equine embryos.	O
268	Comparison of heat production and bone architecture changes in the implant site preparation with compressive osteotomes, osseodensification technique, piezoelectric devices, and standard drills: an ex vivo study on porcine ribs.	1
267	TGFI reprograms TNF stimulation of macrophages towards a non-canonical pathway driving inflammatory osteoclastogenesis. <b>2022</b> , 13,	О
266	New Insights on Bone Tissue and Structural Muscle-Bone Unit in Constitutional Thinness. 13,	O
265	Induction of a NOTCH3 Lehman syndrome mutation in osteocytes causes osteopenia in male C57BL/6J mice. <b>2022</b> , 162, 116476	0
264	A combined treatment with selective androgen and estrogen receptor modulators prevents bone loss in orchiectomized rats.	O
263	Graphene oxide/gallium nanoderivative as a multifunctional modulator of osteoblastogenesis and osteoclastogenesis for the synergistic therapy of implant-related bone infection. <b>2022</b> ,	
262	Targeted Deletion of the Claudin12 Gene in Mice Increases Articular Cartilage and Inhibits Chondrocyte Differentiation. 13,	O
261	miR-221/222 drive synovial fibroblast expansion and pathogenesis of TNF-mediated arthritis.	0
260	Development of a first-in-class unimolecular dual GIP/GLP-2 analogue, GL-0001, for the treatment of bone fragility.	
259	Single Cell Cortical Bone Transcriptomics Defines Novel Osteolineage Gene Sets Altered in Chronic Kidney Disease.	
258	The Effect of IFT80 Deficiency in Osteocytes on Orthodontic Loading-Induced and Physiologic Bone Remodeling: In Vivo Study. <b>2022</b> , 12, 1147	

257	Sexually Dimorphic Increases in Bone Mass Following Tissue-specific Overexpression of Runx1 in Osteoclast Precursors. <b>2022</b> , 163,	0
256	Csf1 from marrow adipogenic precursors is required for osteoclast formation and hematopoiesis in bone.	
255	Galectin-1 deletion in mice causes bone loss via impaired osteogenic differentiation potential of BMSCs. <b>2022</b> , 36,	
254	CXCL12 in late-stage osteoblasts and osteocytes is required for load induced bone formation in mice.	О
253	Evaluating material-driven regeneration in a tissue engineered human in vitro bone defect model.	
252	Systemic effects of BMP2 treatment of fractures on non-injured skeletal sites during spaceflight. 13,	
251	MicroRNA-101a enhances trabecular bone accrual in male mice. <b>2022</b> , 12,	
250	Characterization of three-dimensional bone-like tissue growth and organization under influence of curvature and directional fluid flow.	
249	Osteoblast lineage cells-derived Sema3A regulates bone homeostasis independently of androgens.	
248	Soy protein intake increased bone mineral density under non-energy deficiency conditions but decreased it under energy deficiency conditions in young female rats. <b>2022</b> ,	О
247	The effects of romosozumab combined with active vitamin D3 on fracture healing in ovariectomized rats. <b>2022</b> , 17,	0
246	The effects of maternal fish oil supplementation rich in n-3 PUFA on offspring-broiler growth performance, body composition and bone microstructure. <b>2022</b> , 17, e0273025	1
245	G-CSF Receptor Deletion Amplifies Cortical Bone Dysfunction in Mice With STAT3 Hyperactivation in Osteocytes.	O
244	Guanylyl Cyclase-B Dependent Bone Formation in Mice is Associated with Youth, Increased Osteoblasts, and Decreased Osteoclasts.	O
243	Bone deconditioning during partial weight-bearing in rodents âlʿA systematic review and meta-analysis. <b>2022</b> , 34, 87-103	
242	Bioinspired Silk Fibroin Mineralization for Advanced In Vitro Bone Remodeling Models. 2206992	3
241	Diet X Gene Interactions Control Femoral Bone Adaptation to Low Dietary Calcium.	
240	Ano5 modulates calcium signaling during bone homeostasis in gnathodiaphyseal dysplasia. <b>2022</b> , 7,	

239	A novel extraction method enhanced the osteogenic and anti-osteoporosis effect of tea extract without any hepatotoxicity in ovariectomized rats. 13,	0
238	The crosstalk between MYC and mTORC1 during osteoclastogenesis. 10,	
237	High doses of zoledronic acid induce differential effects on femur and jawbone microstructure.	
236	Collagen VI ablation in zebrafish causes neuromuscular defects during developmental and adult stages. <b>2022</b> , 112, 39-61	1
235	Quantitative increase in T regulatory cells enhances bone remodeling in osteogenesis imperfecta. <b>2022</b> , 25, 104818	0
234	Mussaendoside O, a N-triterpene cycloartane saponin, attenuates RANKL-induced osteoclastogenesis and inhibits lipopolysaccharide-induced bone loss. <b>2022</b> , 105, 154378	
233	Intramembranous bone regeneration in diversity outbred mice is heritable. 2022, 164, 116524	
232	Lanthanide nanoparticles for near-infrared II theranostics. <b>2022</b> , 471, 214724	4
231	Definition of the Region of Interest for the Assessment of Alveolar Bone Repair Using Micro-computed Tomography.	0
230	Deletion of osteopontin or bone sialoprotein induces opposite bone responses to mechanical stimulation in mice. <b>2022</b> , 17, 101621	O
229	Computer tomography and magnetic resonance for multimodal imaging of fossils and mummies. <b>2022</b> , 94, 7-17	О
228	Noninvasive monitoring of muscle atrophy and bone metabolic disorders using dual-energy X-ray absorptiometry in diabetic mice. <b>2022</b> ,	O
227	Local immune cell contributions to fracture healing in aged individuals âl'A novel role for interleukin 22. <b>2022</b> , 54, 1262-1276	О
226	Suppression of osteosarcoma progression by engineered lymphocyte-derived proteomes. 2022,	1
225	A Beginnerâl Guide to the Characterization of Hydrogel Microarchitecture for Cellular Applications. <b>2022</b> , 8, 535	3
224	Effect of different thresholds on the accuracy of linear and volumetric analysis of native- and grafted-bone. <b>2022</b> , 33, 40-46	1
223	3D render volume CT reconstruction of the bones and arteries of the hind digit of the dromedary camel (Camelus dromedarius). <b>2022</b> , 7,	О
222	The efficacy of a semi-resorbable membrane based on silk fibroin-Glycerol on bone regeneration in rabbit calvarial defects compared to a commercial collagen membrane. 088532822211242	O

221	Controlled mechanical early loads improve bone quality and quantity around implants: An in vivo experimental study.	O
220	Distinct Responses of Modeling- and Remodeling-Based Bone Formation to the Discontinuation of Intermittent Parathyroid Hormone Treatment in Ovariectomized Rats.	O
219	RESULTS of MORPHOLOGICAL ANALYSIS of ANIMAL HARD TISSUES IN NORMAL AND SIMULATED OSTEOPOROSIS USING A NON-INVASIVE COMPUTED MICROTOMOGRAPHY TECHNIQUE. <b>2022</b> , 17-21	O
218	Single-cell spatiotemporal analysis reveals cell fates and functions of transplanted mesenchymal stromal cells during bone repair. <b>2022</b> ,	O
217	Effects of boric acid on alveolar sockets filling after dental extraction in rats.	O
216	Biomechanical, Microstructural and Material Properties of Tendon and Bone in the Young Oim Mice Model of Osteogenesis Imperfecta. <b>2022</b> , 23, 9928	O
215	Mouse embryo phenotyping using X-ray microCT. 10,	O
214	Loss of early B cell protein B decreases bone mass and accelerates skeletal aging. 13,	O
213	Myeloid cell-derived catecholamines influence bone turnover and regeneration in mice. 13,	О
212	Positive programming of the GC-IGF1 axis mediates adult osteoporosis susceptibility in male offspring rats induced by prenatal dexamethasone exposure. <b>2022</b> , 115264	O
211	Partial prevention of glucocorticoid-induced osteocyte deterioration in young male mice with osteocrin gene therapy. <b>2022</b> , 25, 105019	O
210	The Fractalkine-CX3CR1 Axis Regulates Non-inflammatory Osteoclastogenesis by Enhancing Precursor Cell Survival.	O
209	Complement receptor C5aR1 on osteoblasts regulates osteoclastogenesis in experimental postmenopausal osteoporosis. 13,	O
208	Effects of more natural housing conditions on the muscular and skeletal characteristics of female C57BL/6J mice.	O
207	Lifelong Excess in GH Elicits Sexually Dimorphic Effects on Skeletal Morphology and Bone Mechanical Properties.	O
206	Water Extract of Piper longum Linn Ameliorates Ovariectomy-Induced Bone Loss by Inhibiting Osteoclast Differentiation. <b>2022</b> , 14, 3667	O
205	Mitochondrial fatty acid Doxidation is important for normal osteoclast formation in growing female mice. 13,	0
204	The Use of Post-Natal Skeleton Development as Sensitive Preclinical Model to Test the Quality of Alternative Protein Sources in the Diet. <b>2022</b> , 14, 3769	O

203	Estrogen regulation of myokines that enhance osteoclast differentiation and activity. 2022, 12,	0
202	Sustained Morphine Delivery Suppresses Bone Formation and Alters Metabolic and Circulating miRNA Profiles in Male C57BL / 6J Mice.	O
201	Which Histometric Analysis Approach Is More Reliable for Assessing Histological Bone Tissue Samples?. <b>2022</b> , 58, 1364	0
200	Relationship between physical changes in the coffee bean due to roasting profiles and the sensory attributes of the coffee beverage.	o
199	Loss of anti-Milerian hormone signaling in mice affects trabecular bone mass in a sex- and age-dependent manner.	0
198	Sirt3 mediates the benefits of exercise on bone in aged mice.	O
197	Subchondral bone structure and synovial fluid metabolism are altered in injured and contralateral limbs 7 days after non-invasive joint injury in skeletally-mature C57BL/6 mice. <b>2022</b> ,	0
196	Validating Causal Diagrams of Human Health Risks for Spaceflight: An Example Using Bone Data from Rodents. <b>2022</b> , 10, 2187	1
195	Increased concentrations of conjugated bile acids are associated with osteoporosis in PSC patients. <b>2022</b> , 12,	0
194	A20 controls RANK -dependent osteoclast formation and bone physiology.	O
193	HSP90 promotes osteoclastogenesis by dual-activation of cholesterol synthesis and NF-B signaling.	O
192	Beta tricalcium phosphate, either alone or in combination with antimicrobial photodynamic therapy or doxycycline, prevents medication-related osteonecrosis of the jaw. <b>2022</b> , 12,	O
191	Long bones exhibit adaptive responses to chronic low-dose-rate ionizing radiation despite its lifespan-shortening and carcinogenic effects on C57BL /6 mice.	O
190	Roxadustat improves renal osteodystrophy by dual regulation of bone remodeling.	o
189	Effect of vitamin D on bone morphometry and stability of orthodontic tooth movement in rats. <b>2022</b> ,	O
188	P21 deficiency exhibits delayed endochondral ossification during fracture healing. <b>2022</b> , 165, 116572	O
187	Bone Strength and Mechanical Behaviour. <b>2022</b> ,	O
186	Multi-scale constitutive model of human trabecular bone.	O

185	Effect of chitosan/inorganic nanomaterial scaffolds on bone regeneration and related influencing factors in animal models: A systematic review. 10,	О
184	Dietary Hempseed Decreases Femur Maximum Load in a Young Female C57BL/6 Mouse Model but Does Not Influence Bone Mineral Density or Micro-Architecture. <b>2022</b> , 14, 4224	O
183	Changes of cortical bone pores structure and their effects on mechanical properties in tail-suspended rats. <b>2022</b> , 100175	0
182	Context-Dependent Roles for Toll-Like Receptors 2 and 9 in the Pathogenesis of Staphylococcus aureus Osteomyelitis.	О
181	High-fat diet-induced obesity augments the deleterious effects of estrogen deficiency on bone: Evidence from ovariectomized mice.	1
180	Osteosarcoma-enriched transcripts paradoxically generate osteosarcoma-suppressing extracellular proteins.	О
179	Low-intensity pulsed ultrasound partially reversed the deleterious effects of a severe spinal cord injury-induced bone loss and osteoporotic fracture healing in paraplegic rats.	О
178	Degradation behavior and osseointegration of Mg-Zn-Ca screws in different bone regions of growing sheepâll pilot study.	1
177	The Nutraceutical Genistein-Lycopene Combination Improves Bone Damage Induced by Glucocorticoids by Stimulating the Osteoblast Formation Process. <b>2022</b> , 14, 4296	0
176	Serum Amyloid A proteins reduce bone mass during mycobacterial infections.	О
175	Effects of Macrophage Depletion and Transplantation on Bisphosphonate-related Osteonecrosis of the Jaw-like Lesions in Mice.	0
174	Effect of Taraxaci Herba on Bone Loss in an OVX-Induced Model through the Regulation of Osteoclast Differentiation. <b>2022</b> , 14, 4354	O
173	Comparison of three-dimensional digital analyses and two-dimensional histomorphometric analyses of the bone-implant interface. <b>2022</b> , 17, e0276269	О
172	Inflammaging and Bone Loss in a Rat Model of Spinal Cord Injury.	O
171	Histochemical assessment of accelerated bone remodeling and reduced mineralization in Il-6 deficient mice. <b>2022</b> ,	0
170	Microgel-Assisted Delivery of Adenosine to Accelerate Fracture Healing.	O
169	Biomechanical, Histologic, and Micro-Computed Tomography Characterization of Partial-Width Full-Thickness Supraspinatus Tendon Injury in Rats. <b>2022</b> ,	О
168	Mechanical properties of young mice tibia in four circumferential quadrants under nanoindentation. <b>2022</b> , 144, 111350	O

167	Osteocyte Estrogen Receptor [] (Ot-ER[]) Regulates Bone Turnover and Skeletal Adaptive Response to Mechanical Loading Differently in Male and Female Growing and Adult Mice.	О
166	Early patellofemoral cartilage and bone pathology in a rat model of noninvasive anterior cruciate ligament rupture. 1-11	Ο
165	Degradation of Bone Quality in a Transgenic Mouse Model of Alzheimer?s Disease.	1
164	R-spondin 3 deletion induces Erk phosphorylation to enhance Wnt signaling and promote bone formation in the appendicular skeleton. 11,	О
163	Topology Optimization-Based Localized Bone Microstructure Reconstruction for Image Resolution Enhancement: Accuracy and Efficiency. <b>2022</b> , 9, 644	O
162	The gelatinases, matrix metalloproteinases 2 and 9, play individual roles in skeleton development. <b>2022</b> , 113, 100-121	Ο
161	Melatonin suppresses bone marrow adiposity in ovariectomized rats by rescuing the imbalance between osteogenesis and adipogenesis through SIRT1 activation. <b>2023</b> , 38, 84-97	О
160	Evaluating material-driven regeneration in a tissue engineered human in vitro bone defect model. <b>2023</b> , 166, 116597	O
159	A microCT imaging protocol for reproducible and efficient quantitative morphometric analysis (QMA) of joint structures of the in situ mouse tibio-femoral joint. <b>2023</b> , 166, 116606	О
158	CCL3 in bone marrow microenvironment causes bone loss and bone marrow adiposity in aged mice.	O
157	The gut microbiome has sexually dimorphic effects on bone tissue energy metabolism and multiscale bone quality in C57BL/6J mice.	O
156	CXCR4 mediates the effects of IGF-1R signaling in rodent bone homeostasis and fracture repair. <b>2022</b> , 116600	O
155	Microtomographic analysis of surgically-created bone defects in rats: manual versus predefined region-of-interest definition.	O
154	Impact of alcohol on bone health in people living with HIV: integrating clinical data from serum bone markers with morphometric analysis in a non-human primate model.	O
153	The PYY/Y2R-deficient male mouse is not protected from bone loss due to Roux-en-Y gastric bypass. <b>2022</b> , 116608	0
152	Progression of microstructural deterioration in load-bearing immobilization osteopenia. <b>2022</b> , 17, e0275439	1
151	Viable Cryopreserved Human Bone Graft Exhibit Superior Osteogenic Properties In Mandibular Lateral Augmentation.	О
150	Simvastatin Embedded into Poly(Lactic-Co-Glycolic Acid)-Based Scaffolds in Promoting Preclinical Bone Regeneration: A Systematic Review. <b>2022</b> , 12, 11623	1

149	Focal adhesion protein vinculin inhibits Mef2c-driven sclerostin expression in osteocytes to promote bone formation in mice.	О
148	Open-source pipeline for automatic segmentation and microstructural analysis of murine knee subchondral bone. <b>2022</b> , 116616	O
147	Connexin 43 Channels in Osteocytes Are Necessary for Bone Mass and Skeletal Muscle Function in Aged Male Mice. <b>2022</b> , 23, 13506	О
146	Sclerostin antibody promotes bone formation through the Wnt/I-catenin signaling pathway in femoral trochlear after patellar instability. 1-13	O
145	CircFOXO3 protects against osteoarthritis by targeting its parental gene FOXO3 and activating PI3K/AKT-mediated autophagy. <b>2022</b> , 13,	2
144	Protein Kinase G2 Is Essential for Skeletal Homeostasis and Adaptation to Mechanical Loading in Male but not Female Mice.	O
143	Avaliaß da perda Esea utilizando diferentes parEnetros na anlise microtomogrEica. Estudo em ratos. 51,	О
142	Targeting Sclerostin and Dkk1 at Optimized Proportions of Low-Dose Antibody Achieves Similar Skeletal Benefits to Higher-Dose Sclerostin Targeting in the Mature Adult and Aged Skeleton. <b>2022</b> , 13, 1891	O
141	Dysbiotic oral microbiota contributes to alveolar bone loss associated with obesity in mice. 30,	0
140	Global cannabinoid receptor 1 deficiency affects disuse-induced bone loss in a site-specific and sex-dependent manner. <b>2023</b> , 146, 111414	O
139	Differential bone adaptation to mechanical unloading and reloading in young, old, and osteocyte deficient mice. <b>2023</b> , 167, 116646	0
138	In vivo intra-articular contrast enhanced 🛭 T imaging of mouse knee cartilage. <b>2023</b> , 167, 116632	О
137	Antimicrobial and bone repair effects of boric acid in a rat model of dry socket (alveolar osteitis) following dental extraction. <b>2023</b> , 76, 127118	О
136	Dura mater assists 3D printed porous titanium scaffolds in healing rabbit calvarial defects. <b>2023</b> , 34, 105111	O
135	Nuclear factor erythroid 2âlelated factor 2 (Nrf2) deficiency causes age-dependent progression of female osteoporosis. <b>2022</b> , 23,	0
134	Assessment of Bone Microstructure by Micro CT in C57BL/6J Mice for Sex-Specific Differentiation. <b>2022</b> , 23, 14585	O
133	Controllable AgNPs encapsulation to construct biocompatible and antibacterial titanium implant. 10,	О
132	Transcriptome-wide association study and eQTL colocalization identify potentially causal genes responsible for human bone mineral density GWAS associations. 11,	1

131	Osteoblast/osteocyte-derived interleukin-11 regulates osteogenesis and systemic adipogenesis. <b>2022</b> , 13,	O
130	Abaloparatide has the same catabolic effects on bones of mice when infused as PTH (1-34).	О
129	The quantification of 3D-trabecular architecture of the fourth cervical vertebra using CT osteoabsorptiometry and micro-CT.	0
128	Bone loss is ameliorated by fecal microbiota transplantation through SCFA/GPR41/IGF1 pathway in sickle cell disease mice. <b>2022</b> , 12,	1
127	Downregulation of the Autism Spectrum Disorder Gene Shank2 Decreases Bone Mass in Male Mice.	0
126	Effects of growth hormone on muscle and bone in female mice: role of follistatin.	O
125	Performance of Polydioxanone-Based Membrane in Association with 3D-Printed Bioceramic Scaffolds in Bone Regeneration. <b>2023</b> , 15, 31	O
124	Muscle-derived extracellular vesicles improve disuse-induced osteoporosis by rebalancing bone formation and bone resorption. <b>2022</b> ,	О
123	Remarkable Plasticity of Bone Iron Homeostasis in Hibernating Daurian Ground Squirrels (Spermophilus dauricus) May Be Involved in Bone Maintenance. <b>2022</b> , 23, 15858	О
122	Regulation of bone homeostasis by MERTK and TYRO3. <b>2022</b> , 13,	O
121	Experimental models of bone marrow lesions in ovine femoral condyles.	О
120	Prolonged treadmill training is not able to prevent ovariectomy-induced bone loss. 13,	О
119	Investigating effects of locally applied boric acid on fracture healing with and without low-level laser therapy. <b>2023</b> , 38,	O
118	Platelet-Derived Growth Factor B Is a Key Element in the Pathological Bone Formation of Ankylosing Spondylitis.	1
117	Trabecular Bone Volume Is Reduced, With Deteriorated Microstructure, With Aging in a Rat Model of Duchenne Muscular Dystrophy. <b>2022</b> , 44, 323-330	O
116	miR-29 is an important driver of aging-related phenotypes.	О
115	Image-based microstructural simulation of thermal conductivity for highly porous wood fiber insulation boards.	O
114	LâĦrticulation sacro-iliaque : un site dâĦnalyse pertinent pour lâĦude de la microarchitecture osseuse et de lâĦterligne articulaire dans des modြes murins de pathologies osseuses chroniques. <b>2022</b> , 89, A177	О

113	Murine Animal Models in Osteogenesis Imperfecta: The Quest for Improving the Quality of Life. <b>2023</b> , 24, 184	O
112	Examination of the microstructures of the lower cervical facet based on micro-computed tomography: A cadaver study. <b>2022</b> , 101, e31805	O
111	Micro CT Analysis of Microholes Drilled by Focused Electron Beam Drilling Based on Image Noise Reduction Using Masking Layers. <b>2022</b> , 31, 388-395	О
110	Latexâlollagen membrane: an alternative treatment for tibial bone defects. <b>2022</b> , 57, 22019-22041	O
109	3D printed trabeculae conditionally reproduce the mechanical properties of the actual trabeculae - A preliminary study. <b>2022</b> , 8, e12101	O
108	Fragile X Messenger Ribonucleoprotein 1 (FMR1), a novel inhibitor of osteoblast/osteocyte differentiation, regulates bone formation, mass, and strength in young and aged male and female mice	O
107	Serum bone remodeling parameters and transcriptome profiling reveal abnormal bone metabolism associated with keel bone fractures in laying hens. <b>2022</b> , 102438	О
106	Sexual dimorphism of the synovial transcriptome underpins greater PTOA disease severity in male mice following joint injury.	O
105	Involvement of Siglec-15 in regulating RAP1/RAC signaling in cytoskeletal remodeling in osteoclasts mediated by macrophage colony-stimulating factor.	O
104	Tissue Bioengineering with Fibrin Scaffolds and Deproteinized Bone Matrix Associated or Not with the Transoperative Laser Photobiomodulation Protocol. <b>2023</b> , 28, 407	0
103	NIBAN2 promotes osteogenic differentiation and antagonizes osteoporosis by regulating RUNX2 alternative splicing.	O
102	Effect of Dietary Geranylgeraniol and Green Tea Polyphenols on Glucose Homeostasis, Bone Turnover Biomarkers, and Bone Microstructure in Obese Mice. <b>2023</b> , 24, 979	O
101	Longitudinal alterations in bone morphometry, mechanical integrity and composition in Type-2 diabetes in a Zucker diabetic fatty (ZDF) rat. <b>2023</b> , 116672	О
100	Inositol 1,4,5-trisphosphate receptor type 2 is associated with the boneâllessel axis in chronic kidney diseaseâlhineral bone disorder. <b>2023</b> , 45,	O
99	Accuracy of in vivo microCT imaging in assessing the microstructural properties of the mouse tibia subchondral bone. 13,	О
98	Asperosaponin VI Protects Against Bone Loss Due to Hindlimb Unloading in Skeletally Growing Mice Through Regulating Microbial Dysbiosis Altering the 5-HT Pathway.	O
97	D-Mannose prevents bone loss under weightlessness. <b>2023</b> , 21,	О
96	Associations Among Hip Structure, Bone Mineral Density, and Strength Vary With External Bone Size in White Women.	O

95	Bone microstructure in proton pump inhibitor users. <b>2023</b> , 168, 116668	0
94	Colon epithelial cell-specific Bmal1 deletion impairs bone formation in mice. 2023, 168, 116650	O
93	Bone marrow dosimetry for mice: exposure from bone-seeking 89,90Sr.	О
92	Metastatic infiltration of nervous tissue and periosteal nerve sprouting in multiple myeloma induced bone pain.	O
91	Lack of Skeletal Effects in Mice with Targeted Disruptionof Prolyl Hydroxylase Domain 1 (Phd1) Gene Expressed in Chondrocytes. <b>2023</b> , 13, 106	1
90	The Micro-CT Analysis of the Structural Parameters of Collagen-based Porous Scaffolds: The Influence of Image Processing and Binarization.	Ο
89	Quantitative Load Dependency Analysis of Local Trabecular Bone Microstructure to Understand the Spatial Characteristics in the Synthetic Proximal Femur. <b>2023</b> , 12, 170	0
88	Evaluation of Vitamin D Isolated or Associated with Teriparatide in Peri-Implant Bone Repair in Tibia of Orchiectomized Rats. <b>2023</b> , 12, 228	O
87	Lateral Sinus Flour Augmentation by Deproteinized Bovine Bone Material in Severe Alveolar Bone Atrophy: Micro Ct Study.	0
86	Enhanced Antitumor Efficacy of Radium-223 and Enzalutamide in the Intratibial LNCaP Prostate Cancer Model. <b>2023</b> , 24, 2189	O
85	Dietary supplementation of clinically utilized PI3K p110Hnhibitor extends the lifespan of male and female mice.	0
84	Gene Therapy to Treat Osteopenia Associated with Chronic Ethanol Consumption and Aldehyde Dehydrogenase 2 Deficiency.	O
83	Micro-CT Analysis of Implanted Poly-Ether-Ether-Ketone Scaffolds: Plasma Immersion Ion Implantation Increases Osteoconduction. 2201297	0
82	Viable cryopreserved human bone graft exhibit superior osteogenic properties in mandibular lateral augmentation. <b>2023</b> , 13,	O
81	Single cell cortical bone transcriptomics define novel osteolineage gene sets altered in chronic kidney disease. 14,	O
80	Temporal Pattern of micro-CT Angiography Vascular Parameters and VEGF mRNA Expression in Fracture Healing: a Radiograph and Molecular Comparison.	O
79	Platelet-rich fibrin (PRF) membrane isolated and injectable-PRF-mixed particulate bovine bone graft in rattibiae non-critical defects healing.	O
78	Bone strength, bone remodeling, and Biomechanics of fracture. <b>2023</b> , 515-546	O

77	Mitochondrial B-oxidation of adipose-derived fatty acids by osteoblast fuels parathyroid hormone-induced bone formation.	О
76	Analysis of Bone Density and Bone Morphometry by Periapical Radiographs in Dental Implant Osseointegration Process. <b>2023</b> , 2023, 1-9	O
75	FBXO11 regulates bone development. <b>2023</b> , 170, 116709	O
74	LBP1C-2 from Lycium barbarum alleviated age-related bone loss by targeting BMPRIA/BMPRII/Noggin. <b>2023</b> , 310, 120725	О
73	Muscadine grape (vitis rotundifolia) and wine polyphenols alleviated arthritis and restored the gut microbial composition in mice. <b>2023</b> , 116, 109311	0
72	C3a-C3aR signaling is a novel modulator of skeletal homeostasis. <b>2023</b> , 18, 101662	O
71	FLNA-filaminopathy skeletal phenotypes are not due to an osteoblast autonomous loss-of-function. <b>2023</b> , 18, 101668	0
70	Reambulation following hindlimb unloading attenuates disuse-induced changes in murine fracture healing. <b>2023</b> , 172, 116748	O
69	Role of resistance training in bone macro and micro damages in an estrogen absence animal model. <b>2023</b> , 317, 121417	0
68	Degradation-Resistant Hypoxia Inducible Factor-2 <del>II</del> n Murine Osteocytes Promotes a High Bone Mass Phenotype. <b>2023</b> , 7,	1
67	SHP-1 Protein Tyrosine Phosphatase Affects Early Postnatal Bone Development in Mice. <b>2023</b> , 112, 472-482	0
66	Implementation of automated behavior metrics to evaluate voluntary wheel running effects on inflammatory-erosive arthritis and interstitial lung disease in TNF-Tg mice. <b>2023</b> , 25,	O
65	PTH 1-34 promoted bone formation by regulating iron metabolism in unloading-induced bone loss. 13,	0
64	Alpha-ketoglutarate up-regulates autophagic activity in peri-implant environment and enhances dental implant osseointegration in osteoporotic mice. <b>2023</b> , 50, 671-683	O
63	X-ray computedmicrotomography time-dependent analysis of sandwich bread in different storageconditions.	0
62	Regional assessment of male murine bone exposes spatial heterogeneity in osteocyte lacunar volume associated with intracortical canals and regulation by VEGF.	O
61	Continuum finite element analysis generalizes in vivo trabecular bone microstructural strength measures between two CT scanners with different image resolution. <b>2023</b> , 9, 025012	0
60	Copper-deposited diatom-biosilica enhanced osteogenic potential in periodontal ligament stem cells and rat cranium. <b>2023</b> , 111, 1286-1298	О

59	Csf1 from marrow adipogenic precursors is required for osteoclast formation and hematopoiesis in bone. 12,	О
58	A Senomorphic-Conjugated Scaffold for Application of Senescent Cells in Regenerative Medicine. 2200276	O
57	Biglycan regulates bone development and regeneration. 14,	O
56	Influence of antiresorptive/antiangiogenic therapy on the extension of experimentally induced peri-implantitis lesions.	O
55	Wnt/I-Catenin Signaling in Craniomaxillofacial Osteocytes. 2023, 21, 228-240	O
54	HSV1716 Prevents Myeloma Cell Regrowth When Combined with Bortezomib In Vitro and Significantly Reduces Systemic Tumor Growth in Mouse Models. <b>2023</b> , 15, 603	O
53	Acute bone loss following SARS-CoV-2 infection in mice.	O
52	Resolvin D1 improves allograft osteointegration and directly enhances osteoblasts differentiation.	O
51	Zoledronate/Anti-VEGF Neutralizing Antibody Combination Administration Increases Osteal Macrophages in a Murine Model of MRONJ Stage 0-like Lesions. <b>2023</b> , 12, 1914	О
50	Development of a First-in-Class Unimolecular Dual GIP / GLP -2 Analogue, GL -0001, for the Treatment of Bone Fragility.	O
49	3-D structure of snow constructed with successive section planes. <b>2013</b> , 75, 441-447	O
48	Osteocyte-Derived CaMKK2 Regulates Osteoclasts and Bone Mass in a Sex-Dependent Manner through Secreted Calpastatin. <b>2023</b> , 24, 4718	O
47	Investigating the role of dry compaction and layer-wise agglomeration to control the dissolution of granular urea fertilizer. <b>2023</b> , 420, 118382	O
46	Quantitative morphometric analysis in tibiofemoral joint osteoarthritis imaging: A literature review. <b>2023</b> , 3, 100088	O
45	Changes in alveolar bone structure during orthodontic tooth movement in adolescent and adult rats: A microcomputed tomography study.	О
44	Excess Growth Hormone Triggers Inflammation-Associated Arthropathy, Subchondral Bone Loss, and Arthralgia. <b>2023</b> ,	O
43	Gulp1 deficiency augments bone mass in male mice by affecting osteoclasts due to elevated 17 lestradiol levels.	O
42	Callus IT cells and microbe-induced intestinal Th17 cells improve fracture healing in mice. <b>2023</b> , 133,	O

41	Less sclerotic microarchitecture pattern with increased bone resorption in glucocorticoid-associated osteonecrosis of femoral head as compared to alcohol-associated osteonecrosis of femoral head. 14,	О
40	Wnt1 Boosts Fracture Healing by Enhancing Bone Formation in the Fracture Callus.	O
39	Sostdc1 Suppression in the Absence of Sclerostin Potentiates Anabolic Action of Cortical Bone in Mice.	O
38	Effects of the individual three-dimensional printed craniofacial bones with a quick response code on the skull spatial knowledge of undergraduate medical students.	O
37	Repeated unilateral injections of botulinum toxin in masticatory muscles in adult rats do not amplify condylar and alveolar bone loss nor modify the volume of the hypertrophic bone proliferation at enthesis.	O
36	Hox genes are crucial regulators of periosteal stem cell identity. <b>2023</b> , 150,	O
35	Mouse Models of Mineral Bone Disorders Associated with Chronic Kidney Disease. <b>2023</b> , 24, 5325	O
34	Enhanced µCT Imaging Protocol to Enable High-Resolution 3D Visualization of Microdamage in Rat Vertebrae. <b>2023</b> , 13, 3625	O
33	Lrp5 p. Val667Met Variant Compromises Bone Mineral Density and Matrix Properties in Osteoporosis.	O
32	Doseâlesponse effect of Montelukast on post-extraction dental socket repair and skeletal phenotype of mice.	O
31	Bone metastases do not affect the measurement uncertainties of a global digital volume correlation algorithm. 11,	О
30	Extracellular Vesicles Secreted by TGF-[1-Treated Mesenchymal Stem Cells Promote Fracture Healing by SCD1-Regulated Transference of LRP5. <b>2023</b> , 2023, 1-17	O
29	Cysteine carboxyethylation generates neoantigens to induce HLA-restricted autoimmunity. <b>2023</b> , 379,	1
28	Microtomographic, histomorphometric, and molecular features show a normal alveolar bone healing process in iNOS-deficient mice along a compensatory upregulation of eNOS and nNOS isoforms. 31,	O
27	Large-scale morphometry of the subarachnoid space of the optic nerve. 2023, 20,	O
26	Differences in the Osseous Ultrastructure in 2 Differing Etiologies of Eagle Syndrome. A Micro-CT Study. Publish Ahead of Print,	O
25	Osteosarcoma-enriched transcripts paradoxically generate osteosarcoma-suppressing extracellular proteins. 12,	О
24	Blockade of Activin Receptor IIB Protects Arthritis Pathogenesis by Non-Amplification of Activin A-ACVR2B-NOX4 Axis Pathway. 2205161	O

23	Single intraoperative infrared laser optimized bone repair in rat femoral osteotomies with experimentally induced osteoporosis. <b>2023</b> , 38,	О
22	Evaluation of Trabecular Microstructure of Cancellous Bone Using Quarter-Detector Computed Tomography. <b>2023</b> , 13, 1240	O
21	FGFR regulator Memo1 is dispensable for FGF23 expression by osteoblasts during folic acid-driven kidney injury. <b>2023</b> , 11,	О
20	Triple-gene deletion for osteocalcin significantly impairs the alignment of hydroxyapatite crystals and collagen in mice. 14,	0
19	Differential bone remodeling mechanism in hindlimb unloaded and hibernating Daurian ground squirrels: a comparison between artificial and natural disuse within the same species.	О
18	Cationic Carrier Mediated Delivery of Anionic Contrast Agents in Low Doses Enable Enhanced Computed Tomography Imaging of Cartilage for Early Osteoarthritis Diagnosis. <b>2023</b> , 17, 6649-6663	O
17	MRI-based vertebral bone quality score for the assessment of osteoporosis in patients undergoing surgery for lumbar degenerative diseases. <b>2023</b> , 18,	О
16	Examining the Role of Hypothalamus-Derived Neuromedin-U (NMU) in Bone Remodeling of Rats. <b>2023</b> , 13, 918	O
15	CCL12 induces trabecular bone loss by stimulating RANKL production in BMSCs during acute lung injury.	0
14	Effects of uphill and downhill walking on post-traumatic osteoarthritis development in mice.	Ο
13	Impact loading intensifies cortical bone (re)modeling and alters longitudinal bone growth of pubertal rats.	0
12	A simple and effective vascular network labeling method for transparent tissues of mice.	O
11	Bone structure and composition in a hyperglycemic, obese, and leptin receptor-deficient rat: Microscale characterization of femur and calvarium. <b>2023</b> , 172, 116747	О
10	KIAA1199 deficiency enhances skeletal stem cell differentiation to osteoblasts and promotes bone regeneration. <b>2023</b> , 14,	O
9	Ensemble deep honey architecture for COVID-19 prediction using CT scan and chest X-ray images.	0
8	Inactivation of the gene encoding procalcitonin prevents antibody-mediated arthritis.	O
7	The quantification of 3D-trabecular architecture of the fourth cervical vertebra using CT osteoabsorptiometry and micro-CT. <b>2023</b> , 18,	О
6	Osteocytes contribute via nuclear receptor PPAR-alpha to maintenance of bone and systemic energy metabolism. 14,	O

5	Reversal of the diabetic bone signature with anabolic therapies in mice. <b>2023</b> , 11,	O
4	Serum amyloid A proteins reduce bone mass during mycobacterial infections. 14,	O
3	Histochemical assessment on osteoclasts in long bones of toll-like receptor 2 (TLR2) deficient mice. <b>2023</b> ,	O
2	Characterization of three-dimensional bone-like tissue growth and organization under influence of directional fluid flow.	O
1	Effects of more natural housing conditions on the muscular and skeletal characteristics of female C57BL/6J mice. <b>2023</b> , 39,	O